Hydrogen trapping in steel: site determination via ab initio modeling

Craig Van Heirweghe

Promotoren: prof. dr. Stefaan Cottenier, prof. dr. ir. Kim Verbeken
Begeleider: Kurt Lejaeghere

Masterproef ingediend tot het behalen van de academische graad van
Master in de ingenieurswetenschappen: materiaalkunde

Vakgroep Toegepaste Materiaalwetenschappen
Voorzitter: prof. dr. ir. Joris Degrieck
Faculteit Ingenieurswetenschappen en Architectuur
Academiejaar 2012-2013

UNIVERSITEIT
GENT

This work has been performed at the Center for Molecular Modeling, in collaboration with the Department of Materials Science and Engineering.

Preface

This work could not have been completed without the help of many people. First of all, I would like to thank my promotors Stefaan Cottenier and Kim Verbeken, who offered me as one of the first Materials Science and Engineering students the opportunity to explore the fascinating world of computational materials science. I would also like to thank both of them for their constant belief in the skills that I have obtained during my engineering studies. A special thanks goes to my supervisors Kurt Lejaeghere and Stefaan Cottenier, for their time and patience to provide such clarifying answers to my innumerable questions, and for their time to revise my thesis several times. Many spelling mistakes would not have been eliminated from this work without Kurt and his unbelievable eye for detail.

Last but not least, I would like to thank my parents and my fiancee Charlotte Depicker. I presume that they still have no clue at all of what I have investigated in this thesis (they usually lost complete interest or started to freak out when I pronounced the words 'ab initio'), but they were nevertheless an immense support during the past few months. They have been there for me at the most depressing moments and helped me to hold on and keep on writing, which has eventually lead to this work.

Toelating tot bruikleen/Permission for usage

De auteur geeft de toelating dit afstudeerwerk voor consultatie beschikbaar te stellen en delen van het afstudeerwerk te kopiëren voor persoonlijk gebruik.
Elk ander gebruik valt onder de beperkingen van het auteursrecht, in het bijzonder met betrekking tot de verplichting de bron uitdrukkelijk te vermelden bij het aanhalen van resultaten uit dit afstudeerwerk.

The author gives permission to make this master dissertation available for consultation and to copy parts of this master dissertation for personal use. In the case of any other use, the limitations of the copyright have to be respected, in particular with regard to the obligation to state expressly the source when quoting results from this master dissertation.

Craig Van Heirweghe
Ghent, June 3th 2013

Hydrogen trapping in steel: site determination via ab initio modeling

Craig Van Heirweghe

Promotors: prof. dr. Stefaan Cottenier, prof. dr. ir. Kim Verbeken
Supervisors: prof. dr. Stefaan Cottenier, ir. Kurt Lejaeghere

Master dissertation submitted to obtain the academic degree of Master of Science in Materials Science and Engineering

Department of Applied Materials Science
Head of Department: prof. dr. ir. Joris Degrieck

Faculty of Engineering and Architecture
Academic year 2012-2013

Summary

Calculations of defect properties via the DFT-based supercell approach suffer from errors due to interactions between the defect and its periodic images for common supercell sizes. The supercell finite-size convergence was therefore investigated for several properties in the particular case of a substitutional Zr-impurity in a fcc Cu host lattice, by means of the plane-wave-based DFT-program VASP. Properties that depend on the local electronic structure of the supercell, such as the LDOS and the local charge difference, were found to converge rapidly with supercell size. It has also been showed that calculations for large supercells do not necessarily improve the supercell finite-size convergence behavior of system-size dependent defect properties, such as the defect formation energy and the force. All parameters that induce errors who scale with system size, such as the number of k-points, will cause problems for such supercells if calculations are performed with a constant relative accuracy. A procedure was however developed that enables us to estimate the necessary parameter requirements for each supercell size and, taking computational limitations into consideration, which supercell sizes can be included in the supercell finite-size convergence investigation. Hence, if all parameter requirements with respect to the defect property of interest are taken into account, reliable supercell finite-size convergence studies can be performed for any defect/lattice-system.

Keywords

Density functional theory (DFT), supercell method, spurious defect interactions, finite-size error, absolute error

Hydrogen trapping in steel: site determination via ab initio modeling

Craig Van Heirweghe

Promotoren: prof. dr. Stefaan Cottenier, prof. dr. ir. Kim Verbeken
Begeleiders: prof. dr. Stefaan Cottenier, ir. Kurt Lejaeghere

Masterproef ingediend tot het behalen van de academische graad van Master in de ingenieurswetenschappen: materiaalkunde

Vakgroep Toegepaste Materiaalwetenschappen
Voorzitter: prof. dr. ir. Joris Degrieck

Faculteit Ingenieurswetenschappen en Architectuur
Academiejaar 2012-2013

Samenvatting

Berekeningen van defecteigenschappen via de DFT-gebaseerde supercelmethode vertonen voor normale supercelgroottes fouten als gevolg van interacties tussen het defect en zijn periodiek kopieën. Daarom werd een grondige studie uitgevoerd op de supercelconvergentie van verschillende eigenschappen in het bijzonder geval van een substiutionele Zr-onzuiverheid in een fcc Cu gastrooster. Alle berekeningen werden hierbij uitgevoerd met het DFT-programma VASP. Eigenschappen die enkel afhangen van de lokale elektronenstructuur in een supercel, zoals de LDOS en lokale ladingsverschillen, bleken snel te convergeren met supercelgrootte. Grote supercellen bleken echter niet noodzakelijk het supercelconvergentie-gedrag te verbeteren voor supercelgrootte-afhankelijke eigenschappen, zoals de defect-vormingsenergie en de kracht. Alle parameters die supercelgrootte-afhankelijke fouten induceren, zoals het aantal k-punten, veroorzaken problemen voor dergelijke supercellen indien de berekeningen uitgevoerd worden met een constante relatieve nauwkeurigheid. Een procedure werd echter ontwikkeld, die ons toelaat om de noodzakelijke parametervereisten te schatten voor elke supercelgrootte en om zo een idee te verkrijgen wat de computationeel grootst haalbare supercel is die beschouwd kan worden in de supercelconvergentie-studie. Wanneer alle parametervereisten met betrekking tot een zekere defect-eigenschap bijgevolg in rekening gebracht worden, kunnen betrouwbare supercelconvergentie-studies uitgevoerd worden voor eender welk defect/rooster-systeem.

Trefwoorden

Density Functional Theory (DFT), supercelmethode, defect-interacties, finite-size fout, absolute fout

Hydrogen trapping in steel: site determination via ab initio modeling

Craig Van Heirweghe

Supervisor(s): Prof. dr. Stefaan Cottenier, Prof. dr. ir. Kim Verbeken, ir. Kurt Lejaeghere

Abstract—**The supercell finite-size convergence was investigated for several properties of the Cu-Zr system, where Zr is a substitutional impurity in the fcc Cu host lattice. It was found that finite-size effects in the Cu-Zr system were small for local properties such as the LDOS and the local charge (distribution), while properties such as the Zr dissolution energy and the atomic force, who depend on the electronic structure of the entire supercell, were difficult to converge with supercell size. However, the latter properties also suffered from supercell-size-dependent errors w.r.t parameter settings, making it impossible to interpret their convergence behavior correctly, especially for the largest supercells. This was a consequence of performing all calculations with a constant relative accuracy. Hence, supercell convergence studies of supercell-size-dependent defect properties in the literature cannot be trusted due to insufficient settings, either w.r.t the supercell size, either w.r.t parameter settings such as the number of k-points. A procedure was developed in order to attain a constant, low absolute error on the Zr dissolution energy w.r.t the number of k-points for all supercell sizes, which clearly improved its supercell finite-size convergence behavior. This procedure can therefore be applied in supercell finite-size convergence investigations of defect properties in other systems, such as hydrogen-related defects in Fe, for absolute errors w.r.t parameters that induce significant absolute error for large supercells.**

Keywords—**Density functional theory (DFT), supercell method, spurious defect interactions, finite-size error, absolute error**

I. Introduction

HYDROGEN embrittlement of high-strength steels is considered as one of the main issues in the development of the hydrogen fuel technology. This phenomenon is still not completely understood however, due to the high complexity of the embrittling mechanism(s), the incapability of visualizing H-defect interactions in the (bcc) Fe lattice and a large scatter in experimentally measured binding energies between H and various defects. Ab initio DFT-calculations by means of the supercell method can provide the required information on the atomic scale about defect structures and binding energies. For common supercell sizes in the literature, however, the calculated defect properties suffer from unphysical interactions between the defect and its periodic images, due to the applied periodic boundary conditions in the supercell approach. Several correction schemes have been developed for defect calculations in semiconductors, especially for defect formation energies. Probert and Payne [1], for example, suggested to first converge the electronic structure of the unrelaxed supercell with supercell size. The supercell which yields the smallest error w.r.t the extrapolated, unrelaxed dissolution energy of the isolated defect, is then used to relax the structure. The energy obtained from the relaxation procedure can then be used to compare with experiments. The research group of Castleton et al. [2] performed additional finite-size scaling procedures to their supercell finite-size convergence data. The dilute limit value of both unrelaxed and relaxed defect formation energies is then obtained by means of a scaling equation, which relates the finite-size error to the supercell size. Similar supercell finite-size convergence investigations are however not known to be performed for metallic systems. A particularly interesting defect/lattice combination is the substitutional Zr-impurity in a fcc Cu host lattice: a recent study by Caestecker at the Center for Molecular Modeling has showed that the Zr dissolution energy is very hard to converge with supercell size [3]. The supercell finite-size convergence behavior of the unrelaxed Zr dissolution energy (conform the methodology suggested by Probert and Payne), and other properties in unrelaxed supercells that can be obtained computationally, were therefore investigate in more detail. Once an efficient procedure is found to remove these finite-size errors in the Cu-Zr system, it can be applied to all kinds of metallic defect/lattice-combinations in order to obtain defect properties that are well converged with supercell size, such as hydrogen-related defects in Fe.

C. Van Heirweghe is with the Materials Science and Engineering Department, Ghent University (UGent), Gent, Belgium. E-mail: Craig.VanHeirweghe@UGent.be

II. Methodology

All supercell calculations were performed with VASP (Vienna Ab Initio Simulation Package) [4], [5], a DFT program based on plane-wave basis functions, within the generalized gradient approximation of the PW91(Perdew-Wang 1991) form [6] for the exchange-correlation functional. The projector-augmented wave (PAW) method was used for the potentials, as introduced by Blöchl [7] and implemented by Kresse and Joubert [8]. The PREC-tag in the INCAR-file of VASP was set to "accurate" in order to obtain the highest possible accuracy on the calculations. To limit the calculation time for large supercells, the LREAL-tag in the same file was set to "Auto" .

Cubic Cu-Zr supercells were constructed by means of conventional fcc Cu unit cells with an equilibrium lattice parameter of 3.637 $\mathring{A}$ [3]. The size of the Cu-Zr supercells was varied from 4 atoms to 1728 atoms. Zr is introduced in a supercell by means of a Zr sublattice, which could have a sc, bcc or fcc symmetry. The Zr-concentration was hence varied by changing the supercell size and/or Zr sublattice symmetry. The calculation time for the largest supercells (216 atoms and larger) was reduced by considering the primitive supercell, which contains only one Zr-atom.

The supercell finite-size convergence was investigated for physical properties that are easily accessible with VASP, such as the Zr dissolution energy and local properties like the local density of states (LDOS), local charge difference (distribution) and atomic forces. The LDOS ware obtained with VASP by first performing a self-consistent and then a non-self-consistent calcula-

tion (ICHARG = 11 in INCAR), using the CHGCAR-file from the self-consistent run. The charge density difference distribution was visualized for various supercells by means of the visualization software VESTA [9], whereas charge differences were obtained by integrating the charge density difference in a sphere with a radius of half the nearest-neighbor distance around a particular nucleus. The atomic forces on all nuclei of a supercell can be found in the OUTCAR-file. Finally, the Zr-dissolution energy is calculated by means of the following equation:

$$E_{diss}^{\mathrm{Zr}}(N) = E(\mathrm{Cu}_{N-1}\mathrm{Zr}) - \frac{N-1}{N}E(\mathrm{Cu}_N) - E(\mathrm{Zr}) \quad (1)$$

where $E_{diss}^{\mathrm{Zr}}(N)$ is the Zr dissolution energy as calculated with N-atom supercells, $E(\mathrm{Cu}_{N-1}\mathrm{Zr})$ the total ground-state energy of the Cu-Zr supercell containing N atoms, $E(\mathrm{Cu}_N)$ the total ground-state energy of the N-atom pure fcc Cu lattice and $E(\mathrm{Zr})$ the total ground-state energy for one Zr atom in its hcp reference state at 0K. The latter term needs to be calculated only once and was found to be -8.318 eV/atom (54-atom supercell: E_{cut} = 400 eV, 6×6×6 k-mesh and EDIFF = 1E-6 eV). The total ground-state energy of pure Cu needs to be calculated for every supercell size N that is considered, because the error on the energy of the N-atom Cu-Zr supercell is of the same order as for its corresponding N-atom pure Cu supercell.

Before the finite-size convergence can be investigated for all these properties, the electronic structure of the supercells, represented by the total ground-state energy, needs to be converged with the basis-set size (via the cut-off energy E_{cut}, or ENCUT in the INCAR-file), the k-point density for the sampling of the first Brillouin zone of the supercells and the convergence criterion of the self-consistent procedure on the total ground-state energy (via EDIFF in INCAR). However, forces are an order of magnitude more sensitive to convergence issues than total ground-state energies, causing forces to converge slower with these parameters. The convergence of this property w.r.t parameter settings was therefore considered as well. The forces on the nuclei are represented by a single scalar parameter F_{rms}, the root-mean square force:

$$F_{rms} = \sqrt{\frac{\sum_{i=1}^{N} F_i^2}{N}} \quad (2)$$

The cut-off energy E_{cut} was set to 400 eV, which is 150 eV above the default cut-off energy for fcc Cu and about 250 eV above the default E_{cut} for Zr. This can be expected to guarantee a high enough accuracy on both the total ground-state energy and F_{rms}. The convergence tests w.r.t the number of k-points and EDIFF were performed until the error on the ground-state energy was below 0.001 eV/atom and the error on the force below 0.01 eV/Å. The convergence tests were conducted on two 4-atom Cu-Zr supercells ($\mathrm{Cu_3Zr}$ and $\mathrm{Zr_3Cu}$), where the atoms were slightly displaced to generate non-zero forces. A 21×21×21 k-mesh (21^3 k-points) and EDIFF = 1E-7 eV were found to suffice for both cells. These parameter settings were then used to determine the settings for all other supercells in order to achieve a constant relative accuracy on the total ground-state energy (i.e. error on the total ground-state energy per atom).

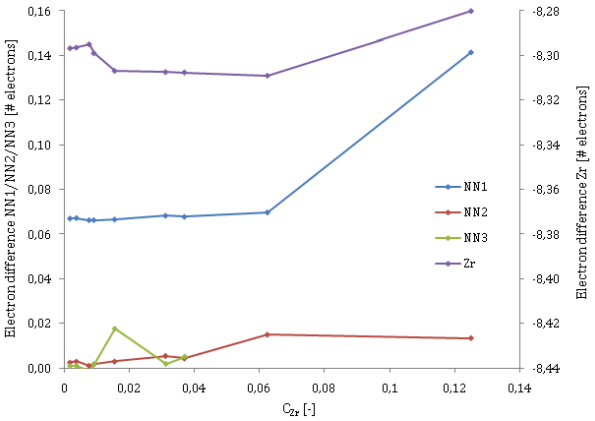

Fig. 1: Integrated charge difference as function of Zr-concentration around Zr and three nearest-neighbor Cu-nuclei of Zr. The integration sphere radius is half the nearest-neighbor distance.

III. Results and Discussion

A. *Supercell finite-size convergence of properties in the Cu-Zr system*

A.1 *Local charge difference and charge density difference distribution*

For all Cu-Zr supercells, charge (density) differences were obtained by subtracting the charge density distribution of the N-atom pure Cu cells from the charge density distribution of their corresponding N-atom Cu-Zr supercells. These differences were then visualized with VESTA by means of 2D-projections of the charge density difference distribution on a $\{100\}$-plane of the supercells. Local charge differences were obtained via the integration method which was explained in the previous section. The supercell finite-size convergence of the local charge difference was investigated for Zr and its three nearest-neighbor Cu-atoms. Fig. 1 shows that all charge differences converge very fast with supercell size (or Zr-concentration, which is equivalent): the second and third nearest neighbors converge more slowly than the first nearest neighbor since they are closer to the periodic images of Zr. The charge difference around Zr is expected to converge the slowest of all due to significant interference effects from its periodic images as a consequence of its highly symmetrical position in the supercell. The Cu-Zr supercell with a Zr-concentration of $\frac{1}{108}$ already reduces the error on the charge difference below 0.01 electrons, which is accurate enough for most applications (such as X-ray diffraction).

The 2D projections of the charge density difference distribution allowed us to visualize the evolution of the magnitude of the spurious defect interactions with supercell size. Such a projection is shown in Fig. 2 for the 1728-atom Cu-Zr supercell with a Zr-concentration of $\frac{1}{1728}$, with an iso-surface value of 0.0002 electrons (yellow lobes represent positive charge density differences, blue lobes represent negative differences). The difference in charge density is the combined effect of Friedel oscillations, which is a purely physical phenomenon (as a consequence of the introduction of a defect in a periodic lattice), and the unphysical interactions between Zr and its periodic im-

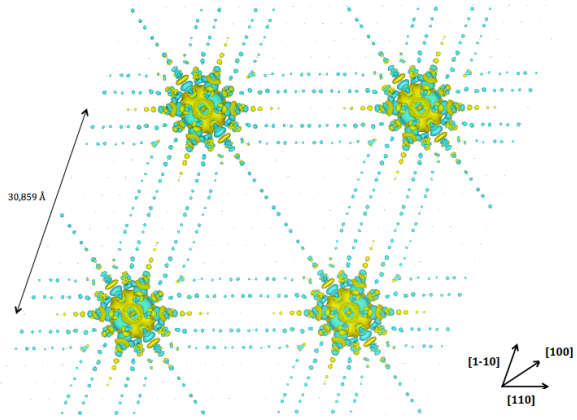

Fig. 2: 2D projection on a $\{100\}$-plane of the charge density difference distribution in the 1728-atom supercell ($c_{Zr} = \frac{1}{1728}$), for an iso-surface value of 0.0002 electrons.

ages. Oscillations in the charge density difference appear along the entire nearest-defect axes ($\langle 110 \rangle$ in the case of a fcc Zr sublattice). Since the iso-surface value is still an order of magnitude above the noise, finite-size effects can still not be considered to be insignificant. Finite-size effects for other substitutional atoms (Ag, Cd and Mg) in fcc Cu were found to be much smaller, indicating that finite-size effects are particularly persistent in the case of the Cu-Zr system. Since finite-size effects still appear in such an extremely large supercell (usual cells contain 10s or 100s of atoms), properties that depend on the electronic structure of the entire supercell, such as the Zr dissolution energy, cannot be guaranteed to yield values that are not influenced anymore by finite-size effects.

A.2 *Local density of states*

The local density of states were determined around Zr, its nearest-neighbor Cu-nucleus and the most bulk-like Cu-nucleus on an lattice site that is not highly symmetrical (and hence for which interference effects such as for Zr would appear). Supercells containing a few hundred atoms were found to suffice in order to obtain highly accurate LDOS around all three types of nuclei. The supercell finite-size convergence is shown in Fig. 3 for the nearest neighbor Cu-nuclei in particular. The LDOS around Zr is again found to converge the slowest with supercell size, most probably for the same reason as in the case of the local charge difference.

A.3 *Zr dissolution energy*

The Zr dissolution energy was calculated for all Cu-Zr supercells, with a Zr-concentration varying between $\frac{1}{4}$ and $\frac{1}{1728}$, with a constant relative accuracy of 0.001 eV/atom on the total ground-state energy for all these supercells. The calculated Zr dissolution energies are plotted as a function of Zr-concentration in Fig. 4a. Different convergence trends appear for different Zr sublattice symmetries, as consequence of geometrical effects (different Zr-Zr distances) and a different number of nearest-neighbor Zr-atoms for each sublattice symmetry. Probert and Payne also suggest that the sublattice symmetry for which the spurious electronic charge distribution (as a consequence of finite-size effects) is commensurate with the electron density of the host lattice, will minimize the finite-size errors and hence would lead to the highest supercell finite-size convergence rate. This would implicate in the particular case of the Cu-Zr system that the fcc sublattice symmetry should convergence the fastest towards the dilute limit, which does clearly not agree with our results.

The supercell finite-size convergence trends are shown in more detail for the lowest Zr-concentration in Fig. 4b. It is remarkable that, apart from the fact that different sublattice symmetries appear to converge toward different dilute limit Zr dissolution energies, deviations from the convergence trend of the fcc sublattice symmetry increase for the largest supercells. Finite-size errors are however expected to further decrease. A thorough analysis of eq. (1) reveals that absolute errors on the total ground-state energy w.r.t parameter settings, such as the number of k-points, increase with supercell size as a consequence of keeping the relative accuracy constant. Since the ground-state energy is converged up to 0.001 eV/atom w.r.t number of k-points, the absolute error on this energy can become in the order of 1 eV for the 1000-atom Cu-Zr supercell. The absolute error on the Zr dissolution energy is proportional with the absolute error on the total ground-state energy of the Cu-Zr and its corresponding pure Cu supercell. The observed supercell finite-size convergence trend therefore cannot be interpreted correctly, especially in the dilute limit of Zr-concentration. Hence, calculations with a constant, low absolute error w.r.t all parameter settings appear to be indispensable for a supercell-size-dependent property such as the Zr dissolution energy.

A.4 *Force*

Net forces were determined on the nearest-neighbor Cu-nuclei to Zr and the most bulk-like Cu-nucleus that is not affected by symmetrically induced interference effects. The net force on the latter type of Cu-nucleus converges relatively fast with supercell size, with remaining errors in the order of 0.001 eV/$\mathring{A}$ for the 216-atom Cu-Zr supercell w.r.t the net force on a

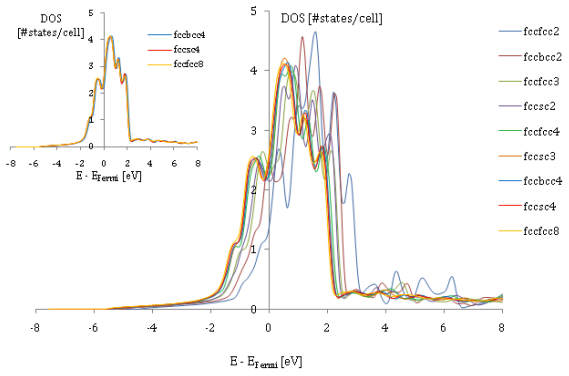

Fig. 3: Local density of states around a nearest-neighbor Cu-atom to Zr for all supercells considered. Inset: The same LDOS, but now exclusively shown for the lowest Zr-concentrations ($c_{Zr} \leq \frac{1}{128}$)

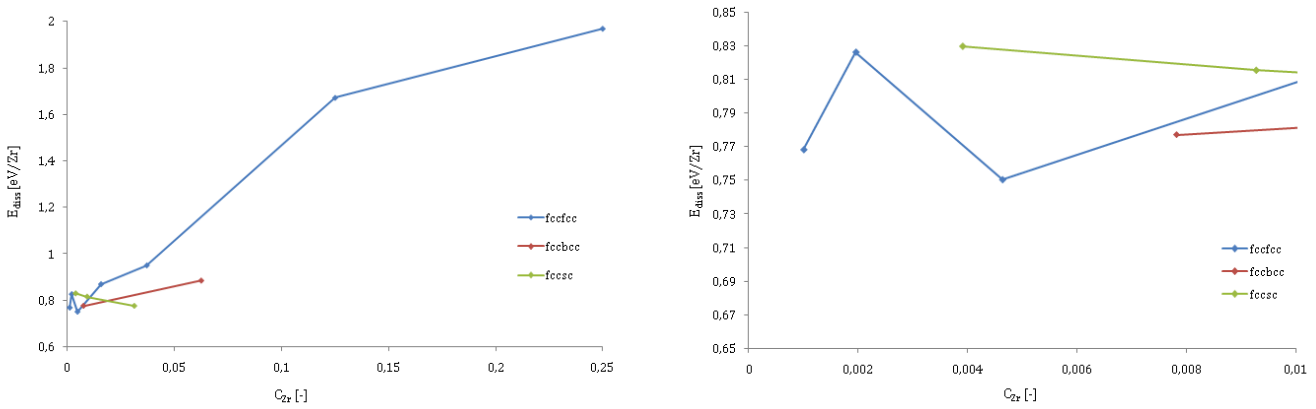

(a) (b)

Fig. 4: (a) Supercell finite-size convergence of the Zr dissolution energy as a function of Zr-concentration (b) Detailed picture of the finite-size convergence towards the dilute limit

true bulk Cu-nucleus, which would be zero. The force convergence rate was also found to be highly dependent on the Zr sublattice symmetry: for similar Zr-concentrations, the net forces were the closest to zero in the case of the sc sublattice symmetry. This was found to be related to the fact that this symmetry maximizes the Zr-Zr distance for supercells with similar Zr-concentrations.

The net force on the nearest-neighbor Cu-nuclei converge more difficult with supercell size, as shown in Fig. 5. Especially the large oscillations in the NN1-force for the smallest Zr-concentration ($c_{\mathrm{Zr}} \leq \frac{1}{216}$), in the order of 0.01 eV/$\mathring{A}$ draw the attention. Such oscillations cannot be expected to be the single result of finite-size effects, since defect interactions should be rather small for such low Zr-concentrations. The atomic force on a particular nucleus is however defined as the derivative of the total ground-state energy with the position of this nucleus. Since large absolute errors w.r.t parameter settings were found in the total ground-state energy in this range of the Zr-concentration, similar effects can be expected to appear in the case of the force as well. This observation implies that all properties that to some extent depend on the electronic structure of the entire supercell, can only be converged correctly with supercell size if all calculations are performed with a constant, low absolute error.

B. K-point requirements for 'constant absolute error' calculations

In order to interpret supercell finite-size convergence trends of supercell-size-dependent properties such as the Zr dissolution energy and atomic force correctly, all calculations need to be conducted with a constant absolute error within the desired degree of accuracy on these properties. Since the total ground-state energy of the Cu-Zr supercells were converged up to a relative accuracy of 0.001 eV/atom w.r.t the number of k-points, large absolute errors will appear for supercells containing 100s or 1000s of atoms, in the order of 0.1-1 eV, due to an insufficient number of k-points for these supercells. The required number of k-points to attain a constant absolute error can be obtained via k-point convergence tests. Such procedures become unfeasible for supercells containing 100s of atoms or more, since calculations need to be performed for various k-meshes. Only one such calculation can take hours or even a few days, however. A procedure was therefore developed in order to estimate the k-point requirements for the largest supercells.

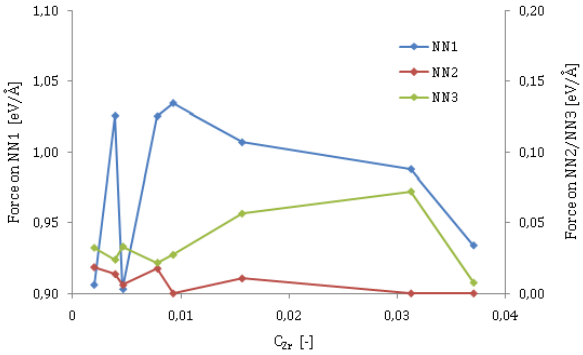

Fig. 5: Forces on the first- (NN1), second- (NN2) and third- (NN3) nearest-neighbor Cu-atoms to Zr for all Zr sublattice symmetries

K-point convergence tests were conducted on the smallest Cu-Zr supercells. From these tests, the relative accuracy $|\Delta E_{atom}|$ (which is N times smaller than the absolute error on the total ground-state energy) was plotted as a function of number of k-points in the one-atom first Brillouin zone k_1 (which is N times the number of k-points in the first Brillouin zone of the N-atom supercell, k_N). An enveloping exponential function of the form $a\exp(-bk_1)$ was determined for these data (with a and b parameters). The choice of this function is a consequence of the observation that the error on the total ground-state energy per atom rapidly decreases with increasing number of k-points. The exponential function envelops the data in such a way that it lies as close as possible, but still above all data points: the error on the total ground-state energy per atom is hence overestimated for all numbers of k-points, which means that an upper limit for the k-point requirements will be obtained for all supercell sizes.

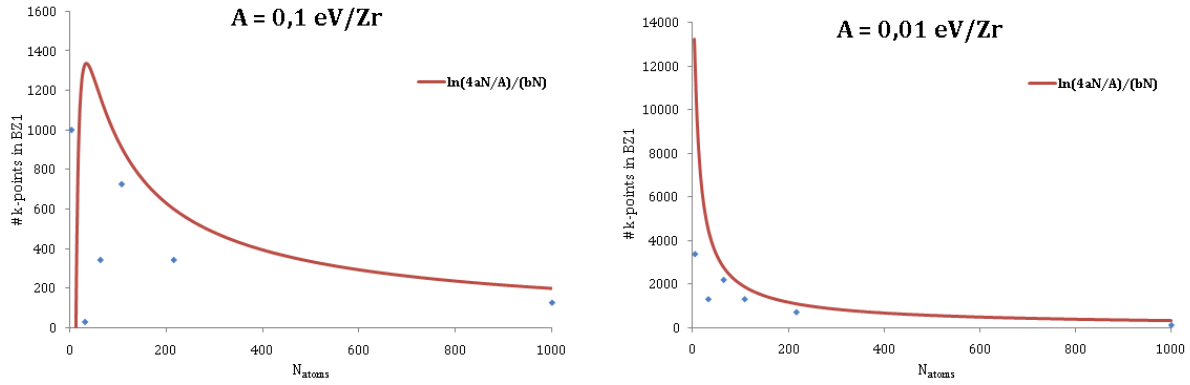

(a) (b)

Fig. 6: The predicted upper-limit k-point requirements as a function of supercell size for (a) $A = 0.1$ eV/Zr and (b) $A = 0.01$ eV/Zr.

It can be shown that if the error on the total ground-state energy per atom $|\Delta E_{atom}|$ is overestimated by the exponential function $a\exp(-bk_1)$, the expression for the upper-limit k-point requirements as a function of system size becomes:

$$k_N = \frac{1}{bN}\ln(\frac{4aN}{A}) \tag{3}$$

with A the desired accuracy on the Zr dissolution energy ([eV/Zr]). Curves of this equation are shown in Figs. 6a and 6b for $A = 0.1$ ev/Zr and $A = 0.01$ eV/Zr respectively. The data points are the k-point requirements for the corresponding supercell sizes as determined by means of the k-point convergence tests (the 1000-atom data point for $A = 0.01$ eV/Zr represents a lower limit for the k-point requirements). The expected trend for the k-point requirements with supercell size for very small supercells is not very well reproduced in the case of $A = 0.1$ eV/Zr: when decreasing the supercell size, the function reaches a maximum, subsequently decreases very fast and even becomes negative for the smallest supercells (12 atoms and less). This is the result of the parameter a (0.002 eV) being much smaller than the accuracy A (0.1 eV/Zr): for small N, the fraction in the $\ln$-factor of eq. (3) then becomes < 1 and the whole term on the right-hand side of this equation becomes negative. This indicates that an exponential function is not a physically correct description of the decreasing relative accuracy with increasing k-point sampling density. The k-point requirements are fortunately (slightly) overestimated in the large-supercell method for both accuracies.

The predicted upper-limit k-point requirements for $A = 0.01$ eV/Zr were used for the 'constant absolute error' calculations in the supercell finite-size investigation of the Zr dissolution energy, except for the 512-atom and 1000-atom, for which lower limit k-point requirements were used. All k-meshes were larger than those used for the 'constant relative accuracy' calculations. The convergence trends as obtained by the 'constant absolute error' calculations are shown in Fig. 7. The convergence trends have clearly improved, even for the smaller supercells, since all trends now appear to converge toward the same dilute limit value of the Zr dissolution energy. This result suggests that, for properties that depend on the electronic structure of the entire supercell, constant absolute error calculations are indispensable in their supercell finite-size convergence investigation in order to interpret the observed convergence trend correctly. The suggested procedure could therefore be used do determine the upper-limit k-point requirements in order to achieve this constant absolute error. The same procedure can however also be used for other parameters, if absolute errors for these parameters become significant for the largest supercells.

The large deviations for the largest supercells in the case of the fcc sublattice symmetry are a result of the use of the lower limit k-point requirements for these supercells. Due to the very high upper-limit k-point density for the largest supercells in the case of the high accuracy $A = 0.01$ eV/Zr, calculations became unfeasible for these cells as a consequence of limited computational resources and calculation time. These supercells should therefore be excluded from the investigation. Hence, when performing a supercell finite-size convergence investigation of a supercell-size-dependent property, the largest supercell that can be included will depend on the desired degree of accuracy on this property.

C. *Supercell finite-size convergence of the H dissolution energy in bcc Fe*

A short additional investigation was performed on unrelaxed dissolution energy of the tetrahedral interstitial H-atom in ferromagnetic bcc Fe. Finite-size errors on this property were found in the literature to be minimal, with remaining errors in the order of 0.01 eV/H for supercells containing a few hundred atoms [10], despite the fact that all calculations were performed with a constant relative accuracy. Similar calculations with supercells up to 251 atoms ($Fe_{250}H$) and a slightly higher, but still constant relative accuracy of 0.001 eV/H compared to the calculations from ref. [10], shown the same, fast convergence behavior of the unrelaxed H dissolution energy. Absolute errors on the total ground-state energy w.r.t the parameter settings hence appear not to dominate the convergence behavior of the H dissolution energy. Nevertheless, since such errors can be in the order of 0.1 eV for the largest cells, a completely correct interpretation of the

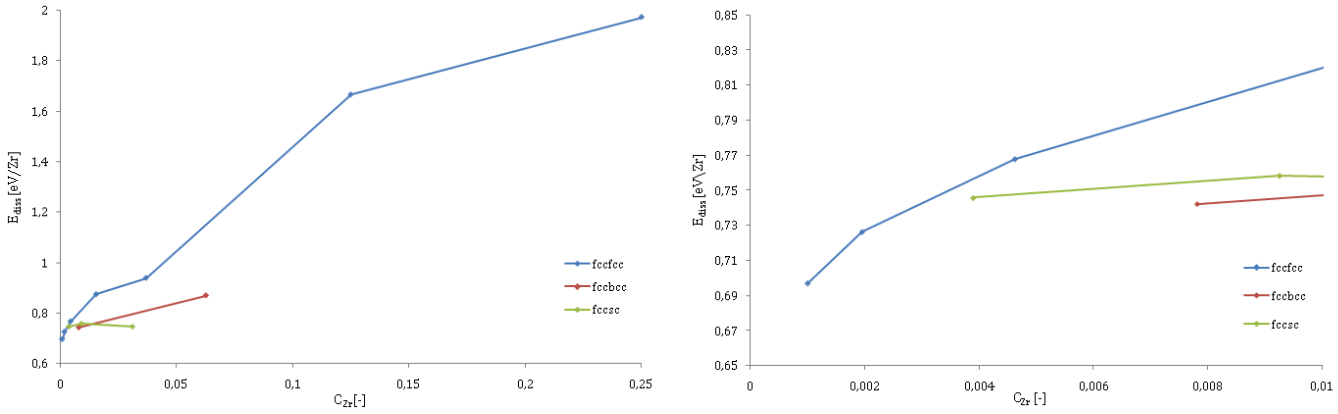

Fig. 7: Supercell finite-size convergence of the Zr dissolution energy as a function of Zr-concentration, using 'constant absolute error' k-meshes ($A = 0.01$ eV/Zr).

convergence trend still requires individual k-point convergence tests for each considered supercell. To achieve a constant degree of accuracy for each supercell, the suggested procedure from the previous section could be useful to estimate the upper-limit requirements of all parameters that induce significant absolute errors for large supercells.

IV. Conclusions

Calculations of defect properties via the DFT-based supercell approach suffer from errors due to interactions between the defect and its periodic images for common supercell sizes. The supercell finite-size convergence was therefore investigated for several properties in the particular case of a substitutional Zr-impurity in a fcc Cu host lattice, by means of the plane-wave-based DFT-program VASP. Properties that depend on the local electronic structure of the supercell, such as the LDOS and the local charge difference, were found to converge rapidly with supercell size. It has also been showed that calculations for large supercells do not necessarily improve the supercell finite-size convergence behavior of system-size dependent defect properties, such as the defect formation energy and the force. All parameters that induce errors who scale with system size, such as the number of k-points, will cause problems for such supercells if calculations are performed with a constant relative accuracy. A procedure was however developed that enables us to estimate the necessary parameter requirements for each supercell size and, taking computational limitations into consideration, which supercell sizes can be included in the supercell finite-size convergence investigation. Hence, if all parameter requirements with respect to the defect property of interest are taken into account, reliable supercell finite-size convergence studies can be performed for any defect/lattice-system.

References

[1] M. I. J. Probert and M. C. Payne, "Improving the convergence of defect calculations in supercells: An ab initio study of the neutral silicon vacancy", *Physical Review B*, vol. 67, pp. 8564-8567, 2003

[2] C. W. M. Castleton, A. Höglund and S. Mirbt, "Density functional theory calculations of defect energies using supercells", *Modelling and Simulation in Materials Science and Engineering*, vol. 17, pp. 084003, 2009

[3] F. Caestecker, "Nauwkeurigheidsstudie voor het ab-initio berekenen van de mengingsenthalpie bij bulk metallic glasses", Universiteit Gent, 2012

[4] G. Kresse and J. Furthmüller, "Efficiency of ab-initio total energy calculations for metals and semiconductors using a plane-wave basis set", *Computational Materials Science*, vol. 6, pp. 15, 1996

[5] G. Kresse and J. Furthmüller, "Efficient iterative schemes for ab initio total-energy calculations using a plane-wave basis set", *Physical Review B*, vol. 54, no. 16, pp. 11169, 1996

[6] J. P. Perdew, J. A. Chevary, S. H. Vosko, K. A. Jackson, M. R. Pederson, D. J. Singh and C. Fiolhais, "Atoms, molecules, solids, and surfaces - Applications of the Generalized Gradient Approximation for exchange and correlation", *Physical Review B*, vol. 46, no. 11, pp. 6671-6687, 1992

[7] P. E. Blochl, "Projector augmented-wave methods", *Physical Review B*, vol. 50, no. 24, pp. 17953, 1994

[8] G. Kresse and D. Joubert, "From ultrasoft pseudopotentials to the projector augmented-wave method", *Physical Review B*, vol. 59, no. 3, pp. 1758, 1999

[9] K. Momma and F. Izumi, "VESTA 3 for three-dimensional visualization of crystal, volumetric and morphology data", *Journal of Applied Crystallography*, vol. 44, no. 6, pp. 1272-1276, 2011

[10] D. E. Jiang and Emily A. Carter, "Diffusion of interstitial hydrogen into and through bcc Fe from first principles", *Physical Review B*, vol. 70, no. 6, pp. 064102, 2004

Hydrogen trapping in steel: site determination via ab initio modeling

Craig Van Heirweghe

Begeleiders: Prof. dr. Stefaan Cottenier, Prof. dr. ir. Kim Verbeken, ir. Kurt Lejaeghere

Abstract— **De supercelconvergentie werd onderzocht voor verschillende eigenschappen van het Cu-Zr systeem, met Zr een substitutionele onzuiverheid in een fcc Cu gastrooster. Eigenschappen die afhankelijk zijn van de lokale elektronenstructuur in de supercel, zoals het lokale ladingsverschil, de lokale ladingsverschil-distributie en de lokale toestandsdichtheid (LDOS) bleken weinig invloed te ondervinden van interacties tussen Zr en zijn periodieke kopieën. Eigenschappen zoals de Zr-oplosenergie en de atomaire krachten, die afhangen van de elektronenstructuur in de gehele supercel, bleken dan weer moeilijk te convergeren met toenemende supercelgrootte. Deze eigenschappen bleken echter ook benvloed te worden door aanzienlijke absolute fouten t.g.v de parameter-instellingen, vooral bij de grootste supercellen, waardoor het waargenomen supercelconvergentiegedrag niet correct kon geïnterpreteerd worden. Deze absolute fouten bleken een gevolg te zijn van het constant houden van de relatieve nauwkeurigheid voor alle supercelgroottes. Supercelconvergentie-studies in de literatuur van eigenschappen die afhankelijk zijn van de elektronenstructuur in de gehele superbel zijn bijgevolg niet betrouwbaar, ofwel omdat de beschouwde supercellen te klein zijn, ofwel omdat parameterinstellingen, zoals het aantal k-punten, onvoldoende zijn voor de vereist absolute nauwkeurigheid. Een procedure werd ontwikkeld om het probleem van de variërende absolute fout met supercelgrootte te verhelpen. Deze procedure verbeterde het supercelconvergentie-gedrag van de Zr-oplosenergie aanzienlijk, waardoor ze uiterst geschikt is om toegepast te worden in supercelconvergentie-studies van defecteigenschappen in andere systemen, zoals voor waterstof-gerelateerde defecten in Fe.**

Keywords— **Density Functional Theory (DFT), supercelmethode, defect-interacties, finite-size fout, absolute fout**

I. Inleiding

WATERSTOFVERBROSSING in hoogsterkte staalsoorten wordt aanzien als één van de voornaamste problemen in de ontwikkeling van de waterstof brandstoftechnologie. Dit fenomeen is nog steeds niet volledig begrepen a.g.v de complexiteit van de verbrossingsmechanismen, de moeilijkheid om H-defect interacties te visualiseren en de grote spreiding in experimenteel bepaalde H-defect bindingsenergieën. Ab initio DFT-berekeningen via de supercelmethode vormen een mogelijk alternatief omdat ze de noodzakelijke informatie op atomaire schaal kunnen leveren. Niet-fysische interacties tussen het defect en zijn periodieke kopieën, a.g.v de door de supercelmethode opgelegde periodieke renvoorwaarden, kunnen echter fouten induceren in berekende defecteigenschappen. Verschillende correctieschema's werden reeds ontwikkeld voor defectberekeningen in halfgeleiders en dan voornamelijk voor de defect-vormingsenergie. Probert en Payne [1] stelden bijvoorbeeld voor om de elektronenstructuur eerst te convergeren met supercelgrootte voor de niet-gerelaxeerde supercellen. The supercel die de kleinste fout oplevert t.o.v de geëxtrapoleerde defect-vormingsenergie voor het geïsoleerde defect wordt dan gebruikt voor de relaxatieprocedure. De vormingsenergie die via deze procedure verkregen wordt kan dan vergeleken worden met experimentele waarden. Castleton et al. [2] voegden daar een zogenaamde "finite-size scaling" aan toe: de vormingsenergie voor het geïsoleerde defect wordt verkregen via een schalingsvergelijking, die de finite-size fout relateert aan de supercelgrootte. Gelijkaardige supercelconvergentie-studies werden echter tot nader order nog niet uitgevoerd voor metallische systemen. De substitutionele Zr-onzuiverheid in een fcc Cu gastrooster bleek een interessant geval van een dergelijk systeem te zijn: Caestecker vond in een recente studie aan het Center for Molecular Modeling dat de Zr-oplosenergie in dit Cu gastrooster moeilijk convergeerde met supercelgrootte [3]. De supercel-convergentie van de niet-gerelaxeerde Zr-oplosenergie (conform de methodologie van Probert en Payne) werd daarom, samen met enkele andere toegankelijke eigenschappen van niet-gerelaxeerde supercellen, meer in detail onderzocht. Eenmaal een efficiënte procedure ontwikkeld gevonden is om finite-size fouten te elimineren in het Cu-Zr systeem, kan diezelfde procedure toegepast worden voor supercelconvergentie-studies van allerlei andere metallische defect/rooster-combinaties, zoals voor H-gerelateerde defecten in Fe.

C. Van Heirweghe is with the Materials Science en Engineering Department, Ghent University (UGent), Gent, Belgium. E-mail: Craig.VanHeirweghe@UGent.be

II. Methodologie

Alle supercelberekeningen werden uitgevoerd met VASP (Vienna Ab Initio Simulation Package) [4], [5], een DFT-programma dat gebaseerd is op vlakke golven as basisfuncties, in combinatie met de GGA-PW91 (Perdew-Wang 1991) uitwisselings-correlatiefunctionaal [6]. Voor de potentialen werd geopteerd voor de PAW-methode, geïntroduceerd door Blochl [7] en geïmplementeerd door Kresse en Joubert [8]. De PREC-tag in de INCAR-file van VASP werd op "accurate" gezet om de hoogst mogelijke nauwkeurigheid te bereiken. De LREAL-tag in diezelfde VASP-file werd op "Auto" gezet om de rekentijd voor de grootste supercellen te beperken.

Kubische Cu-Zr supercellen werden geconstrueerd d.m.v conventionele fcc Cu eenheidscellen, met een evenwichtsroosterparameter van 3.637 $\AA$ [3]. De supercelgrootte werd gevarieerd van 4 tot 1728 atomen. Zr werd geïntroduceerd d.m.v een Zr-subrooster, die een sc, bcc of fcc symmetrie kan hebben. De Zr-concentratie werd aldus gevarieerd door de supercelgrootte en/of de Zr-subroostersymmetrie te wijzigen. De rekentijd voor de grootste supercellen (216 atomen en meer) werd beperkt door de primitieve supercel te beschouwen, welke slechts 1 Zr-atoom bevat.

De supercelconvergentie werd onderzocht voor fysische grootheden die gemakkelijk toegankelijk zijn via VASP, zoals de Zr-oplosenergie en lokale eigenschappen zoals de LDOS, de lokale ladingsverschillen en de atomaire krachten. De LDOS

werden verkregen met VASP door eerst een zelf-consistente berekening uit te voeren en daarna een niet-zelf-consistente berekening uit te voeren, gebruikmakende van de CHGCAR-file van de zelf-consistent berekening. De ladingsdichtheidsverschillen werden gevisualiseerd m.b.v VESTA [9], terwijl ladingsverschillen berekend werden door de ladinsdichtheidsverschillen te integreren rond in een bol met de halve dichtste-nabuur afstand als straal. De atomaire krachten kunnen teruggevonden worden in de OUTCAR-file van een VASP-berekening. The Zr-oplosenergie wordt ten slotte berekend m.b.v de volgende formule:

$$E_{diss}^{\mathrm{Zr}}(N) = E(\mathrm{Cu}_{N-1}\mathrm{Zr}) - \frac{N-1}{N}E(\mathrm{Cu}_N) - E(\mathrm{Zr}) \quad (1)$$

waarbij $E_{diss}^{\mathrm{Zr}}(N)$ de Zr-oplosenergie is voor N-atomige supercellen, $E(\mathrm{Cu}_{N-1}\mathrm{Zr})$ de energie van de grondtoestand van de N-atomige Cu-Zr supercel, $E(\mathrm{Cu}_N)$ de energie van de N-atomige Cu-supercel en $E(\mathrm{Zr})$ de energie van een Zr-atoom in zijn hcp referentietoestand bij 0K.De laatste term dient slechts één keer berekend te worden. $E(\mathrm{Zr}) = -8.318$ eV/atoom werd gevonden via een berekening met een 54-atomige supercel (E_{cut} = 400 eV, 6×6×6 k-mesh en EDIFF = 1E-6 eV). The energie voor puur Cu dient berekend te worden voor elke supercelgrootte N, aangezien de fout op deze energie in dezelfde grootte-orde is als deze voor de corresponderende N-atomige Cu-Zr supercel.

Vooraleer de supercelconvergentie van al deze eigenschappen onderzocht kan worden, moet de elektronenstructuur a.d.h.v de grondtoestandsenergie van de niet-gerelaxeerde supercellen eerst geconvergeerd worden m.b.t de basissetgrootte (via de cut-off energie E_{cut}, of ENCUT in INCAR), de k-puntdichtheid voor het samplen van de eerste Brillouin zone en het convergentiecriterium voor de zelf-consistente berekening (EDIFF in INCAR). Krachten zijn nog een grootteorde gevoeliger voor convergentie-gerelateerde fenomenen, waardoor ze trager convergeren m.b.t deze parameters. De krachten werden daarom ook geconvergeerd m.b.t al deze parameters, m.b.v een enkele scalaire grootheid, meer bepaald de root-mean-square kracht:

$$F_{rms} = \sqrt{\frac{\sum_{i=1}^{N} F_i^2}{N}} \quad (2)$$

Een cut-off energy van 400 eV werd gekozen voor alle supercelberekeningen. Dit is 150 eV groter dan de default-waarde voor fcc Cu en 250 eV groter dan de default-waarde voor Zr. De nauwkeurigheid van de grondtoestandsenergie en de F_{rms} kan met voldoende zekerheid verondersteld worden hoog genoeg te zijn m.b.t E_{cut}. De k-punt en EDIFF-convergentietesten werden uitgevoerd tot een nauwkeurigheid op de grondtoestandsenergie van 0.001 eV/atoom en een nauwkeurigheid van 0.01 eV/Åop F_{rms}. Deze testen werden uitgevoerd op twee 4-atomige supercellen ($\mathrm{Cu_3Zr}$ en $\mathrm{Zr_3Cu}$), waarbij de atomen lichtjes verplaatst werden om krachten verschillend van nul te genereren. Een 21×21×21 k-mesh (21^3 k-punten) en EDIFF = 1E-7 eV bleken ruim te voldoen aan de nauwkeurigheidsvereisten. Deze parameterinstellingen werden vervolgens gebruikt om de instellingen te bepalen voor alle andere Cu-Zr supercellen op een zodanige manier dat de relatieve nauwkeurigheid 0.001 eV/atoom is voor elke supercel.

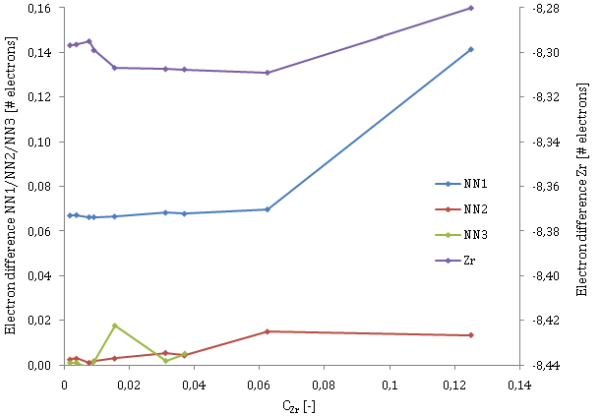

Fig. 1: Het geïntegreerde ladingsverschil i.f.v de Zr-concentratie rond Zr en zijn drie dichtste-nabuur Cu-atomen. De straal van de integratiebol is de helft van de dichtste-nabuur afstand.

III. Resultaten en discussie

A. *Supercelconvergentie van eigenschappen in Cu-Zr*

A.1 *Lokale ladingsverschillen en ladingsdichtheidsverschil-distributie*

Verschillen in lading(dichtheid) werden bekomen door de ladingsdichtheidsdistributie van de N-atomige Cu-supercellen af te trekken van de ladingsdichtheidsdistributie van de corresponderende N-atomige Cu-Zr supercellen. Deze verschillen werden dan voor alle supercellen m.b.v VESTA gevisualiseerd als 2D projecties van de ladingsdichtheidsverschil-distributie op een $\{100\}$-vlak. Lokale ladingsverschillen worden verkregen via de eerder uitgelegde integratiemethode. De supercelconvergentie van de lokale ladingsverschillen werd onderzocht voor Zr en zijn drie dichtste-nabuur Cu-atomen. Fig. 1 toont dat alle ladingsverschillen snel convergeren met supercelgrootte: de tweede en derde dichtste naburen convergeren trager dan het dichtste-nabuur Cu-atoom omdat ze zich dichter bij de periodieke beelden van Zr bevinden. Door de hoogsymmetrische positie van Zr in het rooster, dat significante interferentie-effecten, afkomstig van de periodieke Zr-kopiëen induceert, convergeert het ladingsverschil rond Zr het traagst. De supercel met een Zr-concentratie van $\frac{1}{108}$ reduceert de fout op het ladingsverschil reeds beneden 0.01 elektronen, wat nauwkeurig genoeg voor de meeste toepassingen (zoals X-stralen diffractie).

De 2D projecties van de ladingsdichtheidsverschil-distributie lieten ons toe om de evolutie van de grootte van de defect-interacties met supercelgrootte nader te onderzoeken. Een dergelijke projectie is te zien in Fig. 2 voor de 1728-atomige Cu-Zr supercel ($c_{\mathrm{Zr}} = \frac{1}{1728}$, met een iso-oppervlak waarde van 0.0002 elektronen (de gele oppervlakken wijzen op positieve ladingsdichtheidsverschillen, de blauwe op negatieve). De geobserveerde ladingsdichtheidsverschillen zijn een gevolg van zowel Friedel oscillaties, een natuurlijk fenomeen a.g.v het inbrengen van een puntdefect in een periodiek rooster, als niet-fysische interacties tussen Zr en zijn periodieke beelden. De oscillaties in ladingsdichtheidsverschil lopen over de gehele dichtste-defect assen ($\langle 110 \rangle$ voor een fcc Zr-

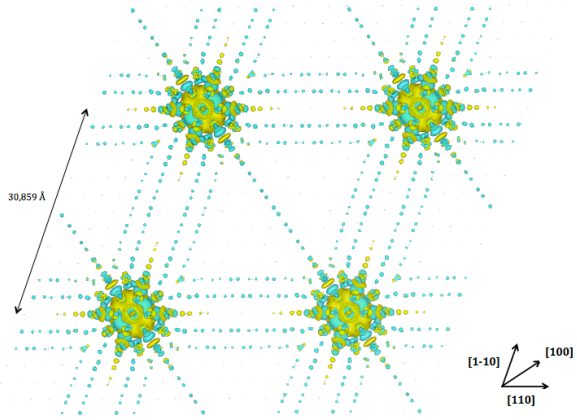

Fig. 2: 2D projectie van de ladingsdichtheidsverschil-distributie op een $\{100\}$-vlak in de 1728-atomige supercel ($c_{Zr} = \frac{1}{1728}$), voor een iso-oppervlak waarde van 0.0002 elektronen.

subroostersymmetrie. Omdat de iso-oppervlak waarde nog een orde groter is dan de ruis, blijken finite-size effecten nog steeds niet helemaal verdwenen te zijn. Voor andere substitutionele elementen (Ag, Cd en Mg) in fcc Cu werden echter veel minder sterke defect-interacties waargenomen, wat erop wijst dat de grootteorde van finite-size effecten erg systeemafhankelijk is. Omdat defect-interacties zelfs nog aanwezig blijken te zijn in een zo'n uitzonderlijk grote Cu-Zr supercel (supercelberekeningen in de literatuur worden uitgevoerd met tientallen of enkele honderden atomen), kunnen finite-size effecten nog steeds verwachten in berekende grootheden die afhangen van de elektronenstructuur in de gehele supercel, zoals de Zr-oplosenergie.

A.2 *Lokale toestandsdichtheid (LDOS)*

De LDOS werden bepaald rond Zr, zijn dichtste-nabuur Cu-atoom en het meest bulkachtige Cu-atoom dat niet zich op een hoogsymmetrische roosterpositie bevindt (en waarvoor dus interferentie-effecten minimaal zijn). Cu-Zr supercellen die slechts een honderdtal atomen bevatten werden reeds voldoende bevonden om voldoende nauwkeurige LDOS te verkrijgen voor all beschouwde types atomen. De supercelconvergentie is afgebeeld in Fig. 3 voor de LDOS van het dichtste-nabuur Cu-atoom van Zr. Ook hier convergeert Zr het traagst met supercelgrootte, vermoedelijk om dezelfde redenen als aangehaald bij de discussie rond de lokale ladingsverschillen.

A.3 *Zr-oplosenergie*

De Zr-oplosenergie werd berekend met een constante relatieve nauwkeurigheid van 0.001 eV/atoom op de grondtoestandsenergie voor alle Cu-Zr supercellen, met een Zr-concentratie tussen $\frac{1}{4}$ en $\frac{1}{1728}$. Deze oplosenergieën worden als functie van de Zr-concentratie weergegeven in Fig. 4a. Er verschijnen verschillende convergentietrends voor de verschillende Zr-subroostersymmetrieën, a.g.v een verschillende Zr-Zr afstand en aantal dichtste-nabuur Zr-atomen voor supercellen van gelijkaardige grootte, maar met verschillende subroostersymmetrie. Probert en Payne opperen eveneens dat die subroostersymmetrie waarvoor de ladingsdistributie a.g.v de defect-interacties commensuraat is met de ladingsdistributie van het gastrooster, de finite-size fout minimaliseert en dus tot een versnelde supercelconvergentie leidt. Dit zou betekenen in het geval van Cu-Zr dat de Zr-oplosenergie voor de fcc subroostersymmetrie het snelst zou convergeren naar de waarde voor oneindige verdunning, wat echter duidelijk niet het geval is.

De supercelconvergentie-trends worden in meer detail getoond in Fig. 4b. Naast het feit dat de verschillende subroostersymmetrieën lijken te convergeren naar verschillen Zr-oplosenergieën bij oneindige verdunning, valt het op dat de afwijkingen van de convergentietrend toenemen voor de grootste supercellen met fcc subroostersymmetrie. Finite-size fouten zouden echter moeten verminderen met toenemende supercelgrootte. Een grondige analyse van vgl. (1) heeft aangetoond dat de absolute fout op de grondtoestandsenergie m.b.t de parameterinstellingen, zoals het aantal k-punten, toeneemt met supercelgrootte door het constant houden van de relatieve nauwkeurigheid in alle berekeningen. Omdat deze energie voor elke supercel geconvergeerd is tot op 0.001 eV/atoom m.b.t het aantal k-punten, kan de absolute fout op deze energie reeds 1 eV bedragen voor een 1000-atomige supercel. De absolute fout op de Zr-oplosenergie is evenredig met de absolute fout op de grondtoestandsenergieën van de Cu-Zr en corresponderende Cu supercellen. Bijgevolg kunnen de supercelconvergentie-trends niet correct geïnterpreteert, vooral voor de grootste supercellen. Zr-oplosenergie-berekeningen met constante, lage absolute fout m.b.t alle parameterinstellingen die een grote absolute fout kunnen induceren voor de grootste supercellen lijkt daarom noodzakelijk te zijn.

A.4 *Kracht*

Netto atomaire krachten werden bepaald op de dichtste-nabuur Cu-atomen van Zr en het meest bulkachtige Cu-atoom dat weinig benvloed wordt door symmetrie-geïnduceerde interferentie-effecten. De kracht op het bulkachtige Cu-atoom convergeert snel met supercelgrootte, met een fout in de grootteorde van 0.001 eV/$\mathring{A}$ voor de 216-atomige supercel, t.o.v de kracht op een echt bulk Cu-atoom (welke nul is). De supercelconvergentie-snelheid bleek eveneens afhankelijk te

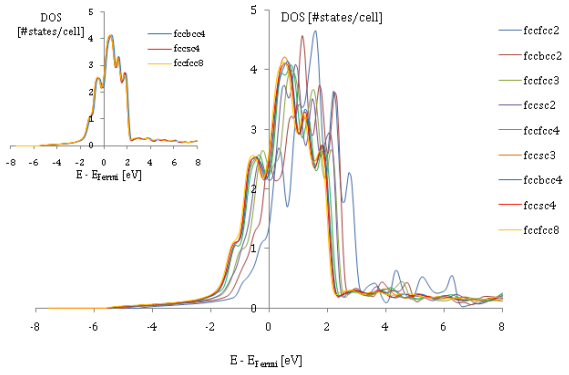

Fig. 3: LDOS rond een dichtste-nabuur Cu-atoom van Zr voor alle Cu-Zr supercellen. Inzet: Dezelfde figuur, maar nu exclusief voor de laagste Zr-concentraties ($c_{Zr} \leq \frac{1}{128}$).

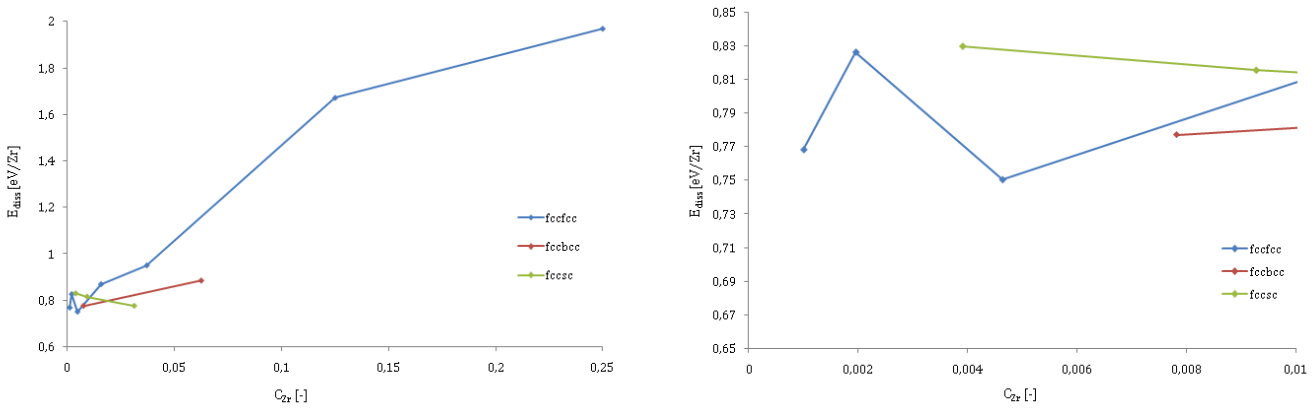

(a) (b)

Fig. 4: (a) Supercelconvergentie van de Zr-oplosenergie i.f.v de Zr-concentratie; (b) Dezelfde figuur, maar in meer detail voor de laagste Zr-concentraties.

zijn van de Zr-subroostersymmetrie: voor gelijkaardige Zr-concentraties bleken de krachten op het meest bulkachtige Cu-atoom in de cellen met sc subroostersymmetrie zich het dichtst bij nul te bevinden dat voor alle andere subroostersymmetrieën. Dit bleek gerelateerd te zijn aan het feit dat voor gelijkaardige Zr-concentraties deze subroostersymmetrie de Zr-Zr afstand maximaliseert.

De netto-kracht op het dichtste-nabuur Cu-atoom convergeert moeilijker met supercelgrootte, zoals te zien is in Fig. 5. Vooral de grote oscillaties in de NN1-kracht bij de grootste supercellen (216 atomen en meer), in de orde van 0.01 eV/$\AA$, vallen op. Zulke oscillaties kunnen niet enkel gerelateerd zijn aan finite-size effecten, aangezien bij dergelijke Zr-concentraties deze effecten reeds vrij klein zouden moeten zijn. De kracht op een bepaald atoom is echter gedefinieerd als de afgeleide van de grondtoestandsenergie tot de positie van het Cu-atoom. Aangezien eerder al grote fouten m.b.t parameterinstellingen werden ontdekt in de grondtoestandsenergie van de grootste Cu-Zr suppercellen, kunnen gelijkaardige effecten optreden voor de kracht. Deze vaststelling impliceert dat alle eigenschappen die in zekere mate afhangen van de elektronenstructuur in de gehele supercel, enkel op een correct manier kunnen geconvergeerd worden met supercelgrootte indien alle berekeningen met een constante, lage absolute fout m.b.t de parameterinstellingen worden uitgevoerd.

B. K-puntvereisten voor 'constante absolute fout' berekeningen

Om de supercelconvergentie-trends van eigenschappen zoals de atomaire kracht en Zr-oplosenergie correct te kunnen interpreteren, moeten all berekeningen uitgevoerd worden met een constante absolute fout op de grondtoestandsenergie van de supercellen m.b.t de parameterinstellingen, binnen de gewenste nauwkeurigheid. Aangezien de grondtoestandsenergie van de supercellen geconvergeerd werd tot op een relatieve nauwkeurigheid van 0.001 eV/atoom m.b.t het aantal k-punten, zijn absolute fouten in de orde van 0.1-1 eV mogelijk voor 100- tot 1000-atomige supercellen. Het vereiste aantal k-punten voor het bereiken van de gewenste absolute fout kan bepaald worden a.d.h.v k-punt convergentietesten. Dergelijke testen zijn echter amper uitvoerbaar voor de grootste supercellen (honderden atomen), aangezien de rekentijd voor één berekening al enkele uren tot dagen kan duren en er berekeningen moeten uitgevoerd worden voor verschillende k-meshen. Daarom werd er een procedure ontwikkeld om de k-puntvereisten te schatten voor de grootste supercellen.

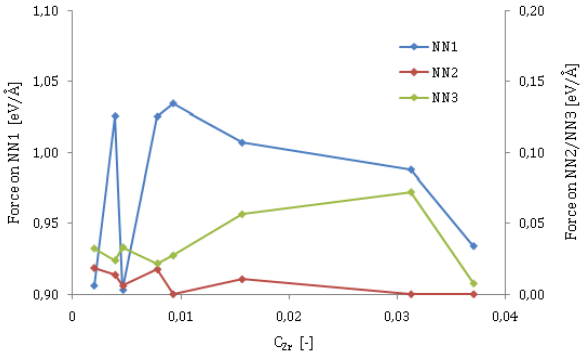

Fig. 5: Krachten op de eerste (NN1), tweede (NN2) en derde (NN3) dichtste-nabuur Cu-atomen van Zr, voor alle Zr-subroostersymmetrieën.

K-punt convergentietesten werden uitgevoerd op de kleinste Cu-Zr supercellen. De relatieve nauwkeurigheid $|\Delta E_{atom}|$ (die N keer kleiner is dan de absolute fout op de grondtoestandsenergie) werd voor elke berekening uitgezet i.f.v het aantal k-punten in de eerste Brillouin zone van de één-atomige supercel k_1 (wat gelijk is aan N keer het aantal k-punten in de Brillouin zone van de N-atomige cel k_N). Een omhullende exponentële functie van de vorm $a\exp(-bk_1)$ (met a en b parameters van de exponentiële functie), werd bepaald aan deze data. Deze functie werd gekozen omdat de fout op de grondtoestandsenergie per atoom snel bleek af te nemen met het aantal k-punten. De exponentële functie omhult de data punten op een zodanige manier dat de curve zo dicht mogelijk bij, maar nog steeds boven de data-punten ligt: de fout op de grondtoe-

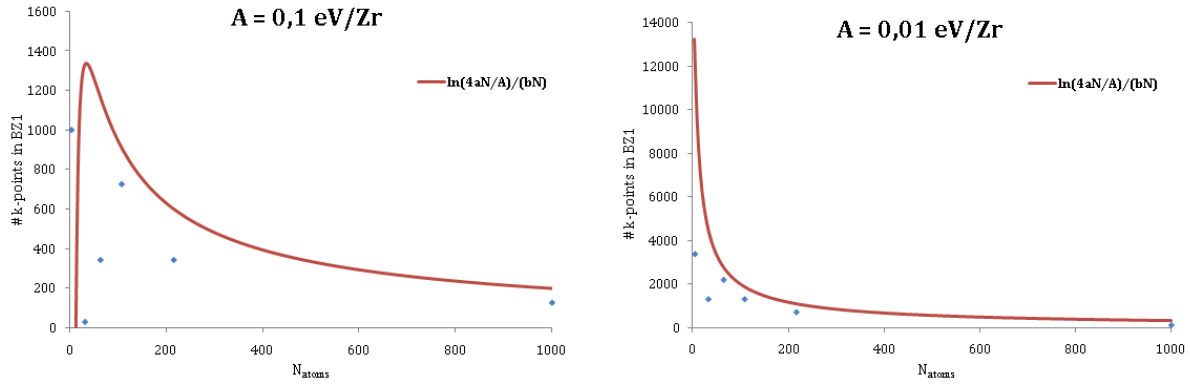

(a) (b)

Fig. 6: De voorspelde bovenlimiet k-puntenvereisten i.f.v de supercelgrootte voor (a) $A = 0.1$ eV/Zr en (b) $A = 0.01$ eV/Zr.

standsenergie per atoom (relatieve nauwkeurigheid) wordt dus overschat voor alle k-meshen. Hierdoor zal voor alle supercelgroottes een bovenlimiet voor de k-puntenvereisten gevonden worden. Men kan aantonen dat de als de fout op de grondtoestandsenergie per atoom $|\Delta E_{atom}|$ overschat wordt door de exponentële functie $a\exp(-bk_1)$, de volgende uitdrukking wordt gevonden voor de k-puntenvereisten i.f.v de supercelgrootte:

$$k_N = \frac{1}{bN}\ln(\frac{4aN}{A}) \tag{3}$$

met A de gewenste nauwkeurigheid voor de Zr-oplosenergie ([eV/Zr]). Curven voor deze vergelijking worden getoond in Fign. 6a en 6b, voor respectievelijk $A = 0.1$ ev/Zr en $A = 0.01$ eV/Zr . De data-punten in deze figuren zijn de k-puntvereisten bepaald via de k-punt convergentietesten voor de corresponderende supercelgroottes (het data-punt voor de 1000-atomige cel bij $A = 0.01$ eV/Zr stelt daarentegen een onderlimiet voor de k-puntvereisten voor). De verwachte trend wordt voor $A = 0.1$ eV/Zr niet goed voorspeld door deze vergelijking voor de kleinere supercellen: de functie bereikt een maximum met afnemende supercelgrootte, waarna ze heel snel afneemt en zelfs negatieve k-puntenvereisten voor de allerkleinste supercellen (minder dan 12 atomen). Dit komt omdat de waarde van de parameter a (0.002 eV) veel kleiner is dan de nauwkeurigheid A (0.1 eV/Zr): voor kleine N wordt de breuk in de ln-factor in vgl. (3) kleiner dan 1 en de hele term aan de rechterzijde van de vergelijking dus negatief. Dit geeft aan dat een exponentiële geen fysisch correcte beschrijving is van het verloop van de relatieve nauwkeurigheid met aantal k-punten. Gelukkig worden de k-puntvereisten consistent (lichtjes) overschat voor beide nauwkeurigheden A in het geval van de grootste supercellen (honderden atomen).

De voorspelde bovenlimiet k-puntvereisten voor $A = 0.01$ eV/Zr werden gebruikt voor de 'constante absolute fout' berekeningen in de supercelconvergentie-studie van de Zr-oplosenergie, behalve voor de 512- en 1000-atomige cel, waar een onderlimiet k-mesh voor deze nauwkeurigheid werd gebruikt. Alle k-meshen bleken groter te zijn dan deze voor de 'constante relatieve nauwkeurigheid' berekeningen uit de vorige sectie. De convergentietrends zijn gevisualiseerd in Fig. 7. De supercelconvergentie vertoont duidelijk beterschap voor alle subroostersymmetrieën, zelfs voor de kleinere supercellen, aangezien alle trends nu lijken te convergeren tot dezelfde Zr-oplosenergie bij oneindige verdunning. Dit suggereert dat 'constante absolute fout' berekeningen inderdaad van primordiaal belang zijn om supercelconvergentie-trends correct te kunnen interpreteren voor supercelgrootte-afhankelijke eigenschappen zoals de Zr-oplosenergie. Een dergelijke procedure blijkt dus nuttig te zijn om een constante absolute fout te creëren voor alle supercelgroottes m.b.t aantal k-punten. Ook voor andere parameters, waarvoor absolute fouten significant kunnen zijn voor de grootste supercellen, kan een dergelijke procedure eventueel aangewend worden.

De grote afwijkingen voor de grootste supercellen met fcc subroostersymmetrie in Fig. 7 zijn een gevolg van het feit dat een onderlimiet voor de k-puntvereisten werd gebruikt voor de 512- en 1000-atomige cellen. Berekeningen met de bovenlimiet k-puntvereisten voor deze cellen bleken computationeel niet meer haalbaar te zijn om een nauwkeurigheid van 0.01 eV/Zr te halen. Deze supercellen dienen daarom geëlimineert te worden uit de convergentiestudie. Het blijkt dus dat bij een supercelconvergentiestudie van en supercelgrootte-afhankelijke eigenschap zoals de Zr-oplosenergie, de grootste supercel die gebruikt kan worden zal afhangen van de gewenste nauwkeurigheid voor deze eigenschap, omwille van computationele beperkingen.

C. *Supercelconvergentie van de H-oplosenergie in bcc Fe*

Er werd nog een kort bijkomend onderzoek uitgevoerd op de supercelconvergentie van de oplosenergie van een tetrahedraal interstitieel H-atoom in ferromagnetisch bcc Fe. Uit de literatuur bleek dat finite-size fouten voor deze eigenschap minimaal zijn, met resterende oscillaties in de orde van 0.01 eV/H voor supercellen van een honderdtal atomen [10], ondanks het feit dat alle berekeningen met een constante relatieve nauwkeurigheid werden uitgevoerd. Gelijkaardige berekeningen met supercelgroottes tot en met 251 atomen ($Fe_{250}H$) en een constante, maar verhoogde relatieve nauwkeurigheid van 0.001 eV/atoom t.o.v de nauwkeurigheid van ref. [10], gaven eenzelfde supercelconvergentie-gedrag van de H-oplosenergie weer. Desondanks kan een dergelijke convergentietrend nog

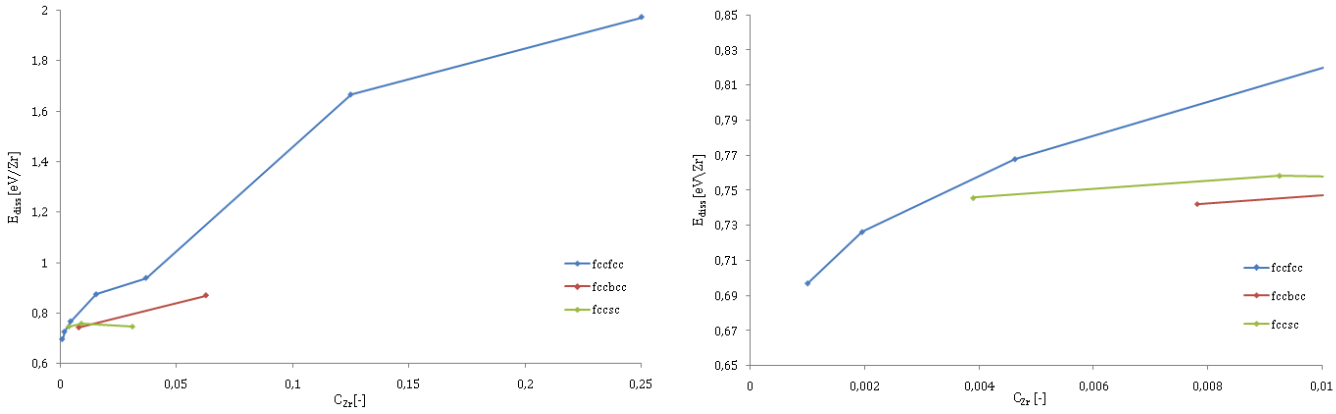

(a) (b)

Fig. 7: Supercelconvergentie van de Zr-oplosenergie i.f.v de Zr-concentratie, m.b.v 'constante absolute fout' k-meshes ($A = 0.01$ eV/Zr)

steeds enkel correct geïnterpreteerd worden als de berekeningen met een constante absolute fout worden uitgevoerd: absolute fouten m.b.t parameter instellingen kunnen immers reeds 0.1 eV bedragen. Om een constante absolute fout op de H-oplosenergie te bewerkstelligen kan de uitgewerkte procedure uit de vorige sectie aangewend worden om bijvoorbeeld de bovenlimiet k-puntvereisten te schatten voor alle supercelgroottes.

IV. Conclusie

Berekeningen van defecteigenschappen via de DFT-gebaseerde supercelmethode vertonen voor normale supercelgroottes fouten als gevolg van interacties tussen het defect en zijn periodiek kopieën. Daarom werd een grondige studie uitgevoerd op de supercelconvergentie van verschillende eigenschappen in het bijzonder geval van een substiutionele Zr-onzuiverheid in een fcc Cu gastrooster. Alle berekeningen werden hierbij uitgevoerd met het DFT-programma VASP. Eigenschappen die enkel afhangen van de lokale elektronenstructuur in een supercel, zoals de LDOS en lokale ladingsverschillen, bleken snel te convergeren met supercelgrootte. Grote supercellen bleken echter niet noodzakelijk het supercelconvergentie-gedrag te verbeteren voor supercelgrootte-afhankelijke eigenschappen, zoals de defect-vormingsenergie en de kracht. Alle parameters die supercelgrootte-afhankelijke fouten induceren, zoals het aantal k-punten, veroorzaken problemen voor dergelijke supercellen indien de berekeningen uitgevoerd worden met een constante relatieve nauwkeurigheid. Een procedure werd echter ontwikkeld, die ons toelaat om de noodzakelijke parametervereisten te schatten voor elke supercelgrootte en om zo een idee te verkrijgen wat de computationeel grootst haalbare supercel is die beschouwd kan worden in de supercelconvergentie-studie. Wanneer alle parametervereisten met betrekking tot een zekere defect-eigenschap bijgevolg in rekening gebracht worden, kunnen betrouwbare supercelconvergentie-studies uitgevoerd worden voor eender welk defect/rooster-systeem.

Referenties

[1] M. I. J. Probert en M. C. Payne, "Improving the convergence of defect calculations in supercells: An ab initio study of the neutral silicon vacancy", *Physical Review B*, vol. 67, pp. 8564-8567, 2003

[2] C. W. M. Castleton, A. Höglund en S. Mirbt, "Density functional theory calculations of defect energies using supercells", *Modelling en Simulation in Materials Science en Engineering*, vol. 17, pp. 084003, 2009

[3] F. Caestecker, "Nauwkeurigheidsstudie voor het ab-initio berekenen van de mengingsenthalpie bij bulk metallic glasses", Universiteit Gent, 2012

[4] G. Kresse en J. Furthmüller, "Efficiency of ab-initio total energy calculations for metals en semiconductors using a plane-wave basis set", *Computational Materials Science*, vol. 6, pp. 15, 1996

[5] G. Kresse en J. Furthmüller, "Efficient iterative schemes for ab initio total-energy calculations using a plane-wave basis set", *Physical Review B*, vol. 54, nr. 16, pp. 11169, 1996

[6] J. P. Perdew, J. A. Chevary, S. H. Vosko, K. A. Jackson, M. R. Pederson, D. J. Singh en C. Fiolhais, "Atoms, molecules, solids, en surfaces - Applications of the Generalized Gradient Approximation for exchange en correlation", *Physical Review B*, vol. 46, nr. 11, pp. 6671-6687, 1992

[7] P. E. Blochl, "Projector augmented-wave methods", *Physical Review B*, vol. 50, nr. 24, pp. 17953, 1994

[8] G. Kresse en D. Joubert, "From ultrasoft pseudopotentials to the projector augmented-wave method", *Physical Review B*, vol. 59, nr. 3, pp. 1758, 1999

[9] K. Momma en F. Izumi, "VESTA 3 for three-dimensional visualization of crystal, volumetric en morphology data", *Journal of Applied Crystallography*, vol. 44, nr. 6, pp. 1272-1276, 2011

[10] D. E. Jiang en Emily A. Carter, "Diffusion of interstitial hydrogen into en through bcc Fe from first principles", *Physical Review B*, vol. 70, nr. 6, pp. 064102, 2004

Table of Contents

Nomenclature

k_1	Number of k-points in the one-atom first Brillouin zone
k_N	Number of k-points in the first Brillouin zone of a N-atom supercell
(L)DOS	(Local) Density of States
(M)EAM	(Modified- Embedded-Atom Method
A	Accuracy of the defect formation energy [eV/defect]
bcc	body-centered cubic
BZ(1)	(First) Brillouin zone
CASTEP	Cambridge Serial Total Energy Package
DFT	Density Functional Theory
E_{cut}	Cut-off energy [eV]
E_{diss}	Dissolution energy [eV/impurity atom]
E^{H}_{diss}	H dissolution energy in ferromagnetic bcc Fe [eV/H]
E^{Zr}_{diss}	Zr dissolution energy in fcc Cu [eV/Zr]
EDIFF	Convergence criterion for the self-consistent procedure in the *INCAR*-file [eV]
ENCUT	Cut-off energy in the *INCAR*-file [eV]
F_{rms}	Root-mean-square force [eV/$\AA$]
fcc	face-centered cubic
GGA	Generalized Gradient Approximation functional
GGA-PW91	Perdew-Wang 1991 functional (GGA-type)
LDA	Local Density Approximation functional
N	Number of atoms
NN	Nearest Neighbor
PAW	Projector-Augmented Wave

PBE	Perdew-Burke-Ernzerhof GGA functional
sc	simple cubic
V_{BZ}	Volume of the first Brillouin zone of a supercell
VASP	Vienna Ab Initio Simulation Package
ZPE	Zero-Point Energy

Introduction

Hydrogen fuel is considered to be one of the most attractive solutions to the ever decreasing fossil fuel reserves and the considerable carbon dioxide emission associated with them. One of the problems in the development of hydrogen technology is the severe loss of ductility metallic materials suffer from when exposed to a reducing, hydrogen containing atmosphere. This problem is also referred to as hydrogen embrittlement. High-strength steels are considered to be very interesting materials for hydrogen transport and storage due to their capability of reducing the weight of a structure without loss of mechanical properties, but they are extremely sensitive to hydrogen embrittlement. This phenomenon is however still not completely understood, as a consequence of the high complexity of the mechanism(s) behind hydrogen-induced cracking, the incapability of visualizing H-defect interactions in the (bcc) Fe lattice and a large scatter in experimentally measured binding energies between H and various defects. Density Functional Theory (DFT)-based ab initio calculations can provide the necessary information on the atomic scale about defect structures and binding energies, making them ideally suited for interpreting experimental results and providing details about the embrittling mechanisms which are not experimentally feasible.

DFT calculations of defect properties are generally carried out by introducing a defect in a finite part of the host lattice and subsequently repeating it periodically throughout space. These periodic boundary conditions generate a material that also contains images of the defect. If the defect concentration is too high, the defect will interact with its closest images, thereby introducing errors in the calculated electronic structure of the cell and hence in the calculated defect properties. Therefore, supercell size-related errors need to be removed in order to obtain accurate defect property values. Several correction schemes have been developed for defect calculations in semiconducting materials. Similar supercell finite-size convergence investigations are however not known to be performed for Fe-H related systems. In order to make DFT defect calculations a useful complement to experimentally investigating hydrogen embrittlement in Fe, the finite-size convergence behavior of a reference Fe-H system was investigated in this work. The H dissolution energy is an important defect property that needs to be calculated accurately if any H-defect binding energies need to be determined. The tetrahedral interstitial H atom in bulk ferromagnetic Fe was therefore considered as a relevant reference system for the supercell finite-size investigation.

Issues with finite-size errors were also encountered in a previous study at the Center for Molecular Modeling on the mixing enthalpy of bulk metallic glasses: the dissolution energy of a Zr

substitutional impurity atom in a Cu host lattice was found not to be converged with supercell size for cells up to 128 atoms. The calculated dissolution energies of the systems with the smallest considered Zr-concentrations were still observed to suffer from finite-size errors. For this reason, and also because the data of these calculations are available, the Cu-Zr system was considered first in this work. The supercell finite-size convergence behavior was investigated for properties such as the Zr dissolution energy, forces and (local) density of states, whereas defect interactions as a function of supercell size were studied by visualizing differences in electronic charge distribution between the defect-containing and the pure Cu supercell. Results from the Cu-Zr study were subsequently transferred to the Fe-H system in order to obtain a H dissolution energy that is well converged with supercell size.

This Master's thesis is built up as follows: Density Functional Theory is outlined in the first chapter, in order to comprehend the principles behind the ab initio calculations performed in this work. The sources of supercell size-related errors and correction schemes to these errors as proposed in the literature are reviewed in the second chapter. In addition, since to our knowledge no correction schemes have been suggested for Fe-H related systems, the applied methodologies behind and results from DFT supercell calculations of defect formation energies in Fe in the literature are summarized as well. The methodology behind our Cu-Zr and Fe-H calculations is explained in the third chapter and results from the supercell finite-size convergence investigation are presented in chapter four. Conclusions from our study are summarized in the fifth and last chapter.

Chapter 1

Density Functional Theory

In this chapter we outline Density Functional Theory [1, 2], a quantum-mechanical modeling method for solving quantum many-body problems, which is used for all solid-state ab initio calculations in this Master's thesis.

A solid material can be defined as a system of $N = \sum_i N_i$ heavy, positively charged nuclei (where different indices i represent nuclei of different elements) and $\epsilon = \sum_i Z_i N_i$ lighter, negatively charged electrons, all electromagnetically interacting with each other. Z_i represents the atomic number of an individual nucleus N_i. Since all particles in this system are very light ($m_e = 9.11\times10^{-31}$ kg, $m_p = 1.67\times10^{-27}$ kg), quantum effects need to be considered. Hence, we need to solve the system's stationary Schrödinger equation to obtain its ground state. The exact many-particle Hamiltonian for this system is:

$$\begin{aligned}\hat{H} = &-\frac{\hbar^2}{2}\sum_{\alpha}\frac{\nabla^2_{\vec{R_\alpha}}}{M_\alpha} - \frac{\hbar^2}{2}\sum_{i}\frac{\nabla^2_{\vec{r_i}}}{m_e} - \frac{1}{4\pi\epsilon_0}\sum_{\alpha,i}\frac{e^2 Z_\alpha}{|\vec{R_\alpha} - \vec{r_i}|} \\ &+\frac{1}{8\pi\epsilon_0}\sum_{i,j}\frac{e^2}{|\vec{r_i} - \vec{r_j}|} + \frac{1}{8\pi\epsilon_0}\sum_{\alpha,\beta}\frac{e^2 Z_\alpha Z_\beta}{|\vec{R_\alpha} - \vec{R_\beta}|}\end{aligned} \tag{1.1}$$

M_α is the mass of the nucleus at $\vec{R_\alpha}$, the electrons have a mass m_e at positions $\vec{r_i}$. The first term on the right hand side of the equation describes the kinetic energy of the nuclei. The second term is the kinetic energy operator for the electrons. The last three terms correspond to the Coulomb interactions between electrons and nuclei, between electrons and other electrons and between nuclei and other nuclei, respectively. The ground-state solution to this Schrödinger equation is the eigenfunction with the lowest corresponding eigenvalue, which is a many-body wave function with four times as many variables as there are particles (three spatial and one spin coordinate for each particle):

$$\Psi(x_1, y_1, z_1, \alpha_1, \ldots x_{N(Z+1)}, y_{N(Z+1)}, z_{N(Z+1)}, \alpha_{N(Z+1)})$$

It is impossible to solve this equation exactly: even for a small Pt cluster of 100 atoms, the full many-body wave function already requires 23.000 dimensions [2]. It is impossible to solve this high-dimensional Schrödinger equation exactly (even a 3-body problem cannot be described exactly). Furthermore, even if the many-body wave function would be approximated with a product of single-particle wave functions, we would end up with a set of coupled differential equations. Such a problem however can only be solved numerically. To obtain acceptably accurate eigenstates, three approximations need to be made. Every one of them will be discussed briefly in the following subsections.

1.1 Born-Oppenheimer approximation

Since nuclei are much heavier than electrons, electrons will acquire a much higher speed than nuclei when both particles feel the same Coulomb force (Fig. 1.1). Hence, any change in position of a nucleus leads to an immediate response by the electrons. This suggests that we can decouple the nuclear positions and thereby reduce the nuclei to a static source of positive charge in the system. The positions of the nuclei then become parameters of the many-body wave function and the positions and spin of the ϵ electrons are the only remaining variables:

$$\Psi(x_1, y_1, z_1, \alpha_1, \dots x_{NZ}, y_{NZ}, z_{NZ}, \alpha_{NZ}; [\vec{R_1}, \vec{R_2}, \dots \vec{R_N}])$$

The above assumption is known as the Born-Oppenheimer approximation, sometimes called the adiabatic principle. The exclusion of the nuclear positions as variables also influences the many-particle Hamiltonian of the system: the kinetic energy of the nuclei is zero - since they are assumed to be static - and the term concerning the mutual Coulomb interaction between the nuclei reduces to a constant. We are now left with a much simpler Hamiltonian, containing the kinetic energy of the electrons, the potential energy due to the electron-electron Coulomb interactions and the potential energy due to the interaction of the electrons with the *external* potential of the nuclei:

$$-\frac{\hbar^2}{2}\sum_i \frac{\nabla^2_{\vec{r_i}}}{m_e} - \frac{1}{4\pi\epsilon_0}\sum_{i,j}\frac{e^2 Z_i}{|\vec{R_i} - \vec{r_j}|} + \frac{1}{8\pi\epsilon_0}\sum_{i,j}\frac{e^2}{|\vec{r_i} - \vec{r_j}|} \tag{1.2}$$

Observe that the kinetic ($\hat{T}$) and electron-electron interaction ($\hat{V}$) term are independent of the type of many-electron system: only the external potential term ($\hat{V}_{ext}$) contains system-specific information. The Born-Oppenheimer approximation is already a major simplification of the problem, but the resulting equation is still too hard to solve. Therefore, other approximations are still necessary.

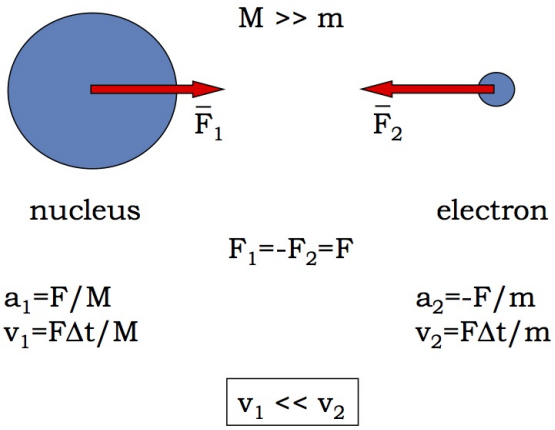

Figure 1.1: Nuclei acquire higher speeds than electrons when feeling the same Coulomb force [3].

1.2 Density Functional Theory

A variety of methods exists to further simplify the quantum many-body problem stated above. One of them, the Hartree-Fock method (HF), is a historically important one, but is not so accurate for solids, so we will not further examine HF in the rest of this paragraph, but rather focus on a method that is much more powerful for accurate calculations of solids: Density Functional Theory (DFT).

1.2.1 The Hohenberg-Kohn theorems

Density Functional Theory is based on two fundamental mathematical theorems proved by Hohenberg and Kohn [4]. The two theorems were originally stated as follows:

Theorem 1: There is a one-to-one correspondence between the ground-state density $\rho(\vec{r})$ of a many-electron system (e.g. a solid) and the external potential ($\hat{V}_{ext}$). An immediate consequence is that the ground-state expectation value of any observable $\hat{O}$ is a unique functional of the exact ground-state electron density:

$$< \psi|\hat{O}|\psi >= O[\rho] \tag{1.3}$$

Theorem 2: For $\hat{O}$ being the Hamiltonian $\hat{H}$, the ground-state total energy functional $H[\rho] \equiv E_{V_{ext}}[\rho]$ is of the form

$$E_{V_{ext}}[\rho] = F_{HK}[\rho] + \int \rho(\vec{r})V_{ext}(\vec{r})d\vec{(r)}) \tag{1.4}$$

where the Hohenberg-Kohn density functional $F_{HK}[\rho]$ is universal for any many-electron system. $E_{V_{ext}}[\rho]$ reaches its minimal value (equal to the ground-state energy[1]) for the ground-state density corresponding to V_{ext}.

[1]The ground-state energy is defined as the energy that is released when bringing all electrons and nuclei, at an infinite distance from each other, to the ground state of the system.

The first theorem seems somewhat counterintuitive: it is no surprise that a certain many-electron system has a unique external potential and - by solving the Schrödinger equation with eq. (1.2) - yields a unique many-particle wave function. However, since the electron density $\rho(\vec{r})$ only depends on three spatial coordinates, it seems to contain much less information than the (4NZ)-dimensional wave function. The first theorem of Hohenberg and Kohn says that the electron density *does* contain the same information as the wave function. Since all observable quantities can be determined via the wave function, the first theorem makes it possible to retrieve the same observable quantities from a unique functional of the electron density. This result is very important: it means that we can think about solving the Schrödinger equation (i.e. finding the ground-state energy) by finding a function that depends on barely three spatial variables - the electron density - rather than a function that depends on 4NZ variables - the wave function.

The first theorem tells us that a (unique) functional of the electron density - that can be used to solve the Schrödinger equation - exists, but unfortunately it does not tell us what it actually *is*. To construct this density functional, we need to know $F_{HK}[\rho]$, the universal Hohenberg-Kohn functional that contains the kinetic energy and electron-electron interactions terms (Theorem 2)[2]. An explicit expression of this functional however is not known. The second theorem says that if the density functional *were* known, we could use the variational principle to find the ground-state density. In practice however, the problem is not solved by means of the second theorem but rather by using the Kohn-Sham equations, which is the topic of the next subsection.

1.2.2 The Kohn-Sham equations

The equations of Kohn and Sham turn DFT into a practical tool, because they provide a practical procedure to determine the ground-state energy. They are in fact an exact transformation of the original problem - a complex coupled differential equation - into rather simple, much easier to handle single-particle equations. They are based on the assumption that the ground-state electron density can be represented by an auxiliary system of non-interacting quasi-particles, which is also known as the Kohn-Sham ansatz. Therefore, the original Hamiltonian is transformed into what will further be called the Kohn-Sham Hamiltonian, and can be written as follows:

$$\hat{H}_{KS} = -\frac{\hbar^2}{2m_e}\nabla_i^2 + \frac{e^2}{4\pi\epsilon_0}\int \frac{\rho(\vec{r}')}{|\vec{r}-\vec{r}'|}d\vec{r}' + V_{xc} + V_{ext} \tag{1.5}$$

or more formally:

$$\hat{H}_{KS} = \hat{T}_0 + \hat{V}_H + \hat{V}_x c + \hat{V}_{ext} \tag{1.6}$$

where the exchange-correlation functional V_{xc} is given by the functional derivative:

$$\hat{V}_{xc} = \frac{\delta V_{xc}[\rho]}{\delta\rho} \tag{1.7}$$

The first term in the Kohn-Sham Hamiltonian (T_0) represents the kinetic energy of the quasi-particles. The second term is the Hartree potential V_H and describes the classical electrostatic

[2]Notice that $F_{HK}[\rho]$ is universal because it does not contain any information about the nuclei and their positions. This functional is the same for any given many-electron system with the same number of electrons.

interaction of the particle with the average, static distribution of all other quasi-particles. V_{ext} is the already defined external potential and V_{xc}, finally, is the additional potential to which the quasi-particle is subject, due to unknown exchange and correlation effects. The above expression can be interpreted as the Hamiltonian corresponding to a non-interacting classical electron gas, subject to two external potentials: one due to the nuclei (V_{ext}) and one due to exchange and correlation effects (V_{xc}). The theorem of Kohn and Sham is stated as follows: *The exact ground-state density $\rho(\vec{r})$ of an N-electron system is*

$$\rho(\vec{r}) = \sum_{i=1}^{N} \phi_i^*(\vec{r})\phi_i(\vec{r}) \tag{1.8}$$

where the single-particle wave functions $\phi_i(\vec{r})$ are the N lowest-energy solutions of the Kohn-Sham equation

$$\hat{H}_{KS}\phi_i = \epsilon_i\phi_i \tag{1.9}$$

So we can find the ground-state density by simply solving the single-particle Schrödinger equation for as many-particles as there are electrons in the original system. The ground-state energy can then be calculated from the ground-state density functional:

$$E_{V_{ext}}[\rho] = T_0[\rho] + V_H[\rho] + V_{xc}[\rho] + V_{ext}[\rho] \tag{1.10}$$

The above defined quasi-particles with quasi-particle wave functions ϕ_i have no physical meaning: they are merely mathematical constructions to determine the ground-state density and energy. The single-particle energies ϵ_i are also no single electron energies.

V_H and V_{xc} both depend on the electron density $\rho(\vec{r})$, which depends on the quasi-particle wave functions ϕ_i that need to be determined via the Kohn-Sham equations. However, to solve these equations, we need to construct the Kohn-Sham Hamiltonian, which requires knowledge about the electron density $\rho(\vec{r})$ to construct V_H and V_{xc}. Obviously, this means that we are dealing with a self-consistent problem: an iterative procedure is required to obtain the electron density up to a desired accuracy (which can be defined via the desired accuracy of the total ground-state energy). An initial guess for the electron density ρ_0 is made, by which the KS-Hamiltonian is constructed. The KS-equations are then solved and the ground-state density is determined via eq. (1.8). If the difference between the calculated density and the guessed density ρ_0 is beneath a certain predefined limit, the final density is said to be consistent with the Hamiltonian and the iteration stops. If the density difference is above this limit, a new iteration starts using the density calculated in the previous iteration. Each iteration of this procedure is called a *self-consistent procedure* and is visualized in Fig. 1.2.

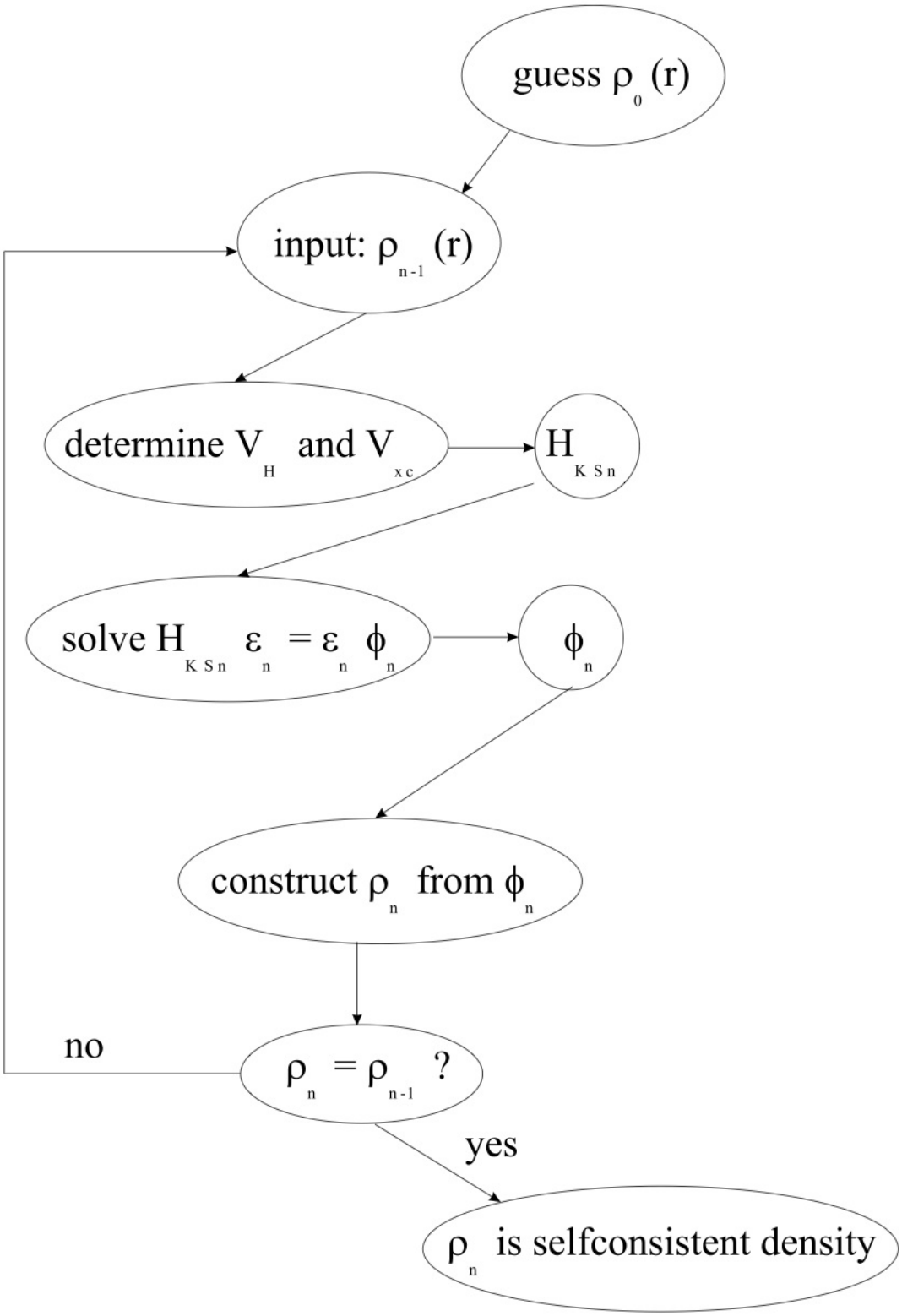

Figure 1.2: The self-consistent procedure as a procedure to solve the Kohn-Sham equations [1].

1.2.3 The exchange-correlation functional

The Kohn-Sham equations are an exact transformation of the original problem: apart from the Born-Oppenheimer approximation, no other approximations were made so far. Exact values for the ground-state density and energy can however not be obtained: a unique expression for the exchange-correlation functional $V_{xc}[\rho]$ exists for any given system of electrons and nuclei, but it is unknown and there is no real hope of ever obtaining one in a closed form. This is a consequence of the fact that this functional is capable of explaining all solid state physics and chemistry: its form will be highly pathological (Fig. 1.3). Therefore, approximations to this functional are made that yield *approximate* values for the ground-state density and energy. A widely used approximation is called LDA (Local Density Approximation), which uses the following expression for the exchange-correlation functional:

$$V_{xc}^{LDA}[\rho] = \int \rho(\vec{r})\epsilon_{xc}(\rho(\vec{r}))d\vec{r} \tag{1.11}$$

with ϵ_{xc} the energy density of a homogeneous electron gas. It means that the exchange-correlation energy for a given density $\rho(\vec{r})$ could be found by dividing the material in infinitesimally small volumes with constant density $\rho(\vec{r})$. Each such volume contributes to the total exchange-correlation energy by an amount equal to the correlation energy of an equal volume filled with a homogeneous electron gas[3], that has the same density as the original material in this volume. There is no guarantee that this works, but it appears to be very accurate in many cases.

The GGA functionals (Generalized Gradient Approximation) are a further improvement to the LDA functionals, making the exchange-correlation contribution of an infinitesimal volume not only depend on its own local density, but also on the density of its neighboring volumes: the *gradients* will play a role. GGA functionals generally perform slightly better, but there are also some drawbacks with respect to LDA functionals: first of all, since there is some freedom to incorporate the gradient, several versions of GGA exist, e.g. PW91 (Perdew-Wang 1991) [5] and PBE (Perdew-Burke-Ernzerhof 1996) [6]. Also, for some GGA's the functional contains some

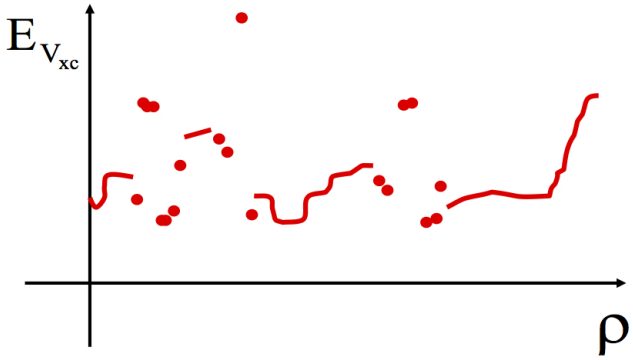

Figure 1.3: The exchange-correlation functional $V_{xc}[\rho]$ will be a highly pathological one [3].

[3]The homogeneous electron gas is the only case for which the exchange-correlation energy can be calculated exactly.

free parameters which are fit to experimental data on atoms and molecules. The best values are fixed and are used for solid-state calculations. As some experimental information is used, this is strictly speaking no longer an ab initio calculation. In this work, all calculations are performed using GGA-PW91 functionals, since good results have already been obtained with these functionals for solid-sate calculations [5].

1.3 Solving the equations

To determine the ground-state density, we need to solve the Kohn-Sham equations:

$$\left(-\frac{\hbar^2}{2m_e}\nabla_i^2 + \frac{e^2}{4\pi\epsilon_0}\int\frac{\rho(\vec{r}')}{|\vec{r}-\vec{r}'|}d\vec{r}' + V_{xc} + V_{ext}\right)\phi_i = \epsilon_i\phi_i \tag{1.12}$$

for all N quasi-particles. Therefore, a basis set ϕ_p^b is defined to approximate the quasi-particle wave functions ϕ_i:

$$\phi_i = \sum_{p=1}^{P} c_p^i \phi_p^b \tag{1.13}$$

Now that a basis set is introduced, the problem can be transformed into matrix algebra and what we are looking for are the coefficients c_p^i. The Kohn-Sham equation for a single quasi-particle can now be written as:

$$HC = SCE \tag{1.14}$$

In this matrix equation, $H = \langle\phi_k^i|H_{KS}|\phi_l^i\rangle(k,l = 1\ldots P)$ and contains matrix elements for all basis functions. Hence, it can be calculated once and for all. The same holds for S, which is called the overlap matrix and contains all dot products $\langle\phi_k^i|\phi_l^i\rangle$. C is a square matrix with all the coefficients we are searching and E, finally, is a diagonal matrix that contains all eigenvalues we are looking for. This can be treated as a generalized eigenvalue problem and diagonalization of the Hamiltonian matrix will lead to P eigenvalues and P sets of coefficients that each define one of the P eigenfunctions, expressed in the given basis.

Since the summation in eq. (1.13) is truncated and not infinite, it is not possible to describe the ϕ_i exactly. An appropriate basis set now has to be found which approximates these quasi-particle wave functions as good as possible and hence allows an as small truncation as possible. Different types of basis sets can be used for solid-state calculations: it is the choice of the basis set that gives the name to the method and determines which computer code will be used. Basis sets should satisfy two principal requirements: they need to be efficient and unbiased. A basis set is called efficient when a relatively low number of basis functions accurately describe the quasi-particle wave function. In that case, the dimensions of the matrices in eq. 1.14 are low and so will be the time required to diagonalize the Hamiltonian matrix. The use of a very efficient basis set, however, assumes that the solution is almost known before one starts solving the problem. Such a basis set cannot be general and will yield results more quickly for some cases, but will be much slower for the majority. The basis set is then *biased*. An ideal basis set is both efficient and unbiased. The most important and widely used basis sets that fulfill both requirements are the

plane-wave basis functions and the augmented plane-wave basis functions. Since all calculations in this Master's thesis are performed with a plane-wave basis set in combination with PAW potentials, this type of basis set is treated briefly in the following section.

1.4 Plane wave basis functions

A basis set that is both unbiased and mathematically simple is the plane-wave basis set. It is related to the Bloch Theorem, which states that *"For a Hamiltonian with lattice periodicity, any eigenfunction $\psi^n_{\vec{k}}(\vec{r})$[4] can be written as a product of a function $u^n_{\vec{k}}(\vec{r})$ that has the periodicity of the lattice, and a plane wave $e^{i\vec{k}\cdot\vec{r}}$ with $\vec{k}$ any vector in the first Brillouin zone*[5]*":*

$$\psi^n_{\vec{k}}(\vec{r}) = \sum_{\vec{K}} c^{n,\vec{k}}_{\vec{K}} e^{i(\vec{k}+\vec{K})\cdot\vec{r}} \tag{1.15}$$

When eq. 1.15 is compared with the general expression in eq. 1.13, it can be seen that $m = (\vec{n}, \vec{k})$ and $p = \vec{k} + \vec{K}$. For a given $\vec{k}$, a single basis function can be written as:

$$\phi^{\vec{k}}_{\vec{K}}(\vec{r}) = e^{i(\vec{k}+\vec{K})\vec{r}} \tag{1.16}$$

Observe that when $\vec{k}$ differs for any two eigenstates, different basis sets have to be used, each with their own $\vec{k}$: the basis set is said to be $\vec{k}$-dependent.

It is impossible to work with an infinite basis set, so it needs to be truncated. For the above defined plane-wave basis set, this done by putting a limit to the set of the vectors $\vec{K}$ with $K \leq K_{max}$. All reciprocal lattice vectors that are inside a sphere with radius K_{max} and center at the origin of reciprocal space, are included into the basis set. Typically, this outer limit is not specified by the value of K_{max} but rather by the free electron energy for the specified K_{max}.

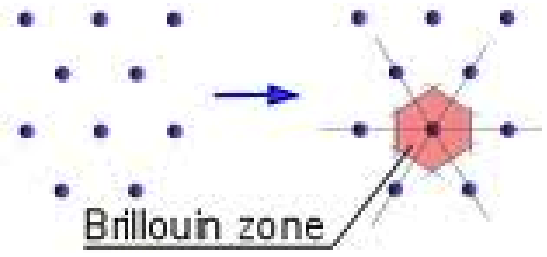

Figure 1.4: The first Brillouin zone of a 2D hexagonal Bravais lattice [7].

[4] n is the so-called band index: the set $(n,\vec{k})$ describes a given vector $\vec{g}$ which can be located anywhere in reciprocal space. For $n = 1$ e.g., this set describes a vector $\vec{g}$ inside the first Brillouin zone, so $\vec{g} = \vec{k}$. For $n = 2$, this set describes a vector $\vec{g}$ located in the second Brillouin zone, and so on.

[5] The first Brillouin zone is the primitive Wigner-Seitz cell of the reciprocal lattice of a given Bravais lattice (Fig. 1.4). This particular choice of unit cell describes all points of reciprocal space that are closer to the origin than to any other point of the reciprocal lattice. Analogously, the second Brillouin zone contains all points that have the origin as their second nearest neighbor, and so on.

This specific value is called the *cut-off energy*:

$$E_{cut} = \frac{\hbar^2 K_{max}^2}{2m_e} \tag{1.17}$$

Once the basis set is defined with E_{cut}, the matrices H and S in eq. (1.14) are calculated for each quasi-particle KS-equation, the Hamiltonian matrix is diagonalized and the KS-orbitals are determined. To calculate properties such as the electron density or the density of states, integrals over the first Brillouin zone are necessary. The electron density, for example, can be determined using the following expression:

$$\rho(\vec{r}) = \frac{1}{V_{BZ}} \int_{BZ} \sum_{i=1}^{N} n_i |\phi_i^{\vec{k}}(\vec{r})|^2 d\vec{k} \tag{1.18}$$

Because those properties need to be calculated by computer, such integrals can be approximated by evaluating the integrand in the integral at a set of discrete $\vec{k}$-points and summing the values of the functions at these points with a proper weight for each point. This means that the wave functions need to be calculated at a discrete number of $\vec{k}$-points. Performing such an integration over a discrete number of $\vec{k}$-points is also-called *Brillouin zone sampling*. More accurate results are obtained if more $\vec{k}$-points are included in the summation and in the limit of using a very large number of points, the numerically obtained value will converge towards the exact solution. Several methods exist for making efficient choices of such $\vec{k}$-points and the one that is used for the calculations in this Master's thesis is the Monkhorst-Pack method [8].

Plane-wave potentials

In the discussion above, it was mentioned that plane waves are suitable basis functions, because they are unbiased. The efficiency however, being an equally important property for a basis set, was not yet discussed for plane-wave basis functions. Recall that the efficiency of a basis set is determined by the number of basis functions necessary to describe the quasi-particle wave functions accurately. The smaller the length scales to be described in real space, the more plane-waves need to be included. Only a large basis set contains strongly oscillating plane-waves on a short length scale in real space[6]. Wave functions of tightly bound core electrons show very steep behavior close to the nucleus (at distances in the order of 0.1 Å), however. This means however that very large basis sets need to be used, in the order of 10^8 [1]! To solve the KS-equations, diagonalization of $(10^8 \times 10^8)$-matrices is required, which is beyond the capability of even supercomputers. The efficiency of the plane-wave basis set as such is hence very low.

The amount of basis functions can however be dramatically reduced. For this purpose, it has to be considered that the core electrons are not especially important in defining chemical bonding and other physical characteristics of materials, because they are quite shielded from the more outer

[6]The wave vector of the plane-wave basis function is equal to $\vec{k} + \vec{K}$: a higher cut-off energy means that longer $\vec{K}$-vectors are included.

regions of the atoms where chemistry happens. These electrons will not behave very differently from free-atom electrons. One can therefore substitute the true potential by a pseudopotential, which replaces the electron density from a chosen set of core electrons with a smoothed electron density in such a way that the most important physical and mathematical properties of the true ion core remain unchanged. Since the electron density near the nuclei varies much smoother now, there are only a few number of plane waves necessary to describe the quasi-particle wave functions. Subsequently, the core electrons are removed from the many-electron system: one atomic calculation is performed on these electrons and its contribution is held constant in all further calculations. This method is therefore called the *frozen-core approximation*.

An alternative way of reducing the basis-set size is the PAW (projector-augmented wave) method as introduced by Blöchl [9] and implemented by Kresse and Joubert [10]. Via a linear transformation, using projector operators within a sphere that contains the rapid oscillations, the original solutions to the Kohn-Sham equation ϕ_i are transformed into a sum of auxiliary wave functions $\tilde{\phi}_i$ that are smooth everywhere [11]. The smooth auxiliary wave functions can be determined by solving the transformed Kohn-Sham equations via a self-consistent procedure, which now requires much less computational effort since these wave functions do not contain the rapid oscillations near the core. The original single-particle wave functions can then be obtained via the inverse linear transformation. It is emphasized that the PAW method is an extension of the pseudopotential approach, and *not* a pseudpotential method as such.

Chapter 2

The DFT-based supercell approach for defect property calculations

2.1 Supercell finite-size errors in calculated defect properties

During the past decades, DFT has proved to be a valuable tool for calculations of bulk properties in solid-state materials. Equally important, however, is the study of defects, since they have a pronounced influence on the properties of a material: the mechanical behavior of a metal, for example, is heavily dependent on its chemical composition (impurities and alloying elements), the precipitate distribution, the grain size and the type of grain boundaries, the dislocation density, ... Calculations of defect properties by means of DFT-based codes could therefore provide an attractive complement to experimental results. The key properties to be obtained by these calculations are the defect formation energy and the equilibrium structure of the defect and its immediate surroundings in the 'bulk' of the material. In the study of the interaction of hydrogen with traps in steel, for example, knowledge of the defect formation energy is important to determine H-defect binding energies, so the strength of hydrogen traps can be compared. Knowing the equilibrium structures of these traps, on the other hand, provides valuable information for the prediction of the location of hydrogen atoms in the traps.

There are generally two ways of modeling defects in solids: the cluster method and the supercell method. In the former approach, a cluster of atoms is created, representing the defect introduced in the host lattice. Open boundary conditions are applied, which means free surfaces are present. The surface atoms are usually terminated with hydrogen atoms, but are otherwise surrounded by vacuum. In the supercell method on the other hand, a unit cell is created - also representing the defect in the host lattice - and is then periodically repeated throughout space, which means that there is no empty space at all. Both methods have strengths and weaknesses: while in cluster calculations errors are introduced due to interactions between the defect and the surface of the cluster, introduction of a defect in a supercell leads to the calculation of a periodic array of defects and not of an isolated defect, creating interactions between the defect and its images if the supercell is not large enough. These defect interactions will cause calculated properties

such as the defect formation energy to alter, making them supercell size-dependent [12, 13]. Furthermore, a reliable equilibrium structure can only be obtained after the finite-size errors are removed, since the structure is created by a relaxation procedure of the atoms around the defect: if the atoms from an unconverged calculation (i.e. with defect interactions still present) would be relaxed, the correct equilibrium structure can not be guaranteed to be the result of this relaxation procedure. This phenomenon is comprehensibly described for the case of the neutral vacancy in silicon by Probert and Payne [13]. Density Functional Theory is compatible with both cluster and supercell method. The latter method will however exclusively be discussed, since in all calculations in this work the DFT supercell method has been used. Convergence of unrelaxed defect properties with respect to supercell size will therefore be of particular interest here.

In order to obtain reliable defect properties from the supercell method, all errors that depend on the supercell size have to be removed. Many studies during the last two decades focussed on the source of these finite-size errors and correction methods to obtain well converged formation energies of point defects with respect to supercell size. All of these investigations however are related to point defect properties in semiconductors, due to the considerable influence of native defects (vacancies and self-interstitials) and impurities (dopants) on the electrical conductivity of these materials [14]. Some features from these studies are nevertheless expected to be applicable - to some extent - in calculations of unrelaxed defect properties in transition metals too, as will be discussed below. In the rest of this section, the main sources of errors that are found in literature, attributed to the finite size of supercells, will be discussed first, whereafter a review will be given of the proposed solution techniques to these finite-size errors.

2.1.1 Sources of errors

The occurrence of interactions between a defect and its images in neighboring supercells when distances between them are relatively small (in the order of tens of Ångströms) shouldn't be a suprise. Different types of interactions will however appear, all contributing to some extent to errors in calculated properties such as the defect formation energy. The identification of these interactions and their influence on calculated defect properties in semiconducting materials has recently been treated extensively by Castleton, Höglund and Mirbt [15]. They make a distinction between supercell size-dependent (either *rational* or *non-rational*) and supercell size-independent errors. Supercell size-dependent errors are considered to be rational when some kind of functional form should exist for them. They usually depend in a monotonic way on the supercell size. Non-rational errors vary irregularly with supercell size, requiring individual treatment for every supercell included in the data set. Supercell size-independent errors on the other hand can be calculated for a defect in a supercell of moderate size and then used to correct the results in all other supercells [15]. All sources and types of errors can be described as follows:

1. ***Rational supercell size-dependent errors***

   (a) *Elastic effects*

   Elastic errors arise because the supercell is not large enough to contain all atomic relaxations around the defect, which leaves the calculated defect energy too high. Direct elastic interactions between a defect and its periodic images also occur, but can be truncated to some extent by freezing the atoms lying in the surface of the supercell during relaxation. Earlier investigations by Castleton et al. [12,16,17] showed that the elastic errors of relaxed defect energies scale with L^{-1} (L is the linear dimension of the supercell). They will however not appear in our calculations since only unrelaxed defect properties are studied.

   (b) *Electrostatic interactions*

   These interactions occur predominantly in supercells containing charged defects, but they need not be negligible even for neutral defects due to dipolar and quadrupolar interactions. This is for example observed in defect energy calculations of the neutral unrelaxed vacancy in silicon by Corsetti et al. [14] . In contrast to elastic interactions, these interactions cannot be truncated or removed. The electrostatic errors scale with L^{-1} and L^{-3} [12, 16, 17]. They are however expected to play only a negligible role in defect calculations in transition metals due to strong screening by electrons in crystal orbitals.

   (c) *Dispersion*

   Dispersion of the defect state levels can occur due to overlap of the defect wave functions with their images from the periodic boundary conditions, introducing another type of error to the defect formation energy (Fig. 2.1). According to Castleton et al., the errors related to dispersion are fairly small for defects in semiconductors and should have a rather short-ranged exponential effect with respect to supercell size [12, 15]. Corsetti et al. however found a very slow convergence of the defect energy of the neutral silicon vacancy with supercell size, which they also blame on dispersion effects [14]. The way dispersion of defect states will affect the defect formation energy in transition metals is more difficult to predict, because the defect levels are not localized as those in the band gaps of semiconductors: they are intrinsically dispersed due to interactions with the valence and conduction bands. Remark that defect level dispersion is a consequence of interactions between a defect and its images and *not* a type of interaction.

2. ***Non-rational supercell size-dependent errors***

   These errors arise from incomplete convergence of the defect energy with respect to k-point integration. They are in themselves not related to the finite supercell size, but it is rather the effect of incomplete k-point convergence that depends on the size of the supercell in question. This effect appears to vary irregularly with supercell size, so full k-point convergence will be necessary for each supercell individually to remove these additional terms in the supercell approximation errors [15]. Only then the rational finite-size errors can be removed during what is usually called the supercell finite-size convergence.

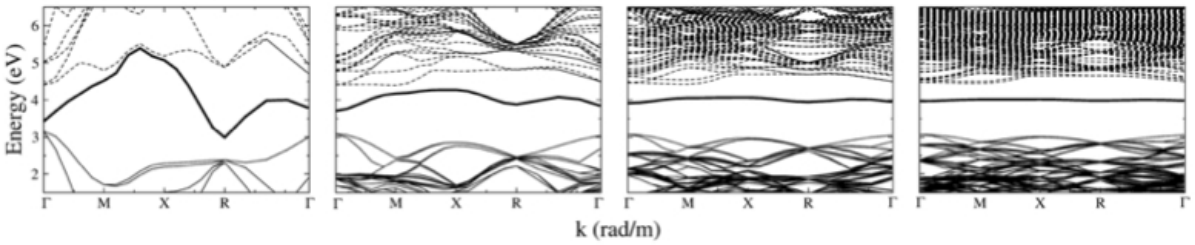

Figure 2.1: Band structure of the neutral P anti site in GaP. The deep defect level is represented by the thick black line. The dispersion is shown for 8, 64, 216 and 512 atom supercells. The small supercells clearly show the strongest defect level dispersion [15].

3. ***Supercell size-independent errors***

   (a) *Choice of exchange-correlation functional*
   LDA functionals typically overbind bonds, while GGA functionals underbind them. Castleton et al. found errors of O(0.1 eV) after comparison between LDA and GGA energies for different types of defects in various semiconductors, without a significant supercell dependence [15]. However, the order of magnitude of these errors is highly dependent on the materials system [18].

   (b) *Choice of potential*
   The defect energy has also been observed to depend on the choice of potential in VASP[7] calculations by Castleton et al. [15], with PAW potentials producing more accurate results than ultrasoft pseudopotentials in the case of various defects in InP semiconductors [12]. Differences in defect energies are typically in the order of O(0.1 eV) or less. Interestingly, in the case of InP, defect energy values also depend on the treatment of the 4d-electrons - either as valence or as core electrons - in the In pseudopotential, especially for In related defects. This phenomenon is illustrated in Fig. 2.2, where the difference in defect formation energy between ultrasoft pseudopotentials (USPPs) treating the In 4d-electrons either as valence or as core electrons, is plotted as a function of the defect's charge. Energy differences are usually well below 0.1 eV for P related defects, but can be of the same order as the finite-size errors for In related defects. The errors are observed to be even larger when *unrelaxed* defect energies are calculated. While treating the In 4d-electrons as valence is physically more correct and hence produces more accurate energies (the In 4d states lie fairly deep beneath the valence band edge, but could still make a contribution to the formation energy), computer limitations often require to treat these electrons as core, especially in the larger supercells (512 atoms) [12].

   (c) *Finite basis set*
   A last supercell size-independent error in calculated defect properties arises due to the finite size of the plane-wave basis set, reflected in the cut-off energy E_{cut} (see section 1.4). To ensure a high accuracy in these and other convergence procedures,

[7]VASP is a quantum-mechanical code that uses DFT to calculate properties of materials. Other codes that are frequently used are CASTEP and Wien2k [19].

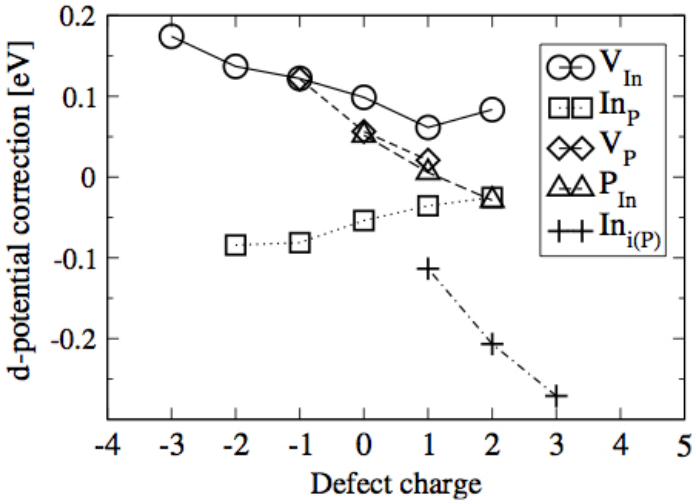

Figure 2.2: Difference in formation energy between using a USPP with In 4d-electrons treated as valence and that using a USPP with the same electrons treated as core, as a function of the charge of the defect [15].

the defect structure needs to be converged with respect to basis-set size before any k-point or supercell finite-size convergence test is performed. This is usually carried out by converging the defect formation energy with E_{cut} up to a predefined error. The variational principle, which guarantees monotonic convergence of the total ground-state energy of the system with increasing basis-set size, does not apply for defect formation energies, since it involves a ground-state energy difference between two dissimilar systems (the bulk and the defect-containing system). A monotonic convergence is however often observed in practice [13]. The convergence tolerance for the defect energy is usually restricted to 0.01 eV (at most) [13, 15].

2.1.2 Solutions to supercell size-dependent errors

2.1.2.1 Convergence of k-point integration

Before rational supercell size-dependent errors can be removed, a complete convergence of the k-point integration needs to be ensured, due to the irrational dependence of the introduced error on the supercell size. For defects in semiconducting materials, a fully converged integration is very important due to the highly localized nature of the defects [13]. This statement is particularly proved by Puska et al. [20], who investigated the convergence of the Si vacancy properties with supercell size. They observed the description of the localized defect states not to straightforwardly improve as the number of k-points increases: the detailed choice of the k-point sampling can affect the convergence strongly, since for some choices of the k-point sampling the dispersed (deep) defect level states hybridize with the bulk energy bands, thereby creating errors in the defect formation energy, and hence postpone the supercell finite-size convergence. Adequate k-point integration convergence has also found to be essential in metallic systems, since defect properties are often incorrectly reproduced when too few k-points are included [21].

To reduce the error induced by k-point sampling below a predefined value, one could simply calculate the defect formation energy with increasing numbers of k-points (for a given supercell) and use the k-mesh for which the error is below the requirement in further calculations. However, a large number of k-points is usually the outcome of such convergence tests: Castleton et al. [12], e.g. , found an 18×18×18 grid[8] (using the Monkhorst-Pack sampling scheme) to be necessary for an 8-atom supercell containing their worst converging defect in InP, to get errors safely below O(0.005 eV). Such k-meshes are already computationally costly, which has made it worthwhile to look for methods that are capable of 'speeding up' the convergence with the number of k-points.

Probert and Payne improved the convergence of the formation energy of the neutral Si vacancy with the number of k-points by introducing a rigid offset $\vec{k_0}$ of the sampling grid in the Monkhorst-Pack sampling scheme [13], which means that the k-point sampling is no longer Γ-centered (where Γ is the origin of the reciprocal lattice). For some supercell symmetries (determined by the symmetry of the introduced defect sublattice) the integration was observed to be not ideally efficient when a Γ-centered k-point sampling was performed for some numbers of k-points, hence introducing significant oscillations in both the total energy and the defect energy when the number of k-points was increased. Using optimal offsets for each combination of supercell symmetry and number of k-points maximizes the efficiency of the integration and hence removes the oscillations. This is well visualized in Fig. 2.3, where the convergence of the vacancy formation energy with the number of k-points is plotted for 16-atom and 32-atom supercells. In both cases, the oscillations are clearly reduced by the inclusion of offsets (black squares in the figure), with the most dramatic effect in the case of one k-point, which is the *Gamma*-point without offset. Note that offsets were found to be more beneficial for some supercell symmetries than for others. Introducing offsets thus proves to be an efficient way of improving the convergence of defect properties with the number of k-points. This method however only becomes useful when the optimal offsets can be derived, such as with the approach created by Moreno and Soler [22].

Castleton et al. [15] improved the k-point convergence for smaller k-meshes by using weighted averages over defect formation energy values E_d calculated using a series of grids. The weighted average up to a certain $N \times N \times N$-grid can then be determined using the following equation:

$$\overline{E_d} = \frac{\sum_N w_N E_d(N)}{\sum_N w_N} \tag{2.1}$$

The best choice for the weight factor w_N was found to be N^3, the number of k-points in the Brillouin zone. The advantage of using such weighted averages is clearly shown in Fig. 2.4, with the most dramatic effect for the 4×4×4 grid. The improved convergence behavior is a consequence of the increased k-point density introduced by the weighted average: the points in the 4×4×4 grid are for example not contained in the 6×6×6 grid if the defect energies are not taken into a weighted average [12]. To minimize the computational cost, ab initio codes further reduce the number of k-points by sampling the *irreducible* Brillouin zone (the BZ can be

[8]When an $N \times N \times N$-grid is created, every reciprocal lattice basis vector is subdivided in N numbers, whereafter an equally spaced grid of k-points is created by making linear combinations with respect to. the reciprocal basis vectors of all these subdivisions. Hence, the full Brillouin zone will be sampled by N^3 k-points.

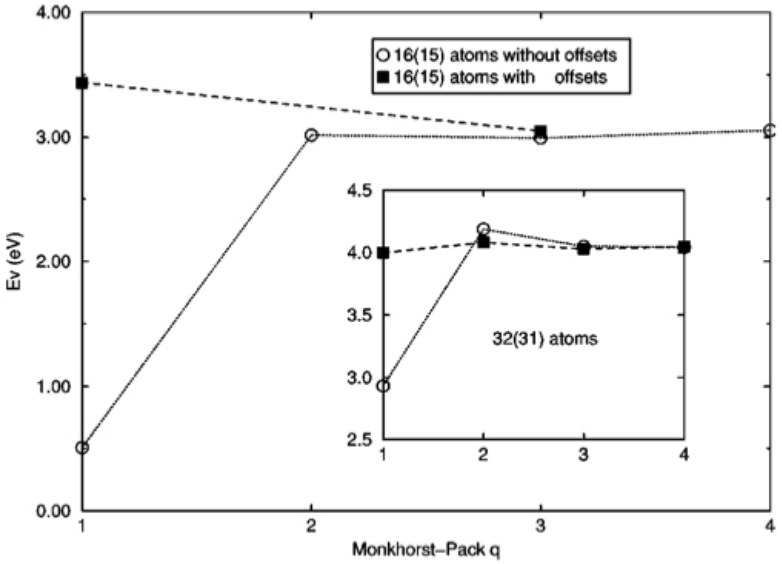

Figure 2.3: Convergence of the unrelaxed neutral vacancy formation energy in Si with the number of k-points for the 16-atom system (without vacancy) and 32-atom system (without vacancy, inset) [13]

reduced by all the symmetries in the point group of the lattice). Setting w_N equal to the number of k-points in the irreducible Brillouin zone (IBZ) also gives an improved convergence, but not as good as in the previous case. Taking unweighted average values (dot-dashed line in Fig. 2.4 is clearly unhelpful. Hence, further calculations of defect formation energies can be performed by taking weighted average values over smaller k-meshes instead of performing one calculation at a high k-point density, which is computationally more costly.

2.1.2.2 Supercell finite-size convergence

Once the electronic structure is converged with respect to the number of k-points, the errors that vary monotonically with supercell size can be removed. Various correction schemes have been suggested during the past decennia, most of them focussing on electrostatic interactions, the leading error terms in the case of semiconductors. The most widely known correction scheme is that of Makov and Payne [23], who predicted the leading terms in the errors to scale linearly and cubicly with L^{-1}. This scheme however does not take into account the errors that do not depend on the charge state, such as elastic interactions, making it only useful to some extent for the convergence of unrelaxed formation energies in semiconductors [15].

A more direct method to remove the finite-size errors was introduced by Probert and Payne [13] in their DFT study of the neutral Si vacancy. They considered all possible supercells with sc, bcc and fcc defect sublattice symmetry, containing between 2 and 256 Si atoms (in the vacancy-free system) and determined the vacancy formation energy both as a function of the number of atoms in the supercell and as a function of the defect density (which is inversely proportional to the supercell size). Both data sets are visualized in Fig. 2.5. There is no apparent trend when the energies are plotted as a function of system size, but the scatter disappears as a function of defect density, with different monotonic trends arising for different supercell symmetries. The scatter

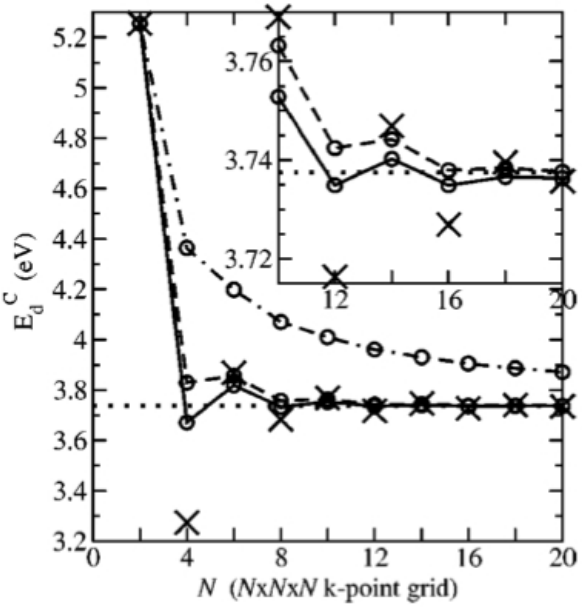

Figure 2.4: Convergence of the defect formation energy of the P interstitial in InP with the number of k-points. ×: calculated values of formation energies. Dotted line: "converged value" from the calculation using a 30×30×30 k-mesh. Dot-dashed: running average over $E_d(N)$. Dashed line: running average weighted by the number of k-points in the IBZ. Solid line: running average weighted over the number of k-points in the full BZ. [12]

in Fig. 2.5(a) is a result of the non-monotonic variation of the defect density when the supercell symmetry changes. Clearly, it is beneficial to plot defect formation energies as a function of inverse supercell size if any trend with respect to supercell size needs to be visualized.

As expected, all trends converge towards the same value in the limit of infinite supercell size, i.e. for a completely isolated defect, which is the system of interest. The rates of convergence however differ for the three symmetries, indicating that an increase in supercell size will not guarantee a better converged solution if the supercell symmetry is changed as well. The differences in convergence rates are explained by Probert and Payne to be the result of two effects: on the one hand, the combination of the geometry of the supercell and the number of nearest neighbors will influence the interaction between the defects. If only this effect would be accounted for, the cells with sc sublattice should converge faster than both bcc and fcc symmetries. The bcc sublattice supercells however converge faster towards the infinite supercell value than both other symmetries. According to Probert and Payne, this is the result of spurious charge movements, caused by the finite size of the supercell, being commensurate with the underlying charge density of the system [13]. In this case, for example, the Si-Si bonds are along ⟨111⟩ directions, whereas the spurious charge movements in the bcc supercell also have a long-ranged component along this direction (Fig. 2.6). For the supercells with sc and fcc sublattices, the long-ranged components of the spurious charge movements are along the ⟨100⟩ and ⟨110⟩ directions respectively, so finite-size effects will be larger and hence convergence will be slower.

Probert and Payne hence demonstrated that large supercells (more than 200 atoms) are required to obtain well converged electronic structures and care needs to be taken if different supercell symmetries are included in the calculations, since different symmetries converge with different

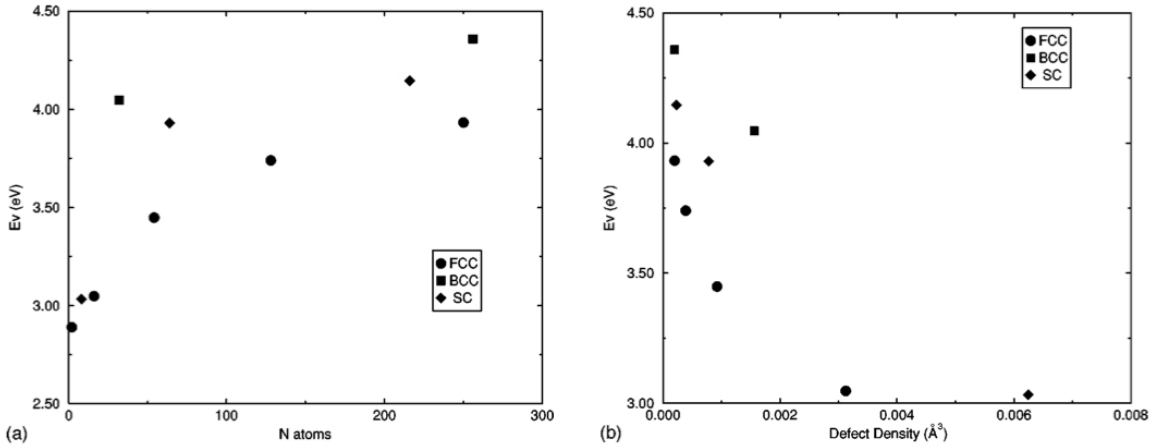

Figure 2.5: Unrelaxed vacancy formation energy as a function of (a) number of atoms in the supercell and (b) defect density [13].

rates towards the physically correct solution. In the case of charged defects, larger cells are expected to be necessary to achieve supercell finite-size convergence due to the presence of long-ranged electrostatic interactions. For such systems correction schemes like that of Makov an Payne could be useful to accelerate the convergence [13]. Interestingly, the same authors expand the basis-set size further before atomic relaxations are performed. The original basis set was converged using the energy differences in the defect formation energy, being correct to second-order errors. The forces on the atoms however are then correct up to first-order errors (forces are proportional to the gradient of the energy), meaning that they converge slower with basis-set size than energies. To ensure accurate relaxations, the forces need to be converged as well, hence the expansion of the basis set. Probert and Payne carried out the k-point and supercell finite-size convergence with a smaller basis set to save computational effort and time [13].

Several authors have performed their calculations using the systematic methodology proposed by Probert and Payne (including their k-point convergence method described in section 2.1.2.1), especially for defect calculations in Si. Corsetti et al. [14] calculated both charged and uncharged Si vacancy properties using this methodology, except for the convergence of the numerical pa-

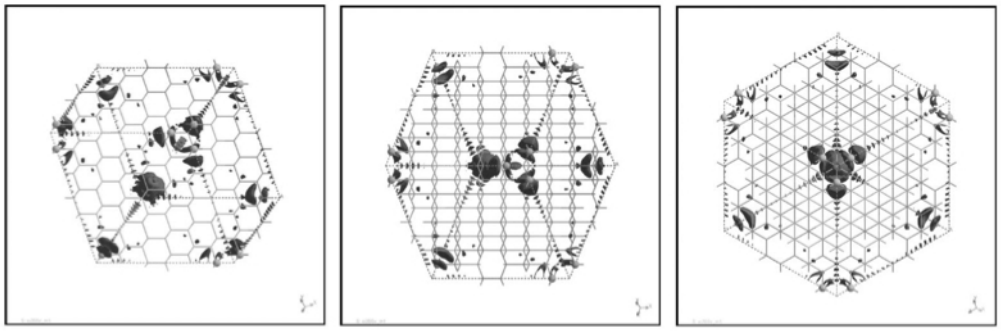

Figure 2.6: Charge density difference isosurface at ρ=0.002 eV/Å^3 between unrelaxed 256- and 255-atom bcc supercells. The leftmost figure is viewed along the [001] direction, the central figure along [011] and the rightmost figure along [111] [13].

rameters (E_{cut}, number of k-points), which they performed for each supercell individually. El-Mellouhi et al. [24] used larger supercells, up to 512 atoms, in their study of diffusion paths of the neutral Si vacancy. The supercell finite-size convergence method of Probert and Payne was also applied by Wierzbowska et al. [25] in their DFT calculations of the Re impurity in Si.

Castleton et al. performed a series of ab initio studies on defect properties in semiconductors during the same period Probert and Payne introduced their methodology [12, 16, 26]. In these studies, they have not only used larger supercells, which was found to be essential by Probert and Payne, but also performed finite-size scalings to the obtained results. This means that for a given supercell symmetry the calculated defect formation energies for different supercell sizes are not only calculated, but also fitted as a function of the inverse supercell size to extract the defect formation energy for the supercell of infinite size [15]. At least three supercells need to be included to perform such a fit. Both unrelaxed and relaxed defect formation energies were found to vary with the supercell size according to a power law:

$$E_d = E_d^{\infty} + a_1 L^{-1} + a_n L^{-n} \tag{2.2}$$

The three fitting parameters are a_1, a_n and E_d^{∞}, where the latter represents the defect formation energy in an infinite supercell and is hence the value of interest. The best value for the exponent n was found to be 3 by means of χ^2-tests, performed on scaling fits to data sets from various defects in InP [12], both relaxed and unrelaxed (using $n = 2, 3$ and 4). This conclusion has been confirmed by others using even larger cells [15]. According to Castleton et al., the linear term (with respect to. L^{-1}) includes both elastic (if relaxed formation energies are investigated) and electrostatic interactions, whereas the volumetric term should predominantly hold for electrostatic interactions. Other studies also included a quadratic term (L^{-2}) in the scaling equation [27], but they are unlikely to be dominant according to the same authors, since this term scales with the surface area: no effects from surfaces are expected to contribute to finite-size errors. The linear and cubic term are more physically justifiable: most error sources should vary with supercell size L (defect-defect distances) and supercell volume L^3 (number of atoms, number of electrons).

Apart from removing the finite-size errors in the calculated defect formation energies, finite-size scaling also offers the possibility to estimate the uncertainty on the energy of the isolated defect E_d^{∞}. Castleton and Mirbt [26] for example determined error bars for the finite-size scalings of various defects in InP. For each defect, 4 calculations were performed (different supercell size, same symmetry) and a finite-size scaling is carried out on this data set. Then, another 4 fitting procedures are performed, in each case omitting one data point from the set. The errors obtained for both relaxed and unrelaxed calculations typically range between 0.01 and 0.1 eV, as can be seen in Fig. 2.7 (E_d^{∞} is the y-axis intersection), and can be further improved by using larger supercells [15]. Remark that in the case of the V_P^0-defect, the extrapolated energy E_d^{∞} differs approximately 0.2 eV from the calculated defect energy of the 512-atom supercell: finite-size scaling could hence be a very attractive tool for determining formation energies of defect that converge slowly with supercell size, since computational limitations make calculations of even larger supercells almost unfeasible.

Other authors have also made use of the finite-size scaling scheme to obtain accurate values for defect properties. Levasseur et al. [28] applied the scheme in their charged defect calculations, in their investigation of the diffusion mechanism of Ga in Si. Puchala and Morgan [29] scaled their data sets of all kinds of defect formation energies in ZnO for their modeling of As diffusion in ZnO. Hine et al. [30] extended the finite-size scaling scheme by also allowing changes in the shape of the supercells, thereby increasing the range of feasible systems in the data set and hence the accuracy of the extrapolated formation energy. This is especially advantageous when the structure's unit cell contains already tens or hundreds of atoms, making it almost impossible to run calculations for larger supercells. According to our knowledge, no authors have so far used the finite-size scaling scheme for defect calculations in transition metals. The question hence remains to which magnitude this scheme is applicable for these materials, since it has especially proved to be very efficient in semiconductors, where electrostatic (and for relaxed energies elastic) interactions are the dominant error term(s). The electrostatic term should however be negligibly small in the case of transition metals due to electronic screening. Elastic contributions on the other hand are even completely absent since only unrelaxed defect calculations are performed.

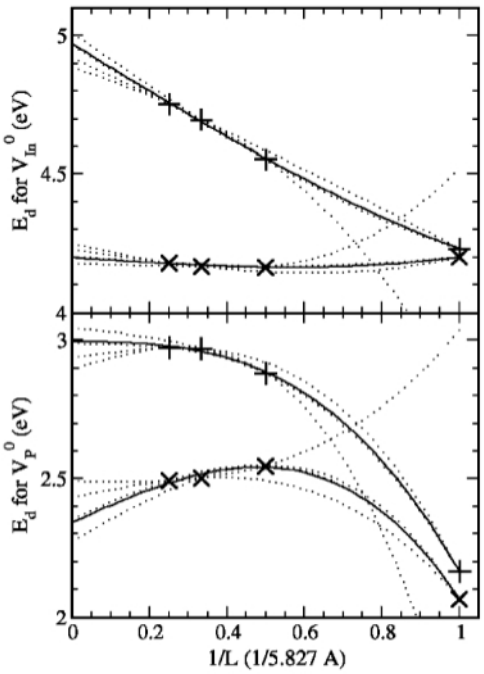

Figure 2.7: Relaxed (×) and unrelaxed (+) formation energies E_d as a function of inverse supercell size, in units of the 8-atom supercell size [26].

2.2 Computational study of point defects in iron

2.2.1 Introduction

Hydrogen fuel cells are considered as relevant future alternatives for internal combustion engines due to their low CO_2-emission and high efficiency [31]. One of the main challenges in the hydrogen fuel technology development concerns the design of materials that are capable of storing and transporting hydrogen-containing fluids safely, i.e. without unexpected failure. High-strength steels are of major interest because of their ability to reduce weight without loss of high mechanical properties, but suffer from (severe) embrittlement when exposed to a hydrogen-containing environment[9], even more than conventional steel grades [32].

To understand this environmentally induced type of fracture, information about the atomic events occurring during hydrogen embrittlement (HE), such as H adsorption on the steel surface, absorption in the bulk and interaction with defects ('hydrogen traps'), is necessary [33]. Several mechanisms have been proposed in the last decennia[10], all supported to some extent by experimental observations [32]. None of these mechanisms can individually explain the complex physics related to hydrogen embrittlement. Instead, a combination is supposed to be responsible for hydrogen degradation in metals [34]. Significant disagreement regarding HE mechanisms however still exists [32]. The complexity of hydrogen-induced embrittlement is not the only problem that prevents a decent understanding of this phenomenon: the low solubility and high mobility of hydrogen in metals make it almost impossible to visualize hydrogen-defect interactions, while the simultaneous effect of different trapping sites available in each microstructure have lead to a wide range of experimentally obtained H-defect binding energies[11] mentioned in the literature [32, 33].

DFT calculations of (point) defect properties in steel have proved to be an important complement to experimental methods, because they can provide information to validate and interpret experimental results and can also provide details that are difficult to access experimentally [**?**]. Several first-principles studies have been performed on the energetics of hydrogen in bulk Fe and its interaction with point defects (acting as hydrogen traps) such as vacancies [**?**, 34, 44–48] and interstitial [44] and substitutional [44, 49] solute atoms in both bcc Fe (α) and fcc Fe (γ). The authors will undoubtedly have been confronted with interactions between a defect and its images due to the finite-size effect of their supercell calculations of defect formation and H-defect binding energies. Very few correction schemes are known to exist for finite-size effects in calculations of defect properties in transition metals, however. The observed supercell finite-size

[9] Either during processing (welding, steelmaking process, galvanizing,...) or in-use (e.g. transportation of hydrogen-containing gases such as hydrogen gas, hydrocarbons or H_2S)

[10] The most viable mechanisms include Hydrogen-Enhanced Decohesion (HEDE), Hydrogen-Enhanced Localized Plasticity (HELP), Adsorption-Induced Dislocation Emission (AIDE) and Hydrogen-Enhanced Stress Induced Vacancy (HESIV), which all rely on the assumption that H accumulates locally in the microstructure at defects, such as grain boundaries, precipitates (interfaces and/or bulk), dislocations and vacancies. These defects act as hydrogen traps because they can retain the hydrogen atoms, either temporarily or permanently, depending on the binding energy between H and the defect. A more detailed description of these mechanisms can be found in Ref. [32]

[11] In the literature, binding energies have been determined using magnetic permeation [35], hydrogen permeation [36, 37], thermal detrapping [38–42] and internal friction [43]

convergence behavior of point defect energies in iron and the applied methods for converging the defect calculations with supercell size are therefore summarized here.

2.2.2 Supercell finite-size convergence methods of point defect properties in Fe

Point defects in α-Fe

Jiang and Carter reported in their DFT study of H-diffusion in bcc Fe in 2004 [33] that examination of the supercell finite-size convergence was lacking in previous studies of interstitial H in bcc Fe. According to these authors, most of them only considered one or two H-concentrations in Fe, the largest cells rarely exceeding 20 atoms. Hence, Jiang and Carter focussed on supercell finite-size convergence of both the unrelaxed and relaxed **dissolution energy** (which is equivalent with the generally defined *defect formation energy* from section 2.1) of an interstitial H defect in the tetrahedral (t-site) and octahedral site (o-site) of bcc Fe (Fig. 2.8). Calculations were carried out for both t-site and o-site since there still remained some doubt about the H site preference in bcc Fe. All calculations were performed with the VASP code, using the PBE functional and an energy cutoff E_{cut} of 350 eV. A 12×12×12 k-mesh was found, during k-point convergence tests, to reduce the error below 0.03 eV for the smallest supercell (Fe_2H), i.e. two Fe-atoms in a bcc lattice with one interstitial H introduced). The H concentrations were varied in 4 supercells from Fe_2H (1×1×1 conventional bcc unit cells) to $Fe_{128}H$ (4×4×4 conventional bcc unit cells). Table 2.1 shows that both the dissolution energy and the energy difference between the o-site and t-site converge rapidly with increasing supercell size, for unrelaxed *and* relaxed calculations. The dissolution energy has converged up to approximately 0.01 eV, which is in the same order of the expected numerical error in their calculations. The authors consider the dissolution energies to be essentially converged with supercell size for the $Fe_{54}H$ system, without investigating the dilute limit. Their calculations however predict that H prefers the t-site over the o-site, with a ZPE-corrected[12], relaxed dissolution energy of 0.301 eV/H-atom at the t-site, which is in good agreement with previous DFT calculations and experiments.

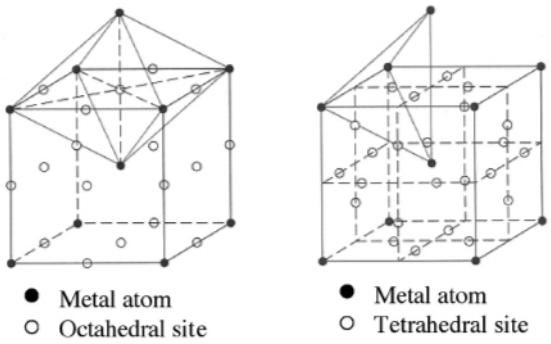

Figure 2.8: Positions of the octahedral (left) and tetrahedral (right) sites in bcc Fe [33].

[12]ZPE correction = Zero-Point Energy correction: the ZPE is obtained by summing up the zero-point vibrational energies of the H's normal modes.

Supercell	$E_{diss,t}$, unrel. (eV)	ΔE_{diss}, unrel. (eV)	$E_{diss,t}$, rel. (eV)	ΔE_{diss}, rel. (eV)
Fe_2H	0.45	0.51	0.20	0.01
$Fe_{16}H$	0.27	0.47	0.16	0.13
$Fe_{54}H$	0.28	0.46	0.19	0.13
$Fe_{128}H$	0.29	0.47	0.20	0.13

Table 2.1: Unrelaxed and relaxed dissolution energies E_{diss} of H in the t-site of bcc Fe and energy differences between H in the o-site and t-site as calculated by Jiang and Carter [33].

Sanchez et al. also investigated interstitial H energetics in bcc Fe [50]. Using CASTEP, they considered a cut-off energy of 375 eV and a 14×14×14 k-mesh from convergence tests on a pure bcc Fe unit cell to be accurate enough for most of their calculations. Only the energy difference between H at the o-site and t-site was converged with supercell size, with $Fe_{54}H$ being the largest system considered. According to these authors, H does not interact with other H atoms at these concentrations. In contrast to Jiang and Carter, they find the o-site to be more stable in Fe_2H. The t-site however becomes preferable for the larger cells, with the energy difference converging to approximately 0.11 eV, in good agreement with Jiang and Carter.

More recently, Wolverton and Counts performed a DFT study concerning the energetics of hydrogen traps in bcc Fe, exclusively focussing on point defects [44]. They also made use of VASP, using the PBE functional and E_{cut} = 450 eV. A k-mesh of 6×6×6 was found to be sufficient for a $Fe_{54}H$ (3×3×3 conventional bcc unit cells) . The supercell finite-size convergence was tested by computing and comparing various relaxed defect formation (H, C, vacancy) and binding energies (H-H, H-C, H-vacancy,. . .) for the supercells with 3×3×3 and 4×4×4 unit cells. According to the authors, the differences were found to be 0.03 eV at most, which is in the same order as the numerical error. They therefore concluded that calculations in 3×3×3 supercells will be fully converged with respect to. supercell size. Their results are in good agreement with previous theoretical and computational studies. In the case of the hydrogen dissolution energy at the t-site, for example, they found a similar value as Jiang and Carter (0.30 eV). The computed vacancy formation energy of 2.17 eV is a bit higher than the one obtained by Tateyama and Ohno (2.0 eV) [48], but their predicted equilibrium H-vacancy configuration and binding energy agree very well. Tateyama and Ohno focussed mainly on k-point convergence of the vacancy formation energy, concluding that a k-mesh of 3×3×3 is sufficient for a 3×3×3 (54-atom) bcc supercell. The difference in formation energy with the 128-atom supercell was found to be approximately 0.1 eV. H-vacancy properties however were not observed to have changed significantly, hence a 54-atom supercell was considered to give well converged properties.

Psiachos et al. dealt in a particular and simple way with the finite-size errors in their study of **H-substitutional atom interactions** [49]. Because they a.o. investigate the evolution of the relaxed binding energy of H and substitutional transition metals with separation distance, the finite-size contribution to the binding energy can be estimated from the non-zero asymptotic value of the distance-dependent binding energy (Fig. 2.9(a)): the authors consider elastic interactions due to a limited supercell size to be the reason for the non-absent interactions at large

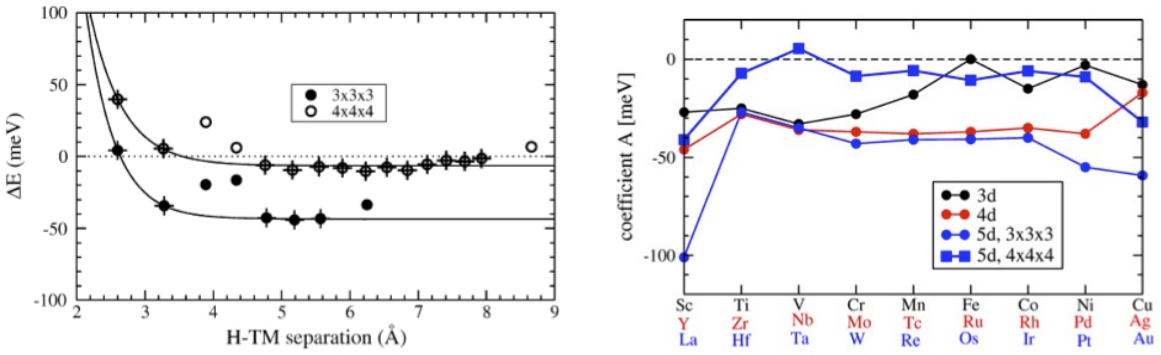

(a) (b)

Figure 2.9: (a) Distance dependence of the H-TM (transition metal) interaction energy for W from DFT calculations. (b) The coefficient A as obtained by fitting the DFT results to eq. (2.3) for different H-transition metal combinations and different supercell sizes. [49]

H-TM separation distance. The data for both the 3×3×3 and 4×4×4 supercell are fit to the simple exponential function

$$\Delta E(R) = A + B\exp(-CR) \tag{2.3}$$

that describes the monotonic decay of the binding energy with separation distance. The fitting parameter A can then be interpreted as a measure of the finite-size effects (since it should be 0 at infinite H-TM distance, which is clearly not observed in the considered supercells). In this way, the finite-size effect introduced by each H-TM pair can be visualized. From Fig. 2.9(b), it can be seen that the value of A is largest for the 5d transition metals (±0.05 eV) but can be significantly reduced by increasing the supercell size to 4×4×4 (±0.01 eV). A plausible reason why 5d transition metals create stronger finite-size effects is the large elastic disturbance these elements induce in the Fe lattice due to their large atomic radii.
Wolverton et al. also performed a DFT study of H binding with substitutional atoms in bcc Fe [**?**]. They investigated the supercell finite-size convergence with similar tests as in their study of the energetics of hydrogen traps in bcc Fe [44], which was discussed earlier. They found differences of at most 0.015 eV between the formation and binding energies of H-H and H-substitutional atom defects in 3×3×3 and 4×4×4 supercells for the same numerical parameters as in their earlier mentioned study. The 54-atom cells were therefore used in their further calculations.

Point defects in γ-Fe

The group of Neugebauer et al. have performed a set of DFT studies [18, 34, 51, 52] on H-defect interactions in fcc Fe, since austenitic steels are under certain conditions also affected by HE, despite the low H permeability and high H dissolution capability in γ-Fe. There were no systematic studies on hydrogen in γ-Fe known to the authors before their first-principles investigation of H solubility and kinetics in austenitic high Mn steels [51]. In this study, DFT calculations were carried out with the VASP code, using the PBE functional and E_{cut} = 270 eV. K-point convergence tests of all 32-atom cells (with varying Mn-concentrations) showed

that a 8×8×8 k-mesh is necessary to achieve an accuracy of 0.01 eV. The supercell finite-size convergence was performed by calculating the relaxed H dissolution energy at the o-site in fcc Fe for 1×1×1 (Fe_4H), 2×2×2 ($Fe_{32}H$) and 3×3×3 ($Fe_{108}H$) supercells. The results in Table 2.2 point out that a 2×2×2 supercell yields an error of 0.02 eV, which is in the order of the numerical error of the k-point integration. The 32-atom cells were therefore considered to produce well converged defect energies. Experimental studies report dissolution energy values between 0.23 and 0.28 eV, however. The large difference between these values and the results in Table 2.2 is a consequence of ZPE and magnetic effects that were not included in the calculations. It is known that fcc Fe has a complex magnetic structure: the magnetic ground-state has been confirmed by both experimental and computational studies to be a spin-spiral structure [51]. Due to its complexity, this state is difficult to implement in DFT calculations, hence magnetic effects were investigated by performing calculations for the ferromagnetic high-spin (FMHS) and antiferromagnetic double-layer (AFMD) collinear structures. For the latter structure, which has already been shown to be the most stable collinear magnetic configuration at 0 K, the solution enthalpy was found to be 0.13 eV. Including a ZPE-correction of 0.07 eV, the dissolution energy amounts to 0.20 eV, in better agreement with experimental values. In their study of H interaction with grain boundaries in α- and γ-Fe [52], the group of Neugebauer nevertheless employed nonmagnetic calculations because of the relatively small magnetic effect (O(0.05eV)). 32-atom supercells were used as a result of their convergence tests in the above mentioned study.
The vacancy formation energy was also converged with supercell size by Neugebauer et al. in their study of H-vacancy interactions in γ-Fe [34]. The same conditions were applied as in the previous investigation, except for the cut-off energy, which was increased to 300 eV. Relaxed vacancy formation energies were calculated for 2×2×2, 3×3×2 and 4×4×4 supercells. Interestingly, the authors searched for the extrapolated limit of the energy at zero-vacancy concentration in the same way as Probert and Payne did [34]. The dilute limit was however only investigated for relaxed formation energies, whereas Probert and Payne first checked the supercell finite-size convergence of unrelaxed energies before any relaxations were performed. Their result for the AFMD magnetic structure (1.84 eV in the dilute limit) is nevertheless in good agreement with experimental results of 1.7 ± 0.2 eV. 3×3×2 supercells yield a formation energy with an error below 0.1 eV compared to the dilute limit and were therefore used in further H-vacancy calculations. In their study of the influence of exchange-correlation functionals on vacancy formation energies in fcc-metals [18] however, a 2×2×2 supercell was found to be sufficient to achieve an accuracy better than 0.1 eV for vacancy formation energy calculations of fcc crystals in general.

	$\mathbf{Fe_4H}$	$\mathbf{Fe_{32}H}$	$\mathbf{Fe_{108}H}$
$\mathbf{E_{diss,o}(eV)}$	0.13	0.06	0.04

Table 2.2: H dissolution energy at the o-site in nonmagnetic fcc Fe (without ZPE-corrections) as a function of supercell size as obtained by Neugebauer et al. [51]

Point defect property calculations in Fe using (semi)-empirical potentials

Some authors have performed calculations of defect properties in the Fe-H system using (semi-) empirical interatomic potentials. These allow to consider more realistic system sizes containing even millions of atoms, but at the cost of a lower accuracy compared to first-principles methods such as DFT [47]. Lee and Jang [45] report the application of the embedded-atom method (EAM) and *modified* embedded atom (MEAM) type potentials to the Fe-H system. In contrast with EAM potentials, MEAM potentials are highly applicable because they can describe a wide range of elements using the same formalism and functional form. Therefore, Lee and Jang developed such a potential for the Fe-H binary system both in bcc and fcc Fe [45] and tested it by calculating physical properties such as the H dissolution energy. The constructed potential contains several model parameters which are fitted to known physical properties of the Fe-H system. The quantities of interest are calculated using a 10×10×10 supercell (containing 2000 atoms) for bcc Fe and a 6×6×6 supercell for fcc Fe. According to the authors, the calculation results were independent of system size for these supercells. Agreement of dissolution energies with experiments and other computational studies is fair: differences are attributed to the lower accuracy of the semi-empirical potential. Ramasubramaniam et al. [47] indeed found this MEAM potential to accurately predict bulk interstitial properties of H in Fe. The core structure of screw dislocations in Fe predicted by this potential however does not agree with results from DFT calculations. To improve the accuracy and predictive capability, Ramasubramaniam et al. fitted their interatomic potentials to a set of DFT calculations in α-Fe. The bulk dissolution energy was modeled using a 54-atom supercell, a cut-off energy of 500 eV and a 6×6×6 k-mesh, giving a convergence of the total energy of the supercell within 1 meV/atom and of the H dissolution energy within 2 meV/atom. The potentials, fitted to the calculated dissolution and binding energies, result in dissolution energies (0.287 eV and 0.297 eV) that are in good agreement with the DFT calculations by Jiang and Carter [33] and Tateyama and Ohno [48]. H-vacancy binding energies are also in good agreement with previous experimental and computational studies. (Semi-) empirical potentials are hence found to be increasingly capable of producing fairly accurate values of defect properties in the Fe-H properties and could hence be an attractive alternative to DFT calculations in the future because of the large system sizes that can be handled.

Conclusions

DFT calculations of point defect formation energies in fcc Fe are generally found to be sufficiently converged with supercell size when a 2×2×2 supercell is used, in contrast to calculations in bcc Fe, where 3×3×3 cells generally result in well converged defect energy values. The H-TM binding energy forms an exception for 5d transition metals, where 4×4×4 cells give better converged values, but the specific correction scheme introduced by Psiachos et al. allows using smaller 54-atom cells. Supercell finite-size convergence has been tested in all of these studies, but no specific correction scheme, as those proposed by Probert and Payne on the one hand and Castleton et al. on the other, is used to attain well converged defect energies. Additionally, 4×4×4 supercells are

the largest cells considered in all of these studies, while residual interactions between H, or other point defects, and its images are never investigated. Rather, the defect energies obtained after E_{cut}- and k-point convergence and atomic relaxation are compared for different supercell sizes. The supercell yielding a formation energy error with respect to a larger cell that is smaller than the assumed numerical error is usually expected to be free of defect interactions and is chosen for further defect calculations, usually to determine H-defect binding energies. Neugebauer et al. are the only authors known to have performed a dilute limit fit as proposed by Probert and Payne, in the case of their calculated vacancy formation energies in fcc Fe, and to have used this dilute limit value of the formation energy. They however made use of relaxed instead of unrelaxed formation energies, hence not entirely following their correction scheme. Jiang and Carter also investigated the convergence of *unrelaxed* energies, showing that the unrelaxed H dissolution energy in the 128-atom cell is already well converged and hence could be assumed to be appropriate for further atomic relaxations according to Probert and Payne's correction scheme. The use of even larger supercells and an investigation of H-image interactions could be critical tests regarding this conclusion. The obtained values of defect formation energies are nevertheless generally in good agreement with experimental results, making the use of such correction schemes seem unnecessary. A systematic study of the supercell finite-size convergence of defect formation energies in the Fe-H system could therefore be very useful to judge the applied convergence tests of previous studies correctly.

Chapter 3

Methodology

3.1 Objective

Due to the lack of correction schemes used in the supercell finite-size convergence tests of Fe-H related systems, a thorough investigation of the supercell size-related errors can provide insight into the need for such correction schemes and in how far defect formation energies obtained in the literature are well converged with supercell size. To our knowledge no study has so far reported the complete isolation of defects in a supercell, meaning that in practice bulk-like atoms between the defects still feel the influence of the spurious defect interactions. The question therefore arises to what magnitude remaining interactions cause calculated observable defect properties, such as energies and forces, to differ from the ideal, isolated defect properties and whether isolated defects actually *can* be obtained for a particular minimum supercell size. Once we are confident about these properties, atomic relaxations (requiring accurate forces) and calculations of defect-defect binding energies can safely be performed.

In this work, the reference system for the Fe-H finite-size convergence investigation was chosen to be the tetrahedral interstitial H impurity in bulk, ferromagnetic bcc Fe. The major advantage of choosing this system is the vast amount of DFT studies reporting their methodology results for their supercell calculations of the H dissolution energy in bulk Fe. This is the defect formation energy corresponding to the tetrahedral interstitial Fe-H system and needs to be calculated as a reference for any H-defect binding energy in Fe. Conclusions from our research can therefore easily be compared with the literature.

Finite-size errors in supercell calculations were already encountered at the Center for Molecular Modeling, and most clearly by Francis Caestecker in his Master's thesis about ab initio calculations of mixing enthalpies in bulk metallic glasses [53]: the calculated dissolution energy of the substitutional Zr-impurity in a Cu host lattice was found to be not well converged for supercells containing up to 128 atoms in both fcc, bcc and sc Cu host lattices. Energies of the fcc sublattice symmetry in a fcc Cu host lattice are not even converged within 0.1 eV for the largest cells considered, as shown in Fig. 3.1. Notice also the different convergence trends for all sublattice symmetries, as observed by Probert and Payne [13]. Since data from Caestecker's

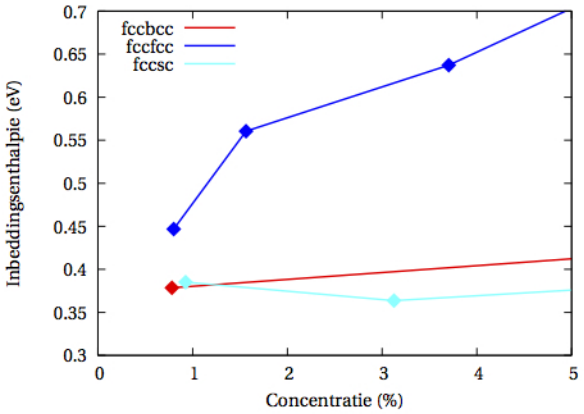

Figure 3.1: Dissolution energy (embedding enthalpy) per Zr-atom added as a function of Zr-concentration in the fcc Cu host lattice [53].

supercell calculations were available to compare with and unanswered questions concerning the supercell finite-size convergence behavior of the Zr dissolution energy remain, the Cu-Zr system was considered to be ideally suited to start our supercell finite-size convergence research of various defect properties. Calculations were performed on the fcc Cu supercells, extending the data set from Caestecker up to 1000 atoms, which is approximately the largest supercell computationally feasible in a realistic time span and with a realistic amount of computational resources. In order to obtain well converged dissolution energies, our investigation was carried out by following the same steps as in the methodology proposed by Probert and Payne [13]:

1. Convergence of the total ground-state energy and forces with respect to basis-set size (E_{cut}) on the smallest (in this case, 4-atom) supercell;
2. k-point convergence of the total ground-state energy and forces on the same supercell;
3. Supercell finite-size convergence of the Zr dissolution energy.

In order to obtain dissolution energies that can be compared with experimental values, the Cu-atoms in the vicinity of the Zr-impurity need to be relaxed. To clearly distinguish between finite-size effects on the dissolution energy and effects due to the relaxation, the positions of all atoms were kept fixed in our calculations. Hence, a 'pseudo'-dissolution energy will be found. Our goal is to establish its value without remaining finite-size errors. Once this problem is solved, it is straightforward to conduct a relaxation procedure in order to compare the calculated dissolution energy to experiments.

Most studies focus exclusively on the supercell finite-size convergence of the formation energy of the particular defect of interest. Other properties, such as forces and (local) density of states, can however also be obtained with ab initio codes. In order to compare the supercell finite-size convergence behavior of all these properties with the dissolution energy, force and density of states calculations were performed as well. In addition, the spurious defect interactions as a function of supercell size were also investigated by visualizing the change in charge distribution due to the introduction of a Zr-atom.

Conclusions drawn from the Cu-Zr supercell finite-size convergence investigation were subse-

quently transferred to the Fe-H system. In order to compare with studies from the literature, the H dissolution energy was calculated for various H-concentrations (i.e. supercell sizes). Since no study has been found to include supercells containing more than 128 Fe atoms (corresponding to a cubic ordering of 64 conventional bcc unit cells), the data set in this work was extended with a supercell of 250 atoms. The dissolution energies were first calculated using the methodology of the Cu-Zr system, as described above, in order to compare with the values obtained via the adjusted methodology, taking into account the conclusions from the Cu-Zr investigation. A study of the supercell size behavior of forces and density of states in the Fe-H system was not performed due to time limitations.

In the following section, the ab initio code that was used for all our calculations and the parameter settings within this code are described, followed by a discussion of the construction of all considered supercells and the methodology behind the calculation of the physical properties of interest. The results from the k-point (and E_{cut}) convergence tests on the Cu-Zr and Fe-H systems are discussed in the last section of this chapter.

3.2 Vienna Ab Initio Simulation Package (VASP)

All ab initio calculations in this work were performed with version 5.2.2 of VASP (Vienna Ab Initio Simulation Package) [54–56], a DFT-based quantum-mechanical code that makes use of a plane-wave basis set in combination with PAW potentials or pseudopotentials (in this work, VASP calculations were performed using PAW potentials). The solutions to the Kohn-Sham equations are determined by VASP via a self-consistent procedure, which was already discussed in chapter 1.

VASP requires 4 input files: *INCAR*, *POSCAR*, *KPOINTS* and *POSCAR*. *INCAR* is the central input file in VASP and contains all desired settings of the calculation, such as the basis-set size (via E_cut) or the self-consistent cycle convergence criterion. The positions of the ions (nuclei) and the geometry of the supercell are written in *POSCAR*. The *KPOINTS*-file determines the k-point settings: the k-mesh in our calculations is generated automatically, using the Monkhorst-Pack sampling scheme [8], which only requires providing the k-grid size and origin in terms of the basis vectors of the reciprocal primitive unit cell. In this way, l×l×l subdivisions of the basis vectors lead to l^3 k-points in the first Brillouin zone. To reduce the number of k-points (and hence calculation time), VASP only considers k-points in the irreducible Brillouin zone, which are called *irreducible k-points*. The k-mesh was always *Gamma*-point centered in our calculations (i.e. centered around the origin of the reciprocal lattice). Finally, information about the pseudopotentials of all species considered, in addition to data such as the valence sate and mass of these species, can be found in *POTCAR*.

VASP calculations on atomic systems containing tens to hundreds of atoms (which are common practice within computational materials research) are impossible to perform on a regular personal computer due to the high computational cost. All calculations were therefore executed using the high-performance computing (HPC) facilities at Ghent University. Especially

the Gengar-cluster was used, since its 192 nodes (where each node consists of 8 CPU's or central processing units) make it very suitable for high-demanding applications: via a Message Passing Interface (MPI) the calculation can be distributed between parallel nodes, thereby reducing the calculation time drastically. The largest calculations, on the other hand, were performed on the new Tier1 infrastructure of the Flemish Supercomputing Center (VSC), which contains 528 16-processor nodes.

3.2.1 Choice of potentials

It was already mentioned in chapter 1 that our calculations were carried out using the PAW method, in combination with the GGA-PW91 (Perdew Wang 1991) exchange-correlation functional [5]. For some elements several PAW potential versions exist, differing in the required basis-set size or the number of electrons treated as valence. Kresse et al. [56] advise for example for d-metals to treat semi-core p-states and sometimes semi-core s-states as valence electrons, giving more accurate results. In the case of Cu, the standard PAW potential is accurate enough for all calculations, meaning that no semi-core p- or s-states need to be included. This seems fairly intuitive: Cu has the [Ar] $3d^{10}4s^1$ valence state, so the energy of the semi-core p- and s-states lie fairly deep beneath the Fermi energy level. Hence, the Cu semi-core states are not expected to contribute a lot to the metallic bonding. In the case of Zr however, with a [Kr] $5s^2 4d^2$ valence state, 4s- and 4p-electrons will have energy levels lying closer to the Fermi energy and could therefore play a role in the metallic bonding. Nevertheless, the standard Zr potential (with only 4 valence electrons) was used for all Cu-Zr supercell calculations to save computational time: including more valence electrons means that a higher E_{cut} is needed and hence the calculation time increases (see section 1.4). For some Cu-Zr supercells, calculations were also performed with the extended potential (including 12 valence electrons) to investigate the influence of the choice of Zr pseudopotential. The Fe and H potentials used for the calculations of interstitial hydrogen in bcc Fe are the standard versions, so in the case of the Fe potential 8 electrons are treated as valence (Fe valence state: $4d^6 5s^2$) and for the H potential the single 1s-electron is treated as valence.

3.2.2 Settings in *INCAR*

It is worth discussing some of the parameter settings in the *INCAR*-file, in view of a comparison with and reproduction of results obtained in this work. The level of accuracy of a self-consistent VASP cycle can be varied with the PREC-tag from "low" up to "accurate" and was set to "accurate" for both Cu-Zr and Fe-H supercell calculations. In this way, the number of lattice points that are used in the mesh for discrete Fourier transformations are maximized. The parameters ISMEAR and SIGMA are related to the partial occupancies of the wave functions. This is particularly important for conducting materials such as metals, since the Fermi level lies in the conduction band: the discontinuity in energy state occupancy at the Fermi level causes difficulties in the Brillouin zone integration. The partial occupancies are therefore slightly altered to remove this discontinuity, i.e. the orbital occupancies near the Fermi level are *smeared*. The

ISMEAR-tag determines the smearing method, whereas SIGMA determines the width of smearing (in eV). Kresse et al. [56] recommend the Methfessel-Paxton smearing method (ISMEAR = 1 in the *INCAR*-file) and a smearing width of 0.2 eV (SIGMA = 0.2) for metals. These settings were therefore also applied to all Cu-Zr and Fe-H calculations.

Another parameter, LREAL, was particularly set to limit the time required for each iteration in the self-consistent procedure. This parameter determines whether the so-called projector operators (see ref. [56]) are evaluated in real space or reciprocal space. The number of operations that need to be carried out scale with the system size when the operators are evaluated in reciprocal space, whereas it becomes independent of system size in real space. Kresse et al. [56] advise to use real space for systems containing roughly more than 20 atoms to save computational time. Therefore, the LREAL-tag was switched to "Auto" for such supercells in our calculations. For smaller systems, LREAL was set to "FALSE".

For the Fe-H system, two other parameters needed to be considered due to the ferromagnetic nature of bcc Fe. Ab initio calculations of magnetic materials need to spin-polarized, meaning for a ferromagnetic material that the magnetic moments of the electrons need to aligned. This is done in VASP by switching the ISPIN-tag from the default ISPIN = 1 (non-spin-polarized calculation, for paramagnetic materials) to ISPIN = 2. An initial guess of the magnetic moments is necessary when starting from scratch or when information on the magnetization density is absent in the *CHGCAR*-file, which contains the electronic charge density data from a VASP calculation. In our Fe-H calculations, a non-spin-polarized calculation (ISPIN = 1) was performed initially to create a non-magnetic *CHGCAR*, followed by a spin-polarized calculation (ISPIN = 2) to converge to a reliable magnetic solution, as recommended by Kresse et al. [56]. They also suggest to set the initial magnetic moments large enough to obtain reliable results. Therefore, the initial magnetic moment was set to $4\mu_B$ for Fe and $1\mu_B$ for H.

The *INCAR*-file also contains the cut-off energy E_{cut} (via the ENCUT-tag) and the EDIFF-tag, which is the allowed error on the total ground-state energy from a self-consistent procedure. The calculation ends when the energy difference between two subsequent iterations in the calculation is lower than EDIFF. The values for these parameters were determined for both systems in the convergence tests, which are discussed in the following section. An overview of all *INCAR*-settings in Cu-Zr and Fe-H is given in Table 3.1.

3.3 Supercell construction

Supercells were constructed for both systems via the *supercell*-tool that comes with Wien2k, another DFT-based quantum-mechanical code [19]. A *POSCAR*-file of each supercell of the pure host lattice is constructed by specifying the desired number of unit cells of the pure lattice in each dimension. In each case, cubic N×N×N supercells are constructed. For the corresponding defect-containing supercells, the impurity atom position(s) were applied in the *POSCAR*-files.

Via this procedure, the size of the pure fcc Cu and Cu-Zr supercells was varied from 1×1×1 (the 4-atom, conventional fcc unit cell) to 4×4×4 conventional fcc unit cells (256 atoms). An

	Cu-Zr	Fe-H
PREC	Accurate	Accurate
ISMEAR	1	1
SIGMA	0.2	0.2
LREAL	Auto	Auto
ISPIN	1	2
MAGMOM	-	N*4 + 1

Table 3.1: Parameter settings in the *INCAR*-file for all Cu-Zr and Fe-H calculations. Remark that LREAL = FALSE for systems smaller than 20 atoms (minority of cells), the Fe-H calculations using ISPIN = 2 are always performed after a non-spin-polarized calculation using ISPIN = 1 and N in the MAGMOM-tag is the number of Fe-atoms in the corresponding Fe_NH-supercell.

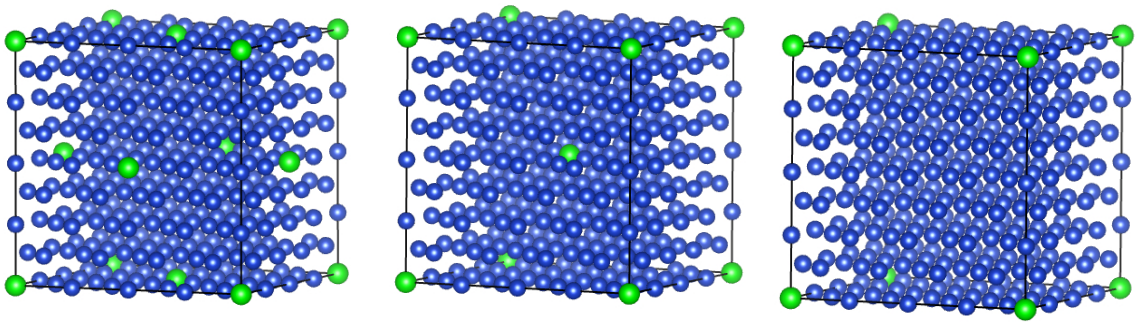

(a) (b) (c)

Figure 3.2: 256-atom Cu-Zr supercells with (a) fcc, (b) bcc and (c) sc Zr sublattice symmetry. Cu-atoms are shown in blue, Zr-atoms in green.

equilibrium lattice parameter of 3,637 Å was found by Caestecker for the conventional fcc Cu unit cell and was used for the construction of all supercells [53]. The Zr sublattice symmetry was varied for each system size, as shown in Fig. 3.2 for the fcc, bcc and sc sublattice symmetry in the 256-atom cell. Additional, larger supercells were created for the fcc sublattice symmetry since for this sublattice symmetry the Zr dissolution energy was found to converge very badly (Fig. 3.1). The Zr-Zr distances were maximized up to the computational limit, resulting in additional supercells containing up to 1000 atoms. The 512-atom and 1000-atom supercells are shown in Fig. 3.3. In contrast to all other supercellls, these cells are primitive unit cells (containing only one Zr-atom). They were calculated with a script from K. Lejaeghere from the $6 \times 6 \times 6$, $8 \times 8 \times 8$ and $10 \times 10 \times 10$ conventional supercells, respectively, by means of the spglib and ASE [57] packages. Using the primitive cells reduces the number of atoms to a quarter of the conventional supercells. Since the calculation time of a self-consistent procedure scales cubicly with the number of valence electrons in the cell, calculations are in this way made computationally feasible for such low defect concentrations.

To discriminate between the different supercells, a particular terminology will be introduced in the context of this thesis. The notation for each supercell is determined by the number of host lattice conventional unit cells considered in each dimension and the host (fcc) and sublattice

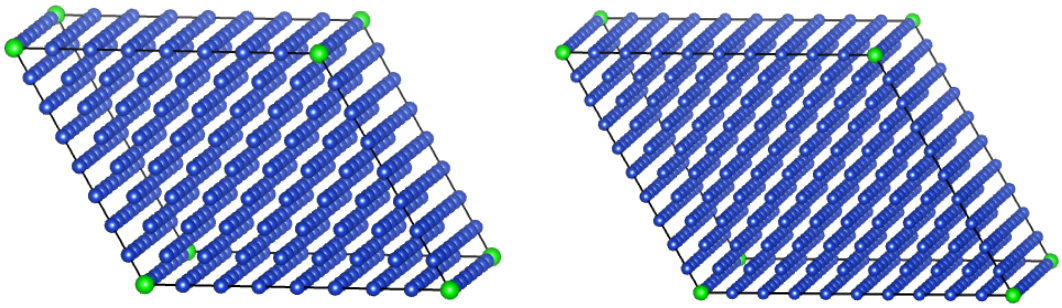

(a) (b)

Figure 3.3: (a) 512-atom (fccfcc8) and (b) 1000-atom (fccfcc10) primitive cells of the corresponding $8 \times 8 \times 8$ and $10 \times 10 \times 10$ conventional supercells with fcc sublattice symmetry. The cell axes lie along [110], the primitive basis vectors of the fcc lattice.

(fcc, bcc or sc) symmetry. A 2×2×2 conventional supercell for example with fcc Cu as host lattice and only Zr-atoms at the corners of the supercell is denoted by fccsc2. All considered Cu-Zr supercells for the supercell finite-size convergence investigation of the Cu-Zr system are listed in Appendix A.

The bcc Fe and Fe-H supercells are constructed with conventional bcc Fe unit cells and a hydrogen atom inserted in a tetrahedral interstitial position. The supercell sizes vary from 1×1×1 to $6 \times 6 \times 6$ conventional unit cells. Each supercell will be denoted by the number of Fe and H atoms: the $2 \times 2 \times 2$ for example, which is also shown in Fig. 3.4, contains 16 Fe atoms (8 conventional bcc Fe unit cells) and 1 H atom and hence will be denoted as $Fe_{16}H$. All Fe-H systems considered in our supercell finite-size convergence calculations are also summed up in Appendix A.

3.4 Determination of physical properties

The supercell finite-size convergence was investigated for physical properties that are easily accessible with VASP. While the dissolution energy of the impurity is the main property of interest for both the Cu-Zr and Fe-H system, forces on and local density of states (LDOS) of particular atoms in the Cu-Zr system were also checked for supercell finite-size convergence. In the following paragraphs, the methods behind the calculation of these properties are described.

3.4.1 Local density of states (LDOS)

A DOS calculation can be done in VASP following a two-step procedure [56]: first, the charge density, written to the *CHGCAR*-file, is calculated via a self-consistent run with a relatively low number of k-points. The k-mesh used for this self-consistent procedure will be discussed in the next section. In the second step, a non-self-consistent calculation is performed using the *CHGCAR*-file from the previous step. This is done by switching the ICHARG-tag in the

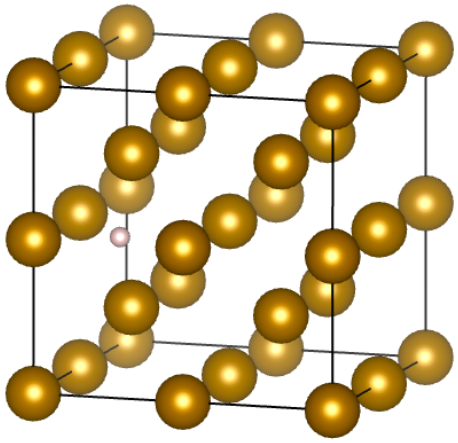

Figure 3.4: $Fe_{16}H$ supercell: the pink hydrogen atom is placed at an interstitial position in the bcc Fe lattice (brown)

INCAR-file to 11. A high quality DOS usually requires a high number of k-points. Therefore, the k-mesh size in the second step was consistently increased for the DOS calculation of each Cu-Zr supercell, as will be discussed in the next chapter.

Via this procedure, the density of states of the whole system, which is called the 'total DOS', can be calculated and visualized. However, in this work the supercell finite-size convergence of the *local* density of states, i.e. in the neighborhood of particular nuclei in the Cu-Zr supercell is investigated. This requires the setting LORBIT = 10 in the *INCAR*-file, making VASP calculate the site-projected wave function character of each energy band using a quick projection scheme that only works with the PAW method [56]. In addition, information about the s-, p- and d-character of the site-projected wave function can be obtained.

3.4.2 Force

The supercell finite-size convergence of the forces in the Cu-Zr system was investigated by determining the force on the first (NN1), second (NN2) and third (NN3) nearest neighbor Cu-atoms to the substitutional Zr impurity for each supercell in Table A.1. In quantum mechanics, the X-component of the force on a particular nucleus γ in the system is equal to [3]:

$$F_{X_\gamma} = -\frac{\partial \langle \psi | \hat{H} | \psi \rangle}{\partial X_\gamma} \tag{3.1}$$

In this equation, ψ is the wave function of the many-electron system and $\hat{H}$ the Hamiltonian of the same system, as defined in Chapter 1. $\langle \psi | \hat{H} | \psi \rangle$ represents the expectation value of the energy for a quantum state ψ of the system with Hamiltonian $\hat{H}$. To determine the force component F_{X_γ}, the derivative $\frac{\partial \psi}{\partial X_\gamma}$, which contains information about the way the wave function of the system changes when the nucleus is moved, needs to be known. This term is very complex to determine and would therefore make the calculation of atomic forces a difficult task. Fortunately,

the Hellmann-Feynman theorem states that:

$$\frac{\partial \langle\psi|\hat{H}|\psi\rangle}{\partial X_\gamma} = \left\langle \psi \left| \frac{\partial \hat{H}}{\partial X_\gamma} \right| \psi \right\rangle \tag{3.2}$$

This simplifies the expression for the force substantially, since only the way the Hamiltonian changes with a change in nucleus position needs to be known. DFT however does not yield the ground state wave function, but the ground state electron density $\rho(\vec{r})$, from which the total ground-state energy $E_{V_{ext}}[\rho]$ can be calculated. Since $E_{V_{ext}}[\rho]$ is exactly $\langle\psi|\hat{H}|\psi\rangle$, with ψ the ground-state wave function of the many-body system, the force can be calculated by evaluating the derivative of the total ground-state energy with respect to the position of the nucleus of interest:

$$\vec{F}(\vec{R}) = -\frac{\partial E_{V_{ext}}[\rho]}{\partial \vec{R}} \tag{3.3}$$

This is exactly the way VASP calculates forces on nuclei. The force on each nucleus in a particular supercell can be found in the *OUTCAR*-file when using the VASP code.

3.4.3 Dissolution energy

The defect formation energy is equivalent with the dissolution energy in the case of the substitutional Zr and interstitial H impurity. This property is a measure of the amount of energy required to form the point defect complex (i.e. to substitute a Cu-atom by a Zr-atom in the Cu-Zr system, or add a H-atom to bcc Fe in the Fe-H system), with the ground-state energy of the pure materials as a reference [44]. The dissolution energy of one impurity atom can be determined for each supercell size with the following formula:

$$E_{diss} = E(h_N + PD) - E(h_N) - E(PD_{bulk}) \tag{3.4}$$

In this equation, E_{diss} denotes the dissolution energy of the point defect (PD) embedded in a supercell containing N host lattice (h) atoms. $E(h_N + PD)$ is the calculated total ground-state energy of a cell containing N host lattice atoms and a point defect PD. The two other terms denote the ground-state energies of the pure materials, with $E(h_N)$ the total energy of a cell containing N host lattice atoms and $E(PD_{bulk})$ the total energy of the impurity element in its pure element reference state. If the supercell contains more than one impurity atom (due to sublattice symmetry), the total ground-state energy of this supercell is divided by the number impurity atoms in the cell.

The dissolution energy for a particular supercell size and materials system thus requires 3 supercell calculations: one for the defect-containing cell, one for the corresponding pure host lattice cell and one for the defect in its reference state. The energy of the impurity element in its reference state needs to be calculated only once: since the number of impurity atoms in the cell

does not scale with supercell size, the error on $E(PD_{bulk})$ does not either. Before the dissolution energy can be calculated for each Cu-Zr supercell, the ground-state energies on the right-hand side of eq. (3.4) need to numerically well converged with basis-set size (via E_{cut}) and number of k-points if accurate values need to be obtained. Convergence tests on one, small supercell are then sufficient to derive the optimal settings for all other defect-containing supercells of the same system.

3.5 K-point convergence tests

3.5.1 Cu-Zr

Accurate dissolution energies $E_{diss}(N)$ can only be calculated if the total ground-state energy of each supercell is well converged with basis-set size (via E_{cut}) and number of k-points. For the Cu-Zr system, forces will also be determined on particular atoms in each supercell to investigate the force convergence with supercell size. Since forces are defined as the derivatives of the total energy with respect to an atomic displacement, they are an order of magnitude more sensitive to convergence issues than total energies, causing the forces to converge slower with basis-set size and number of k-points. A higher E_{cut} and number of k-points are hence expected to be required if accurate forces need to be calculated as well. For the convergence tests of the forces, the root-mean-square force (F_{rms}) is chosen as single scalar parameter to represent the forces on the atoms in each supercell. F_{rms} is calculated using the following equation:

$$F_{rms} = \sqrt{\frac{\sum_{i=1}^{N} F_i^2}{N}} \tag{3.5}$$

In this equation, F_i is the total force on atom i in a supercell containing N atoms.

All convergence tests of the rms force (and total ground-state energy) were performed on the smallest possible cell, in this case fccsc1 with chemical composition Cu_3Zr, to minimize the computational effort. All atoms were slightly displaced from their symmetrical lattice positions in the order of 0.01 Å to create non-zero forces on the Cu-atoms. Extra tests were performed on the equally large Zr-rich supercell with composition Zr_3Cu to confirm the obtained parameter settings from the tests on the Cu-rich cell. Similar settings are expected since the elements are the same in both cells, shown in Fig. 3.5.

K-point convergence tests are of particular interest in this work, for reasons that will be explained in the next chapter. The optimal cut-off energy was therefore not determined via separate convergence tests. Its value was set to 400 eV: this is 130 eV above the default cut-off energy from the *POTCAR*-file of Cu and about 250 eV above the default E_{cut} for Zr. This value can be considered to be high enough in order to reduce the error on the ground-state energy and the rms force sufficiently. E_{cut} convergence tests by Caestecker have shown for the ground-state energy of Cu_3Zr in particular [53] that a cut-off energy of 400 eV already reduced the error on the energy difference (between the energy at the equilibrium volume of the cell and the energy

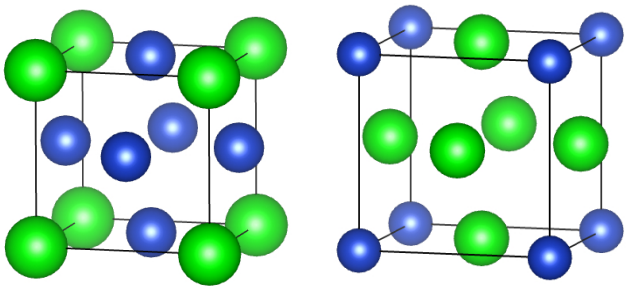

(a) (b)

Figure 3.5: (a) Cu_3Zr and (b) Zr_3Cu supercell used for E_{cut}, k-point and EDIFF convergence tests of the Cu-Zr system. All atoms are slightly displaced from their symmetrical positions to generate non-zero forces.

at 105% of this equilibrium volume) to approximately 0.0001 eV/atom. Larger errors on the total ground-state energy per atom and rms force with respect to E_{cut} hence do not need to be expected.

The total ground-state energy was converged with respect to number of k-points with a tolerance of 1 meV/atom and F_{rms} with a tolerance of 5 meV/Å to achieve reliable dissolution energies, as suggested by Probert and Payne [13]. To further evaluate the accuracy of our supercell calculations, the convergence of F_{rms} and the total ground-state energy with EDIFF was checked as well. Figs. 3.6a and 3.6b show the results for the convergence tests on the total ground-state energy and F_{rms} of the Zr_3Cu-cell, respectively. For every convergence test, E_{cut} was set to 400 eV. The ranges for which the total ground-state energy and rms force lie within the required accuracy (0.001 eV/atom for the total ground-state energy, 0.01 eV/Åfor the rms force) with respect to the most accurate calculation are shown by the dashed lines. The total ground-state energy of the Zr-rich system clearly converges very fast with the number of k-points: approximately 3000 k-points in the first Brillouin zone, corresponding to a 15×15×15 k-mesh, are already enough to achieve an accuracy of 0.0001 eV/atom. The EDIFF-tag can safely be set to 1E-7, since the differences in energy with EDIFF = 1E-8 are negligible. The same settings for both parameters also suffice to keep the error on F_{rms} below 0.001 eV/Å. Surprisingly, the total energy and rms force converge at approximately the same rate with respect to both parameters in the case of the Zr_3Cu. As shown in Figs. 3.6c and 3.6d, the results from the k-point convergence tests on Cu_3Zr are quite different, except for EDIFF, for which 1E-7 still suffices. Both E(Cu_3Zr) and F_{rms} converge much slower with the number of k-points than their Zr-rich counterparts. The rms force also converging at an even slower rate than the total energy. A 21×21×21 k-mesh is observed to satisfyingly reduce the error on the total ground-state energy below 0.001 eV/atom and the error on F_{rms} below 0.01 eV/Å. The number of k-points corresponding to the 21×21×21 k-mesh (9261 k-points) is indicated in each figure by the black arrow.

To avoid significant differences between k-point related errors on the ground-state energy of a Cu-Zr supercell and its corresponding pure Cu supercell, this parameter needs to be set to the same value for each $E_{diss}(N)$-calculation. To check if these parameter settings are also valid for the pure Cu host lattice, additional convergence tests were performed on the fcc Cu conventional

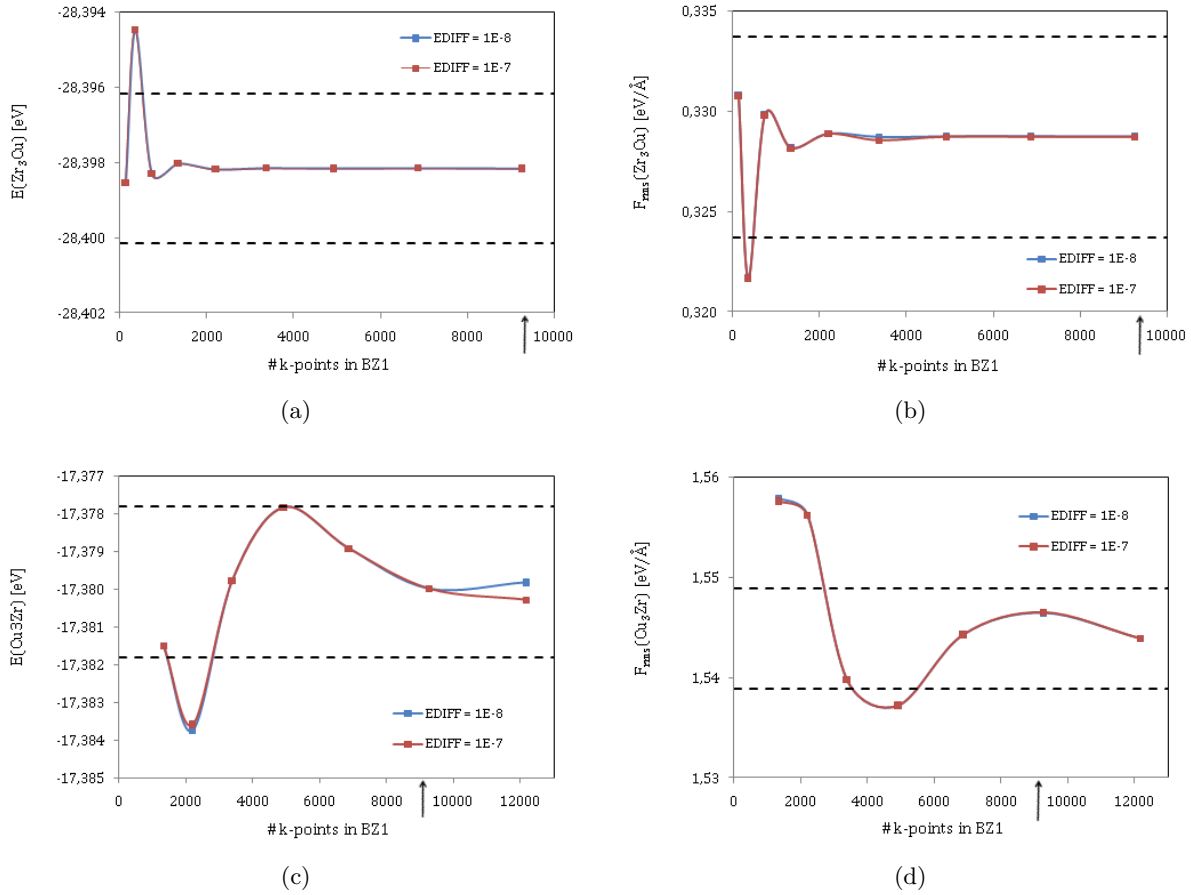

Figure 3.6: Results of k-point and EDIFF convergence tests at E_{cut} = 400 eV. (a) Total ground-state energy of Zr_3Cu; (b) F_{rms} of Zr_3Cu; (c) Total ground-state energy of Cu_3Zr; (d) F_{rms} of Cu_3Zr. The range of the required accuracies with respect to the most accurate calculation (0.001 eV/atom for the ground-state energy, 0.01 eV/$\AA$ for F_{rms}) is shown by the dashed lines in each figure.

unit cell. Since the position of the atoms in pure Cu are fixed by symmetry, forces are zero for all pure Cu supercells and hence only convergence with respect to the total ground-state energy needs to be tested. Increasing the k-mesh from 21×21×21 to 25×25×25 leads to a change in E(Cu) of 0.0001 eV/atom. The influence of a change of EDIFF was also investigated: switching the EDIFF-tag to 1E-8 results in a ground-state energy uncertainty below 10^{-6} eV/atom. Hence,both parameters can safely be copied from the Cu-Zr convergence tests to calculations of pure Cu supercells.

The optimal values for E_{cut} (400 eV) and EDIFF (1E-7) can be used for all considered Cu-Zr and Cu supercells in Table A.1. This however does not hold for the number of k-points, since the same numerical accuracy for the total energy per atom and the rms force in different supercells can only be obtained if the numerical integration over the first Brillouin zone is carried out with the same *k-point density* (i.e. $\frac{\#k-points}{V_{BZ}}$) instead of the number of k-points. The volume of the first Brillouin zone (V_{BZ}), the unit cell of the reciprocal lattice, is inversely proportional to the volume of the real space unit cell. Hence, the number of k-points necessary to maintain a certain k-point density scales inversely with the supercell size as well. The cubic 32-atom

supercells in Table A.1 for example are 8 times as large than fccsc1 (Cu_3Zr), since they are constructed with 8 4-atom cells. The volume of the first Brillouin zone of the 32-atom cells is thus 8 times smaller than that of fccsc1, so only $\frac{1}{8}$ of the number of k-points will suffice. Since fccsc1 will be sampled with a 21×21×2 k-mesh, a grid with half as much subdivisions in each reciprocal lattice dimension will give an equally high k-point density. Since the 21×21×21 grid has an uneven amount of subdivisions in each dimension, an 11×11×11 k-mesh will be used in the particular case of the 32-atom cells to ensure a high enough k-point density. The parameter settings that were used for property calculations in each Cu-Zr supercell are summarized in Appendix B.

3.5.2 Fe-H

The investigation of the Fe-H system exclusively focussed on the supercell finite-size convergence of the H dissolution energy. Therefore, convergence tests were only performed with respect to the total ground-state energy of the defect-containing supercell. Since accurate forces are no prerequisite, less severe parameter settings are expected to suffice.

The convergence of the total ground-state energy with E_{cut}, EDIFF and k-points was investigated for the smallest available cell, Fe_2H. In contrast to the Cu-Zr convergence tests, a different, less time-consuming approach was used. In an earlier study, K. Lejaeghere et al. found in their convergence tests for the elemental crystals a cut-off energy of 400 eV and a 19×19×19 k-mesh to suffice with a convergence criterion of 10^{-4} eV for the self-consistent calculation (EDIFF) [58]. The tests were performed with the standard Fe PAW potential in combination with the PBE functional. To check if these settings ensure a high enough accuracy for the total ground-state energy of the H-containing cell as well, equilibrium cell volumes and total energies of the unrelaxed Fe_2H cell attained with these and 'higher' settings (E_{cut} = 600 eV, 23×23×23) were compared. The self-consistent convergence criterion was set to 10^{-6} eV (EDIFF = 1E-6) for both sets of combinations to slightly enhance the accuracy of our calculations.

In order to compare both total energy and equilibrium supercell volume, energies were created for different cell volumes at both settings. For these settings, $E(Fe_2H)$ was calculated at 13 different (cubic) cell volumes of the conventional bcc Fe unit cell (varying between $V_0' \pm 6\%$, with V_0' the estimated equilibrium volume, corresponding to a lattice parameter of 2.833 Å). The equilibrium cell volume V_0 and total ground-state energy are calculated for each volume range by fitting the data (total energy E and cell volume V) to the Birch-Murnaghan equation of state:

$$E(V) = E_0 + \frac{9V_0B_0}{16}\left\{\left[\left(\frac{V_0}{V}\right)^{2/3} - 1\right]^3 B_0' + \left[\left(\frac{V_0}{V}\right)^{2/3} - 1\right]^2 \left[6 - 4\left(\frac{V_0}{V}\right)^{2/3}\right]\right\} \tag{3.6}$$

Apart from V_0, values for fitting parameters such as the equilibrium bulk modulus B_0 and the first derivative of this modulus with respect to pressure B_0' can also be obtained, but are not of

particular interest here. The results for both combinations of parameter settings are visualized in Fig. 3.7. The difference in total ground-state energy fluctuates for each supercell volume around 0.003 eV, reducing the error to 0.001 eV/atom if $E_{cut} = 400eV$ and a 19×19×19 k-mesh are used. The same holds for the total energy $E(Fe_2H)$ at the equilibrium volume, for which the corresponding lattice parameter was found to be 2.826 Å with an error of 0.001Å between the different settings. Hence a cut-off energy of 400 eV in combination of EDIFF = 1E-6 are used for all Fe-H supercell calculations. The k-meshes of all supercells are based on the constant k-point density criterion as explained in the previous section and were kept as similar as possible to the density obtained with the 21×21×21 grid in the Fe_2H cell. The parameter settings that were used for each supercell are summarized in Appendix B. Each supercell was constructed using conventional bcc Fe unit cells with lattice parameter 2.826 Å .

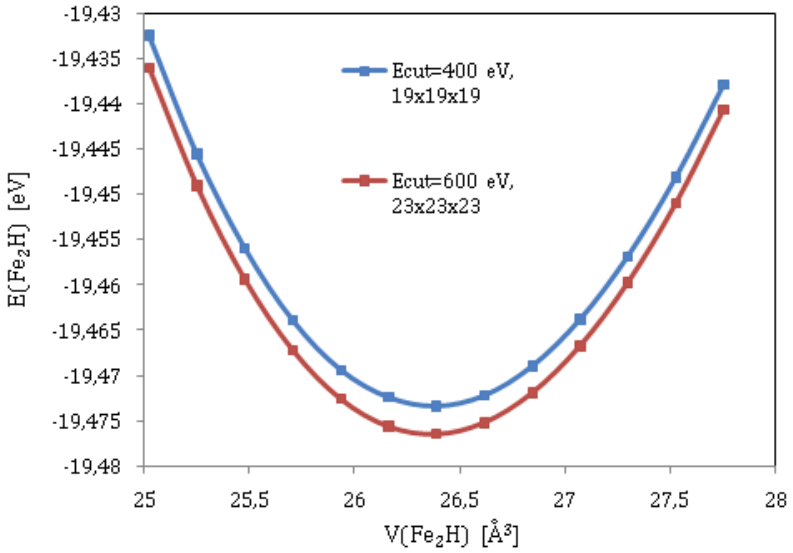

Figure 3.7: Convergence test of the parameter settings of the Fe-H system at EDIFF = 1E-6, using the Birch-Murnaghan fit of the total ground-state energy as a function of supercell volume

Chapter 4

Results

4.1 Supercell finite-size convergence of physical properties in the Cu-Zr system

4.1.1 Electronic charge distribution

A property that will undoubtedly be affected by spurious defect interactions is the distribution of electronic charge around the Cu- and Zr-nuclei in a supercell. As long as Zr-atoms feel each other's presence in the Cu host lattice, the charge distribution in their neighborhood will change when the sublattice symmetry and/or supercell size is modified. For practical applications such as X-ray diffraction, electronic charges in a lattice need to be known within an accuracy of approximately 0.01 electrons. The supercell finite-size convergence of the charge distribution around Zr and the Cu-nuclei in its vicinity is investigated in order to know how low defect concentrations in the Cu-Zr system need to be to achieve this accuracy.

The change in electronic charge distribution was determined and visualized for various Zr-concentrations and sublattice symmetries in the Cu-Zr system. First, self-consistent VASP calculations were performed on each Cu-Zr and corresponding pure Cu supercell to generate the *CHGCAR*-files, which contain the electronic charge density (electronic charge/$V_{supercell}$) at discrete points in the supercell. Subsequently, the *CHGCAR* of the pure Cu supercell is subtracted from the Cu-Zr *CHGCAR* with the visualization software VESTA (Visualization of Electronic and Structural Analysis) [59]. The differences in charge density can then be visualized as iso-surfaces with the same program. Charge differences were determined around particular nuclei by integrating the charge density within a sphere with a radius that is half the nearest neighbor distance in the fcc Cu-lattice. For a fcc Cu lattice parameter of 3.637 Å the sphere radius equals 1.28 Å . The integrations were conducted by means of a script written by Caestecker [53].

2D projections on a {100}-plane were taken of the charge density difference in various supercells with simple cubic and face-centered cubic sublattice symmetry and are shown in Figs. 4.1 and 4.2 respectively. The iso-surface value of the charge density difference was set to 0.0005 electrons for all supercells. Higher iso-surface values would give rise to predominantly spherical surfaces

close to the Zr-nuclei, which is not very suitable for investigating interaction effects on Cu-nuclei in its vicinity. On the other hand, noise would appear for too low iso-surface values. This evidently needs to be avoided in order to analyze and interpret finite-size effects. In Figs. 4.1 and 4.2, blue iso-surface lobes in these figures correspond to negative differences, yellow lobes to positive. Zr was considered to have 4 valence electrons in its pseudopotential, while Cu has 11. The change in electronic charge distribution is therefore overall negative and should add up to -7 electrons in each primitive supercell. The lobes in each figure are however predominantly yellow and hence correspond to positive differences: this is a consequence of the small iso-surface value that was chosen: predominant negative differences can be found at iso-surface values in the order of 0.1/0.01 electrons.

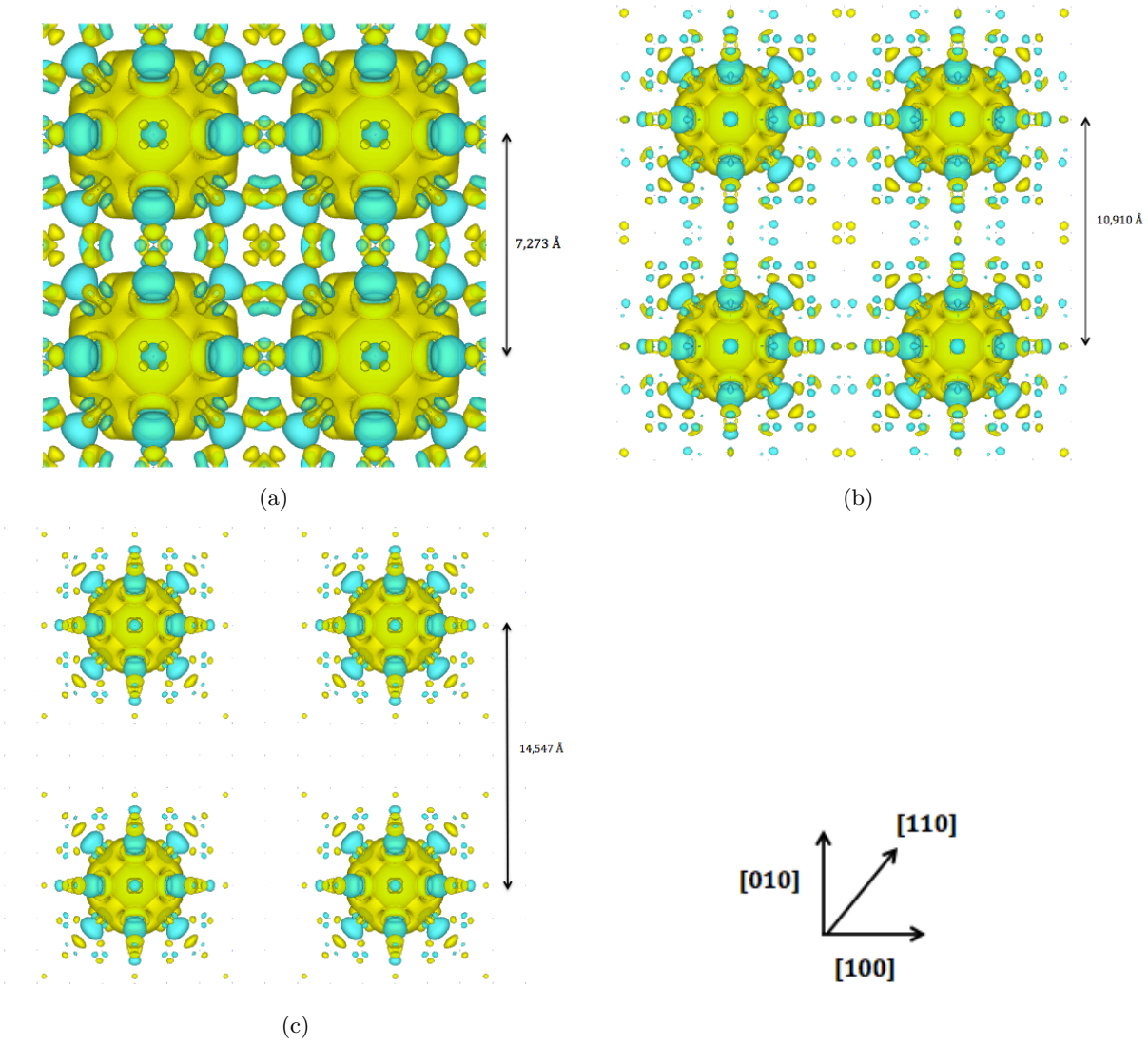

Figure 4.1: 2D projections of the charge density difference on a {100}-plane, at an iso-surface value of 0.0005 electrons for (a) fccsc2 ($c_{Zr} = \frac{1}{32}$), (b) fccsc3 ($c_{Zr} = \frac{1}{108}$) and (c) fccsc4 ($c_{Zr} = \frac{1}{256}$)

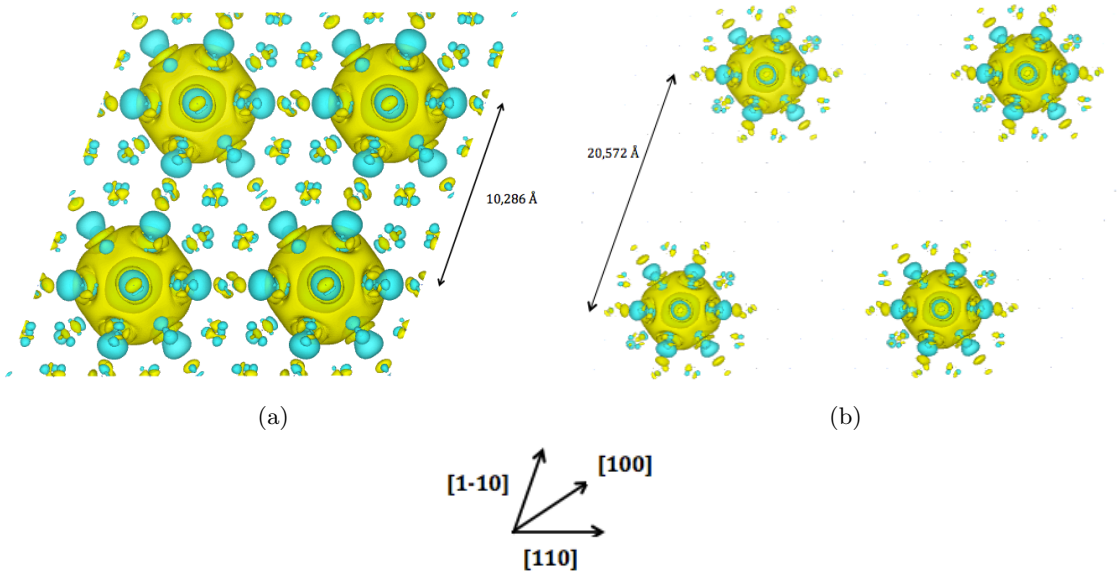

Figure 4.2: 2D projections of the charge density difference on a {100}-plane at an iso-surface value of 0.0005 electrons for (a) fccfcc4 ($c_{Zr} = \frac{1}{64}$) and (b) fccfcc8 ($c_{Zr} = \frac{1}{512}$)

The charge density difference as seen in Figs. 4.1 and 4.2 is of course a consequence of the introduction of Zr into the Cu host lattice. The distribution of electrons is altered due to the combination of two effects. First of all, a purely physical (quantum-mechanical) phenomenon called 'Friedel oscillations' appears. These oscillations arise when electrons of the host lattice near the Fermi level, which have a wave function that is spread over the entire system, are scattered due to the disturbance of the Coulomb potential in the neighborhood of an impurity such as Zr [53]. The charge density is hence disturbed over some distance from the Zr-atom. Since the Coulomb potential is only disturbed locally around the Zr-nucleus, the amplitude of the oscillations decays away from the defect and eventually diminishes completely.

In addition, the charge distribution in a supercell will be influenced by spurious interactions between Zr and its periodic images. This is a purely artificial effect due to the finite size of the supercell. Hence, both finite-size effects and Friedel oscillations will generate charge (density) differences, which cannot be distinguished directly from each other. However, as the Zr-concentration is decreased, finite-size effects diminish due to the increasing distance between Zr and its periodic images. The charge density difference plots and charge integration should therefore converge towards the Friedel contribution in the limit of the largest supercells. In the case of the charge density difference plots, differences in the shape and number of iso-surfaces between different supercell sizes indicate that the electronic distribution is not yet fully converged with supercell size. Integrated charge differences, around particular nuclei, for different supercell sizes can give in the same way an indication of the rate of the supercell finite-size convergence.

Short-range effects

The 2D projections of the charge density difference, for an iso-surface value of 0.0005 electrons, are shown for the cells with simple cubic Zr sublattice symmetry in Fig. 4.1 give a good indication of the convergence rate of the electronic charge in the vicinity of Zr. Differences in shape and number of lobes between the 32-atom (Fig. 4.1a) and 108-atom (Fig. 4.1b) supercells are already quite small, especially close to the Zr-nucleus, within a radius of roughly 3 Å . The iso-surfaces in the 256-atom cell (Fig. 4.1c) within a radius of approximately 5 Å do not even seem to have changed with respect to. the fccsc3 cell, which suggests a fast convergence of the charge distribution in the neighborhood of Zr. The same trend is observed in the fcc sublattice supercells of Fig. 4.2, with iso-surfaces that seem to change very little with decreasing Zr-concentration within approximately the same radius.

These observations were more numerically substantiated by integrating the charge density difference around Zr and around its first, second and third nearest neighbor Cu-nuclei. The integrated electronic charge difference around each type of nucleus is shown as a function of Zr-concentration in Fig. 4.3. Especially the charge difference around the first nearest neighbor (NN1) converges very rapidly with Zr-concentration: the remaining error is even reduced below 0.001 electrons for the fccbcc4 cell with respect to fccfcc8. Since NN2- and NN3-nuclei are further removed from Zr, the charge density around their nuclei are more affected by the geometry of nearby Zr-images and hence converges slower with decreasing Zr-concentration. Oscillations in the integrated values for NN2 and NN3 are a consequence of the change in sublattice symmetry and hence of the geometry of their surroundings.

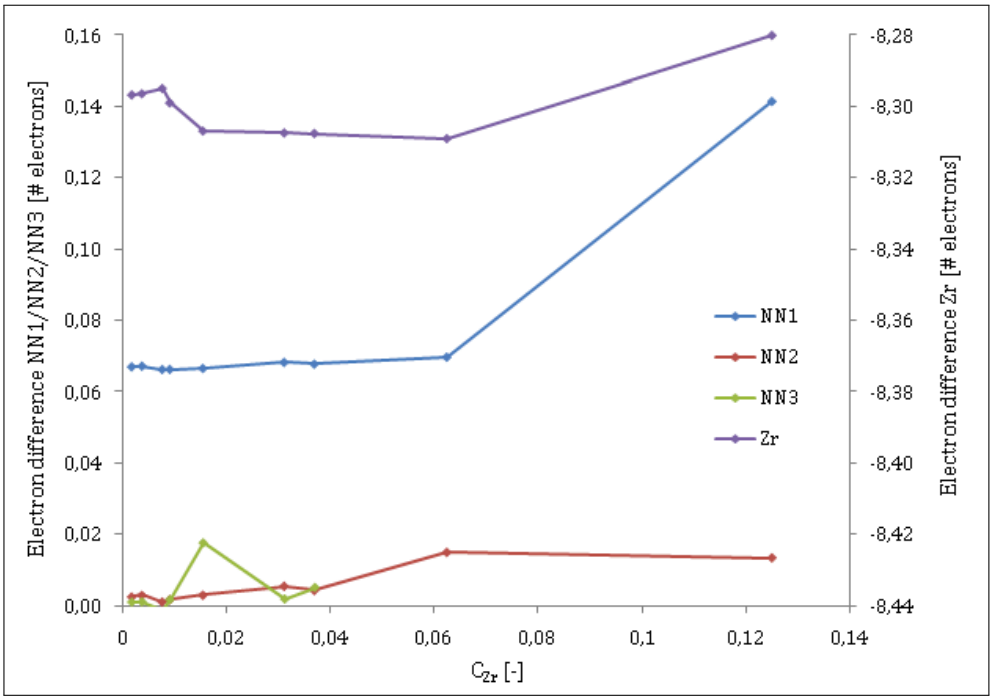

Figure 4.3: Integrated charge difference as a function of Zr-concentration around Zr and three nearest-neighbor Cu-nuclei of Zr. The integration sphere radius is half the nearest-neighbor distance.

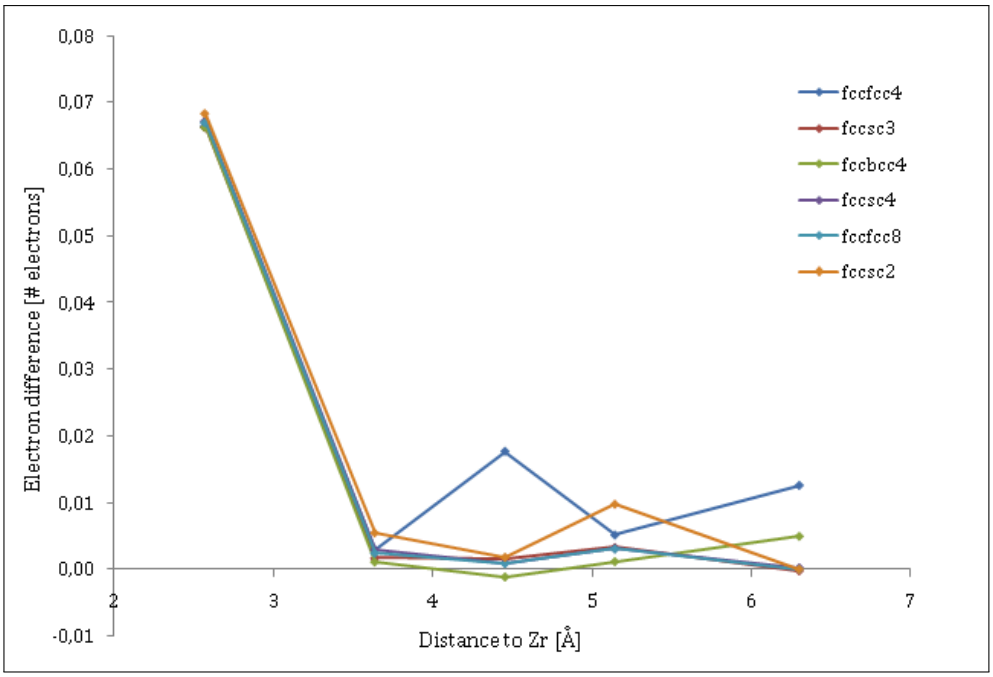

Figure 4.4: Integrated charge difference for the supercells with the smallest Zr-concentrations ($c_{Zr} \leq \frac{1}{32}$) as a function of distance from Zr. The integration sphere radius is half the nearest-neighbor distance.

The charge difference around the Zr-nucleus converges at a similar, but slightly slower rate with Zr-concentration than NN1. Because the distance to the periodic copies is maximal in the case of the Zr-nucleus, the statement that larger distances to the periodic copies of Zr imply a higher convergence rate would not hold anymore. However, in contrast to the Cu-nuclei, Zr resides at a highly symmetrical lattice site. The charge density around such a symmetrically positioned nucleus can strongly interfere, constructively or destructively, with the electronic charge distribution around the periodic Zr-copies. A correct physical description of the electronic charge distribution around Zr will hence be very difficult, even without finite-size errors[13]. Since the nearest neighbor Cu-nuclei reside at less symmetrical positions, such interference effects will be substantially smaller. This then explains why the finite-size convergence behavior of the charge difference around Zr is different from the nearest neighbor Cu-nuclei.

For all these nuclei, the charge difference errors for the fccsc4 cell are around 0.001 electrons with respect to the fccfcc8 cell. The local electronic charge hence appears to be a property that does not suffer a lot from finite-size effects, especially because an accuracy of 0.01 electrons already suffices for most applications. According to Fig. 4.3, this accuracy can already be achieved for concentrations in the order of $\frac{1}{108}$ in the case of the Cu-Zr system, and even higher if the NN3-oscillation for the fccfcc4 cell is not taken into account. The same conclusion can be drawn from Fig. 4.4, where the charge density around Cu-nuclei for supercells with a maximum Zr-concentration of $\frac{1}{32}$ is plotted as a function of distance from Zr. A Zr-concentration of $\frac{1}{108}$ (fccsc3)

[13]If this symmetry phenomenon is still not completely clear, consider then the following example: assume a Cu-nucleus in the middle of a cubic supercell, with a Zr-nucleus at every corner. The Cu-nucleus will feel a force due to the Zr-nuclei at each corner, but as a consequence of the Zr sublattice symmetry, the net force will add up to zero. In reality however, if the Cu-atom is close enough to the Zr-defect, the net force should be non-zero because the Zr-atom should be isolated (the Zr-concentration will be much lower than computationally feasible)

reduces the error on the charge difference below 0.01 electrons, even for NN4 and NN5 Cu-nuclei, which were also included in the data set.

Long-range effects

The electronic charge distribution in the neighborhood of Zr was found to converge well with supercell size, with remaining errors in the order of 0.001 electrons for the fccsc4 supercell. This however does not imply that interactions between Zr and its periodic images have completely vanished, which is especially important for properties that depend on the electronic structure of the complete supercell: while the local charge distribution can be considered to be converged accurately enough with respect to supercell size, the error on the charge distribution can become quite large for the *entire* supercell as long as spurious defect interactions are present. One such a property is for example the Zr dissolution energy, which according to equation 3.4 depends a.o. on the total ground-state energy of the entire Zr-containing supercell. Remaining finite-size errors hence need to be avoided as much as possible. The evolution of the electronic charge difference along the nearest-defect directions was therefore examined in more detail. The shortest distances between Zr-nuclei are along $\langle 110 \rangle$-directions in supercells with fcc sublattice symmetry and along $\langle 100 \rangle$-directions in supercells with sc sublattice symmetry.

The charge density difference oscillations in fccsc3 and fccfcc4 are observed in Figs. 4.1b and 4.2a along the entire $\langle 100 \rangle$- and $\langle 110 \rangle$-directions respectively for an iso-surface value of 0.0005 electrons. This clearly suggests that Zr-atoms in these cells still interact with each other and are hence still not isolated. Figs. 4.1c and 4.2b however indicate that when for each sublattice symmetry the Zr-concentration is approximately halved, the spurious defect interactions seem to disappear since oscillations for a 0.0005 electron iso-surface value are absent halfway the defect-defect distance. Disappointingly, they reappear at lower iso-surface values, for example in the 512-atom fccfcc8 cell, for an iso-surface value of 0.0002 electrons. The same conclusion can be drawn from Fig. 4.5, where the logarithm of the absolute value of the charge density difference is plotted along [110], the nearest-defect direction for the fcc sublattice symmetry. These values correspond to the charge density difference in a *point* along this axis and are hence *not* integrated charges. Charge density differences in the order of 10^{-4} electrons are still found halfway the nearest Zr-Zr distance.

The spurious interactions can be further evaluated by integrating the charge density difference around the Cu-nucleus that is at maximum distance from both Zr and its image along the nearest-defect direction, which is the Cu-nucleus halfway the [110]-axis in the case of fcc sublattice symmetry. Like Zr, this nucleus resides at a highly symmetrical lattice site and therefore strong interference effects for the electronic charge density can be expected as well. The charge distribution around the halfway Cu-nucleus will hence not appear bulk-like, even if finite-size effects would be completely removed. Therefore, the charge density difference is integrated around the Cu-nucleus next to it along the [110]-axis. In the case of an isolated Zr-atom, a charge density difference integration around such a Cu-nucleus should yield zero since charge differences would be pure Friedel oscillations, which at such distances from the defect can be considered

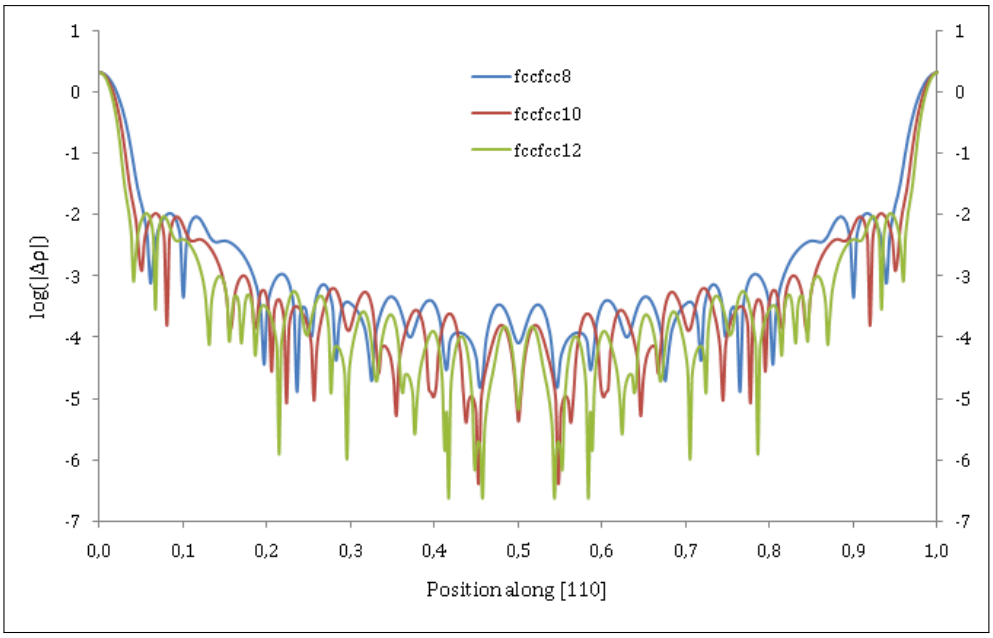

Figure 4.5: Absolute values of the charge density difference along the [110] nearest-defect direction, displayed on a logarithmic y-scale and with the Zr-Zr distance scaled to 1.

to be locally displaced electronic charge originating from nearby Cu valence electrons. The integration with a sphere radius of half the nearest neighbor distance (1.28 $\AA$) however yields a charge density difference of approximately 0.0007 electrons. In order to be completely sure that such low values for the charge difference can still be considered to be a consequence of defect interactions and not due to noise on the charge density difference as calculated by VASP, the noise on the charge difference for pure Cu was estimated by varying the k-mesh (from 11×11×11 to 13×13×13) on a 32-atom pure Cu cell and integrating the difference between the *CHGCAR*s from both calculations. The charge density difference was found to be 6.10^{-5} electrons, which is about ten times smaller than the integrated charge difference on the 'bulk-like' Cu-nucleus in the fccfcc8 cell. Hence, Zr can still not be considered to be isolated from its images in the 512-atom fccfcc8 cell. This indicates that even such large cells, which already require a considerable amount of computational effort[14], would yield ground-state energies that are still affected by finite-size effects.

The question now arises how small the Zr-concentration needs to be made to actually remove Zr-Zr interactions. The supercell size was therefore increased even further: *CHGCAR*-files were created for both the 1000-atom fccfcc10 cell and the 1728-atom fccfcc12 cell. Achieving a completely converged self-consistent procedure is already an exhaustive task for both cells: a VASP calculation for a 1000-atom cell, with a 3×3×3 k-mesh, already takes 16 hours with 512 cores (CPUs), which is equivalent with 64 nodes on the Gengar-cluster, and a maximum memory use of 3 GB per core. In the case of a single k-point VASP calculation for the 1728-atom supercell, 58 hours are necessary, with the same amount of computational resources, for the self-consistent

[14]Recall that the calculation time scales with the third power of the number of valence electrons in the cell for most operations in the self-consistent procedure. A single k-point calculation of an fccfcc8 supercell, for example, takes 5.5 hours on 256 CPUs (equivalent with approximately 60 days on a single-core computer) when all settings are chosen such as in Table B.1.

procedure to end. This requires in addition a maximum memory use of 7 GB per core. This should give a good idea of how exceptional the data acquisition for such large supercells really is.

2D projections of the charge density difference were made on a {100}-plane, from both *CHGCARs* with an iso-surface value of 0.0002 electrons and are visualized in Figs. 4.6b and 4.6c for fccfcc10 and fccfcc12 respectively. According to these figures, the oscillations clearly diminish along the ⟨110⟩ nearest defect axes. Fig. 4.5 also shows how the charge density difference along [110] somewhat decreases with increasing supercell size. The oscillations halfway the nearest-defect distance are however still of the same order as those observed in the 512-atom cell. Remaining defect interactions can hence not be excluded even for a Zr-concentration of $\frac{1}{1728}$! This remarkable conclusion implies that properties such as the total ground-state energy of the cell and hence also the Zr dissolution energy, cannot be guaranteed to yield values that are not influenced anymore by finite-size effects.

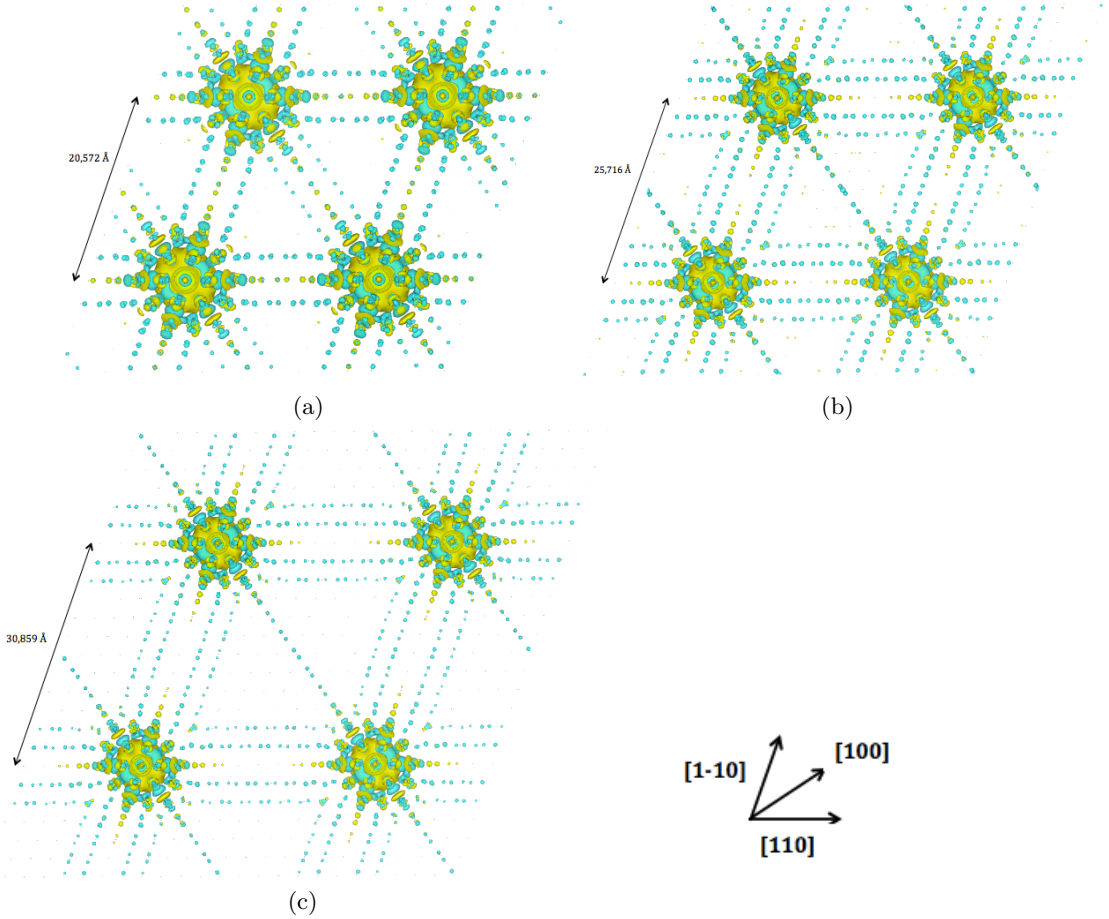

Figure 4.6: 2D projections of the charge density difference on a {100}-plane at an iso-surface value of 0.0002 electrons for (a) fccfcc8 ($c_{Zr} = \frac{1}{512}$), (b) fccfcc10 ($c_{Zr} = \frac{1}{1000}$) and (c) fccfcc12 ($c_{Zr} = \frac{1}{1728}$)

Other substitutional atoms in Cu

The Cu-Zr system was found to suffer from very persistent interactions between Zr and its periodic images: iso-surfaces for a charge density difference of 0.0002 along the nearest-defect directions were even visible in a supercell with a Zr-concentration of $\frac{1}{1728}$. However, other substitutional atoms than Zr have a different chemical and physical nature, implying that the magnitude of defect interactions are expected to differ as well. To investigate the dependence of defect interactions on the system type, Zr was substituted by various elements, all with a different type of electronic structure. First of all, Ag is considered since it has the same electronic valence structure as Cu, the host lattice atom. Cd was also chosen because it has only one extra valence electron compared to Cu. Finally, Mg was also included due to its completely different chemical nature (Mg is a p-block element, whereas al other elements are from the d-block of the periodic table). Charge density difference plots were made for fccfcc8 (512-atom) supercells and are visualized in Fig. 4.7 for an iso-surface value of 0.0002 electrons. The magnitude of spurious defect interactions is clearly observed to be system-dependent: while defect interactions are visible along the entire ⟨110⟩-directions in the case of the Cu-Zr system, they completely disappear for the other systems. Some oscillations are observed in the case of Cu-Mg, but surely not along the entire interaction line. This could indicate that elements with a similar electronic structure as the host lattice atoms suffer less from finite-size effects than elements of chemically and physically different nature. This is however not completely consistent with the fact that substitutional Mg creates less spurious defect interactions than Zr, which is after all still a transition metal. A more detailed investigation of the reasons behind the different defect interaction behavior between different Cu-(solute atom) systems is however beyond the scope of this thesis.

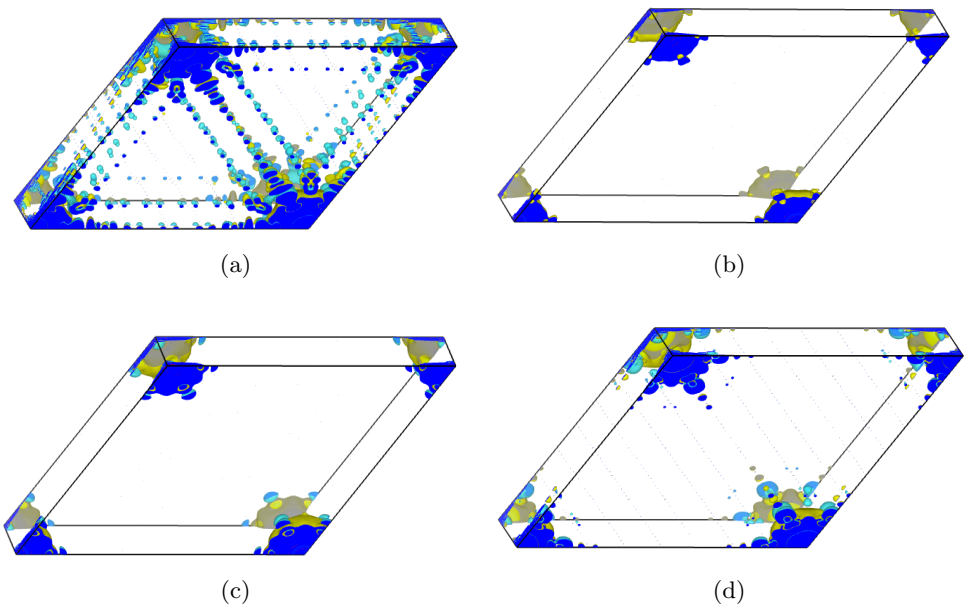

Figure 4.7: Charge density difference plots at an iso-surface value of 0.0002 electrons for 512-atom cells of (a) Cu-Zr, (b) Cu-Ag, (c) Cu-Cd and (d) Cu-Mg. The nearest-defect distance along ⟨110⟩-directions is 20.572 Å in each cell.

Fig. 4.8 shows that if the iso-surface values are further decreased, interactions along nearest-defect directions reappear for all three systems. The iso-surface values are now in the order of 10^{-5}, so integrated charge differences around the most bulk-like Cu-atom (that is not influenced by symmetry) along a nearest-defect direction could be expected to be close to noise on the bulk Cu-atom, which was already found to be in the order of 10^{-5} electrons. However, the charge density difference oscillations in Fig. 4.8 appear predominantly along ⟨110⟩-directions, suggesting that finite-size effects still affect the charge density. Hence, all considered Cu-(solute atom) systems with a solute concentration of $\frac{1}{512}$ still suffer from finite-size effects, but to a (much) smaller magnitude than Cu-Zr.

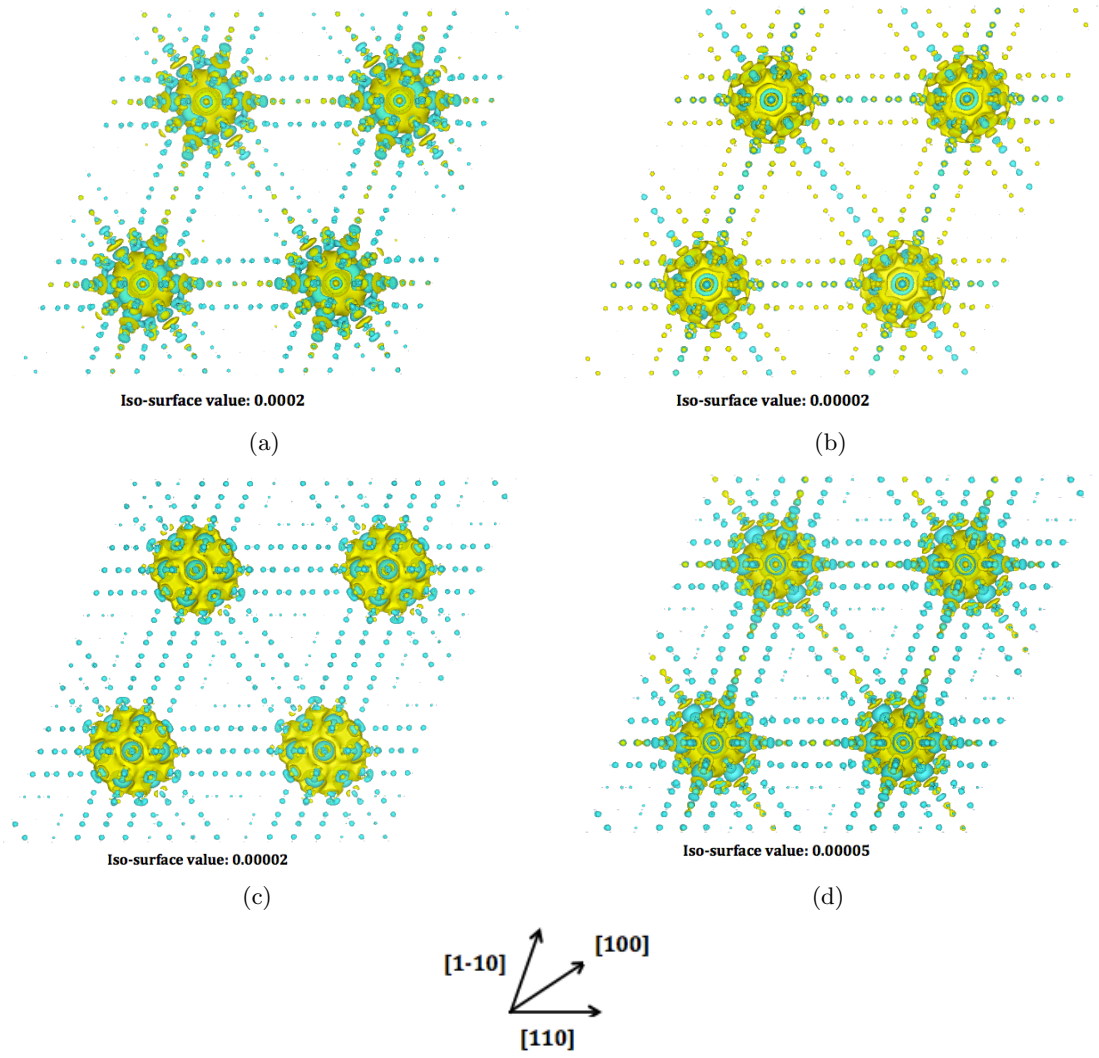

Figure 4.8: 2D projections of the charge density difference on a {100}-plane for 512-atom cells of (a) Cu-Zr (iso-surface value: 0.0002 electrons), (b) Cu-Ag (iso-surface value: 0.00002 electrons), (c) Cu-Cd (iso-surface value: 0.00002 electrons) and (d) Cu-Mg (iso-surface value: 0.00005 electrons). The nearest-defect distance along ⟨110⟩-directions is 20.572 Å in each cell.

4.1.2 Local density of states

As mentioned in the previous section, the introduction of a lattice defect such as the Zr substitutional atom in a periodic lattice affects the electronic structure of the atoms in its vicinity due to a local change in external potential. The local density of electronic states (LDOS) around the nuclei of these elements will hence be influenced as well. These changes in density of states are then a purely physical consequence of the introduction of an isolated Zr-atom. However, since the electronic charge distribution around Zr and the Cu-nuclei in its vicinity, was found to be disturbed due to spurious interactions between Zr and its periodic images, especially in the case of high Zr-concentration supercells, similar errors can be expected both in the total and the local density of electronic states. To compare with the electronic charge convergence, LDOS of the Zr defect and particular Cu-atoms were calculated for each supercell mentioned in Table A.1 in Appendix A[15] to investigate how the electronic structures around these nuclei converge with decreasing Zr-concentration.

The LDOS were determined in each supercell for one of the 12 first-nearest-neighbor (NN1) Cu-nuclei of Zr. Since the Cu host lattice has a fcc lattice symmetry, each NN1 Cu-nucleus lies along the [110]-direction of the conventional axes of the real space lattice, at a distance of $\frac{\sqrt{2}}{2}$ times the lattice parameter of the conventional Cu fcc unit cell. Its position is hence independent of the Zr sublattice symmetry. Fig. 4.9 shows that the density of electronic states around a NN1 Cu-nucleus is already well converged for cells with Zr-concentrations equal to and smaller than $\frac{1}{108}$. While the LDOS of the 256-atom fccfcc4 supercell still shows some differences, the fccsc3 LDOS is in very good agreement with those from the lower Zr-concentration supercells. According to the figure in the upper right corner, differences can be considered to be negligible for even lower Zr-concentrations. Hence, the electronic structure around these nuclei converges very well with supercell size. Since the local electronic charge around NN1 was found to be well converged for similar concentrations, a good correspondence between the supercell finite-size convergence behavior of both properties seems to appear.

For the larger supercells, or equivalently for the lower Zr-concentrations, the supercell size convergence of the density of electronic states around the most bulk-like Cu-nucleus, i.e. the nucleus that maximizes the sum of the distances with the nearest Zr images, was investigated as well. The most bulk-like Cu-nucleus will reside in the middle of the unrelaxed primitive supercell, which is a highly symmetrical lattice site. As already discussed in the previous section, interference effects due to the periodic Zr-images alter the electronic charge distribution around a nucleus at such a lattice site. Hence, its correct physical nature will not be obtained, even without finite-size errors. The same phenomenon will play a role in the case of the LDOS. Therefore, the LDOS was calculated around the Cu-nucleus closest to the middle of the primitive cell of each supercell considered. The analysis of the electronic charge density distribution has showed that finite-size effects are predominantly found along the nearest-defect directions. This suggests that the electronic distribution around the most bulk-like Cu-nuclei in a supercell will not be significantly affected by the presence of the periodic Zr images. A fast supercell finite-

[15]Except for fccfcc10, which requires far too much k-points than computationally feasible in order to obtain an accurate (L)DOS.

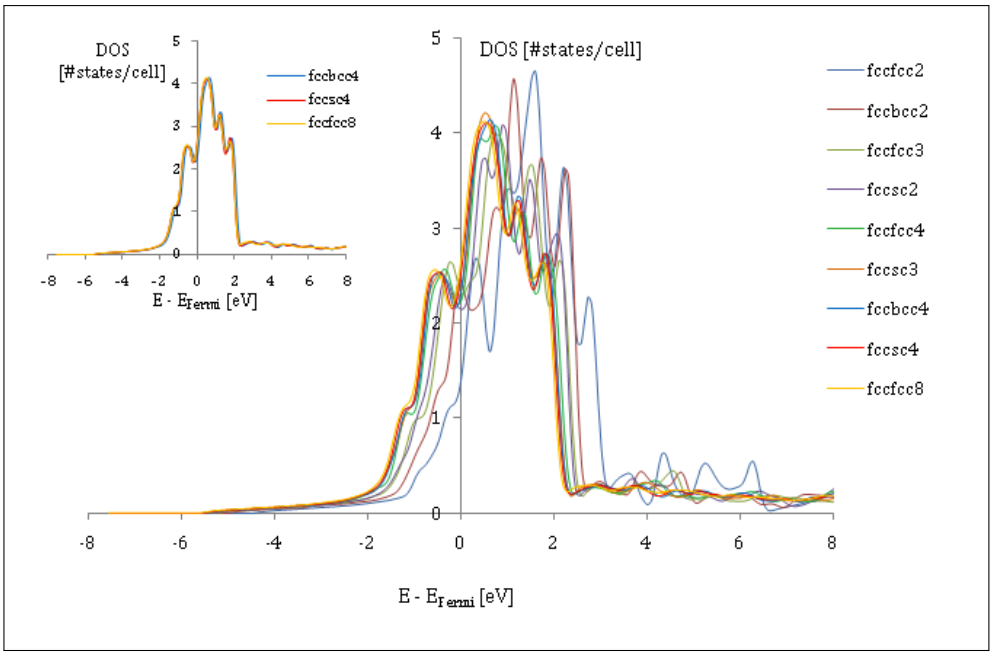

Figure 4.9: Local density of states around a nearest-neighbor Cu-atom to Zr for all supercells considered. Inset: The same LDOS, but now exclusively shown for the lowest Zr-concentrations ($c_{Zr} \leq \frac{1}{128}$)

size convergence of the LDOS can hence be expected. However, since the primitive cell of each supercell depends on the Zr sublattice symmetry, the position of the Cu-nucleus for which the LDOS needs to be calculated does too. Supercells with Zr-concentrations higher than $\frac{1}{64}$ were therefore not included in the analysis: the quasi bulk-like Cu-nuclei in these cells are still far too close to the Zr-nuclei (up to the third nearest neighbor). In addition, the LDOS was calculated around a Cu-nucleus in pure Cu, representing the true (DFT) LDOS of a bulk Cu-atom. The calculation was conducted on a 32-atom pure Cu supercell. All these LDOS plots are collected in Fig. 4.10. This figure points out that even the fccfcc4 supercell, with the highest considered Zr-concentration, appears to be quite close to the pure Cu-LDOS, which is in good agreement with the findings of the electronic charge convergence. The inset of Fig. 4.10 shows that the LDOS of the largest supercell (fccfcc8) is optimally converged with supercell size due to the excellent overlap with the pure Cu-LDOS. Also notice the distinct shape of the LDOS curves for the bulk-like and nearest-neighbor Cu-nucleus, which clearly shows the influence of the Zr-defect on the local density of electronic states (Fig. 4.9 vs 4.10).

The supercell finite-size convergence of the Zr-LDOS was also investigated for all supercells. Fig. 4.11a shows that the Zr-LDOS converges much more difficultly with decreasing Zr-concentration than the Cu-LDOS: especially the 2×2×2-supercells give rise to large errors, with a strong overestimation of the DOS of the unoccupied energy band between 2 and 12 eV above E_{Fermi}. Omitting the LDOS of the supercells with the highest Zr-concentrations (up to $\frac{1}{27}$) allows investigating the convergence of the Zr-LDOS in the low concentration limit in more detail. According to Fig. 4.11b, the lower energy band with partially filled electronic states (up to E_{Fermi}) is already well reproduced by the fccsc3 supercell, which has the highest Zr-concentration considered in this figure. The unoccupied high-energy band differs more significantly for different supercells,

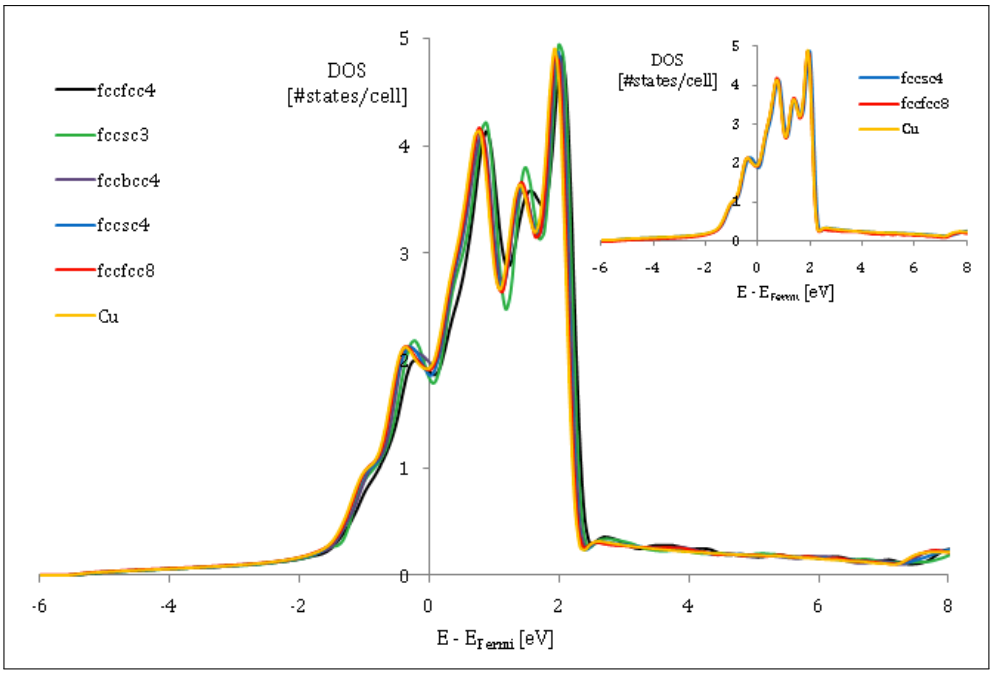

Figure 4.10: (Local density of states around the most bulk-like Cu-atom, that is not completely determined by symmetry, for Cu-Zr supercells with a Zr-concentration of $\frac{1}{64}$ and lower. Inset: The same LDOS, but now exclusively shown for the lowest Zr-concentrations ($c_{Zr} \leq \frac{1}{256}$) and pure Cu

but can be considered to be fairly well converged with supercell size in the case of the fccfcc8 cell, due to the small remaining differences in band structure with fccsc4, which has the second lowest Zr-concentration considered. These results are again in good agreement with the observed slower supercell finite-size convergence rate of the charge distribution around Zr. Interference effects due to the highly symmetrical lattice site of Zr hence also affect the supercell finite-size convergence behavior of the LDOS.

In conclusion, the local density of states of host lattice atoms has proved to be a property that can be accurately calculated with supercells containing a few hundred atoms in the case of the Cu-Zr system - a $\frac{1}{128}$ atomic Zr-concentration already suffices. The Zr-LDOS however converges more slowly than the nearest and bulk-like Cu-atoms and was shown to have converged fairly well only for the largest supercell considered, with a Zr-concentration of $\frac{1}{512}$. Nevertheless, quite accurate LDOS calculations appear to be feasible in a routine fashion since supercells in the order of 100 atoms are comfortably treatable with modern supercomputers.

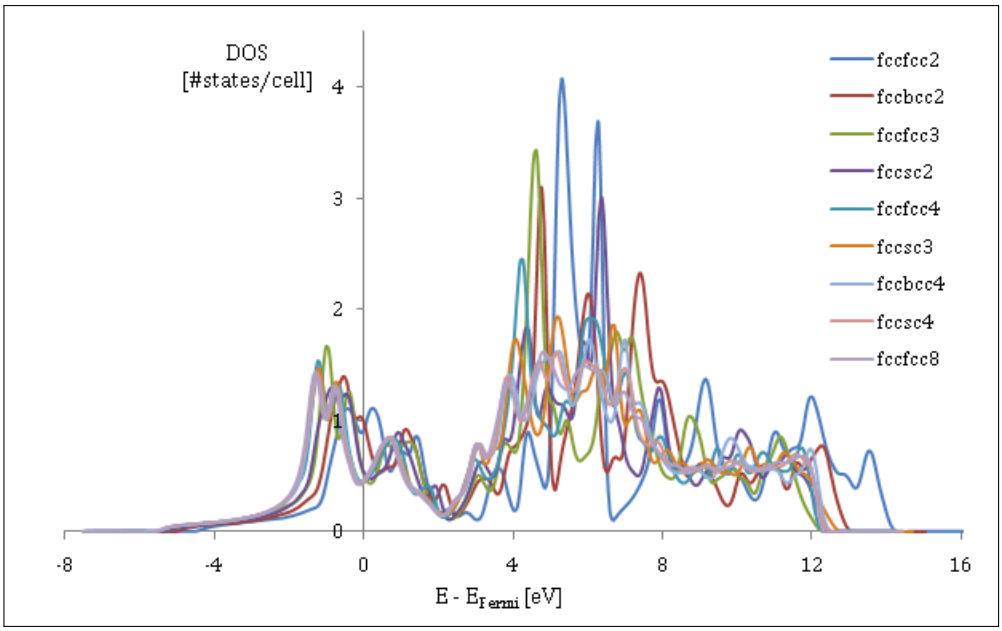

(a)

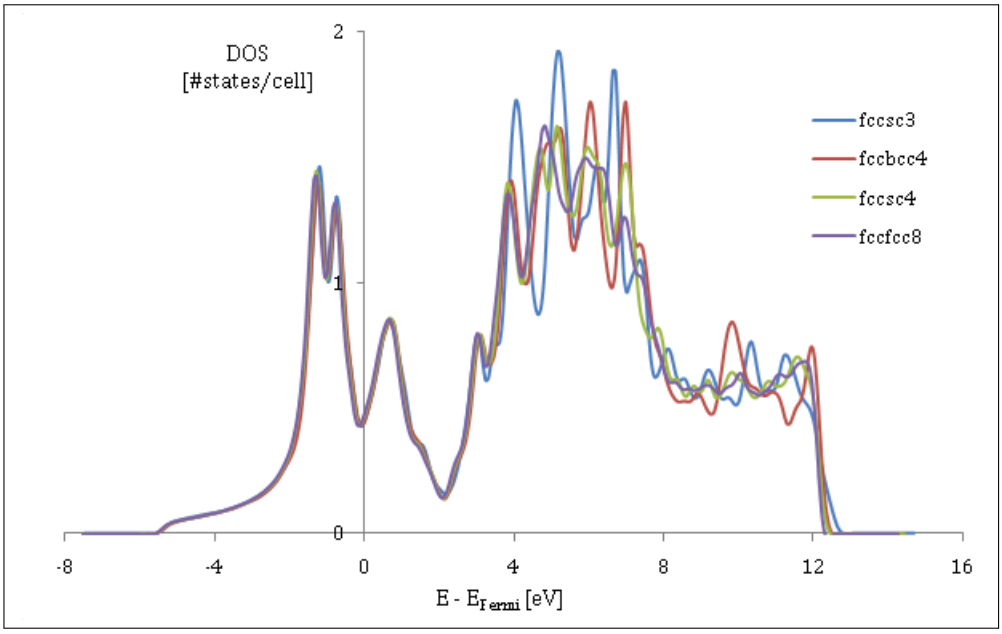

(b)

Figure 4.11: Calculated LDOS for the Zr-defect (a) in each supercell and (b) in supercells with Zr-concentrations equal to and lower than $\frac{1}{64}$.

4.1.3 Zr dissolution energy

The analysis of the electronic charge distribution has showed that spurious Zr-Zr interactions cannot be ruled out even in the largest supercells considered. Since the total ground-state energy of a Cu-Zr supercell - and hence the Zr dissolution energy - is a property that depends on the charge distribution in the complete supercell, it will still suffer from finite-size errors. The magnitude of this error for a given supercell can however not be simply deduced from the same analysis: it could for example still be possible that despite calculated Zr dissolution energies still containing some finite-size errors, they have already converged within an acceptable energy tolerance with respect to supercell size. A thorough examination of the supercell finite-size convergence rate of the Zr dissolution energy is therefore indispensable.

The Zr dissolution energy for each Cu-Zr supercell was calculated according to eq. (3.4) for the defect formation energy in general. For the Cu-Zr system in particular, the expression for the Zr dissolution energy can be rewritten as:

$$E_{diss}^{\mathrm{Zr}}(N) = E(\mathrm{Cu}_{N-1}\mathrm{Zr}) - \frac{N-1}{N}E(\mathrm{Cu}_N) - E(\mathrm{Zr}) \tag{4.1}$$

For each Cu-Zr supercell with Zr-concentration $\frac{1}{N}$, the total ground-state energies of pure Cu and Zr are required as well. Computational details of the pure material reference calculations are therefore discussed first.

Total ground-state energy of pure metals

Since Cu has an fcc structure in its ground state at 0K, fcc Cu is considered as the reference state for pure Cu In order to attain a similar accuracy for $E(\mathrm{Cu}_{N-1}\mathrm{Zr})$ as for $E(\mathrm{Cu}_N)$, its total ground-state energy is calculated in supercells containing as many Cu-atoms as there are atoms in total in the corresponding Cu-Zr supercell. As discussed in section 3.3, all Cu supercells are constructed using fcc unit cells with a lattice parameter of 3.637 Å. The parameter settings for each Cu supercell size are equal to those listed in Table A.1 in Appendix A. Convergence tests on a pure Cu unit cell in the previous chapter have shown that the accuracy of the energy was better than 0.001 eV/atom, as in the case of Cu-Zr. The calculations for the larger pure Cu supercells were conducted with the same E_{cut} (and hence the same number of basis functions per atom) and k-point sampling density as for the Cu unit cell. This guarantees that the accuracy of the total ground-state energy per atom is approximately equal to 0.001 eV/atom for all Cu supercells, which is clearly shown in Fig. 4.12. The calculated total ground-state energy per Cu-atom for each supercell size fluctuates around -3.729 eV/atom, with oscillations of roughly 0.001 eV/atom at most .

In contrast to Cu, the number of Zr-atoms in a supercell does not scale with supercell size. Hence, the error on the pure Zr ground-state energy remains constant for all Zr dissolution energy calculations and thus needs to be calculated only once. Zr has a hexagonal close-packed crystal structure in its pure equilibrium state. In order to determine the equilibrium lattice

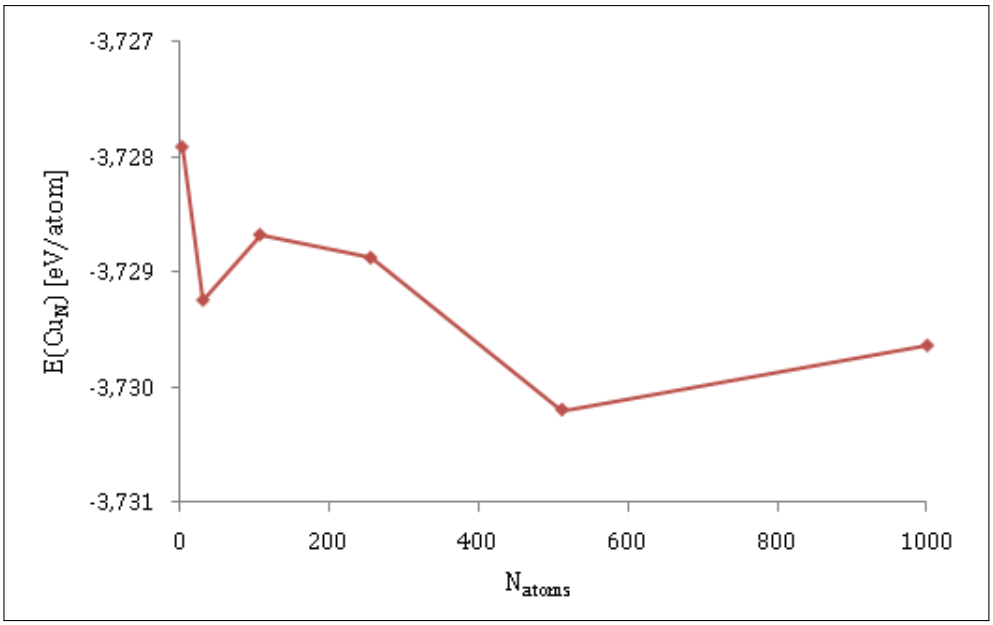

Figure 4.12: Evolution of the total ground-state energy of pure Cu as a function of number of Cu-atoms in the supercell

parameters (hexagon side length a and cell height c) of the hcp unit cell of Zr, the volume of the cell was first optimized by means of the Birch-Murnaghan equation of state. The total ground-state energy of a Zr hcp unit cell was calculated for various cell volumes. The volume was varied between $V_0' \pm 6\%$, with V_0' the initial guess for the cell volume, based on the values for a and c as obtained by Lejaeghere et al. [58] . The c/a-ratio was held constant in all these calculations. The lattice parameters obtained from the Birch-Murnaghan fit were subsequently used for the geometrical optimization with VASP. By fixing the cell volume, the c/a-ratio was optimized. Via this procedure, a = 3.231 Åand c = 5.169 Åwere found to be the equilibrium values of the Zr lattice parameters, which is close enough to experimentally obtained values of 3/230 Å for a and 5.145 Å for the cell height c [60].

The ground-state energy $E(Zr)$ could now be calculated from this optimized Zr unit cell. $E(Zr)$ was calculated using a 3×3×3, 54-atom Zr supercell. By means of k-point and E_{cut} convergence tests, the total-ground state energy of the Zr unit cell was found to be accurate up to 2.10^{-4} eV for a 17×17×17 k-mesh, a cut-off energy of 400 eV and EDIFF = 1E-6. For the 54-atom supercell, the k-mesh was adjusted to 6×6×6 subdivisions to attain a similar k-point density as in the unit cell. Eventually, a total ground-state energy of -8.318 eV/atom was found for pure Zr, which was used for all Zr dissolution energy calculations.

Effect of Zr sublattice symmetry

Now the energies of the reference states have been determined, the Zr dissolution energy can be calculated for all supercells considered in Table A.1 in Appendix A. To visualize the finite-size convergence behavior of this property, E_{diss}^{Zr} is plotted as a function of Zr-concentration in Fig. 4.13a. Different convergence trends can be clearly distinguished for the three considered

Zr sublattice symmetries. This representation method was suggested by Probert and Payne to visually separate trends for different defect symmetries, which proves to be valid for the Zr dissolution energy as well. This does not come as a surprise however: the same authors already indicated that differences in rate of convergence between different sublattice symmetries are a consequence of differences in geometry of the defect sublattice and number of nearest defects for similar concentrations. All these phenomena are observed in our supercell series as well, hence the different convergence rates.

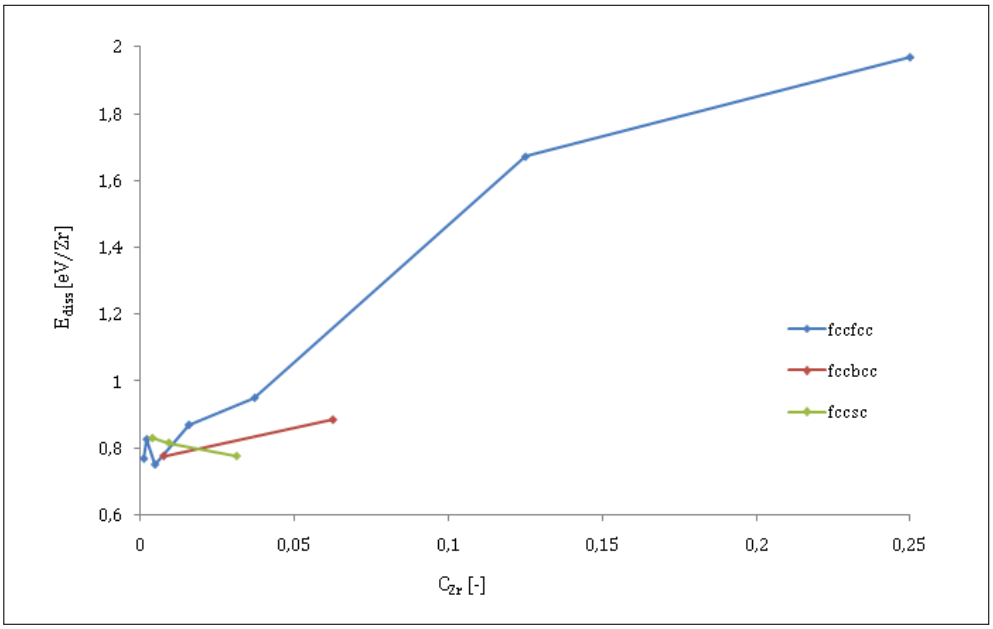

(a)

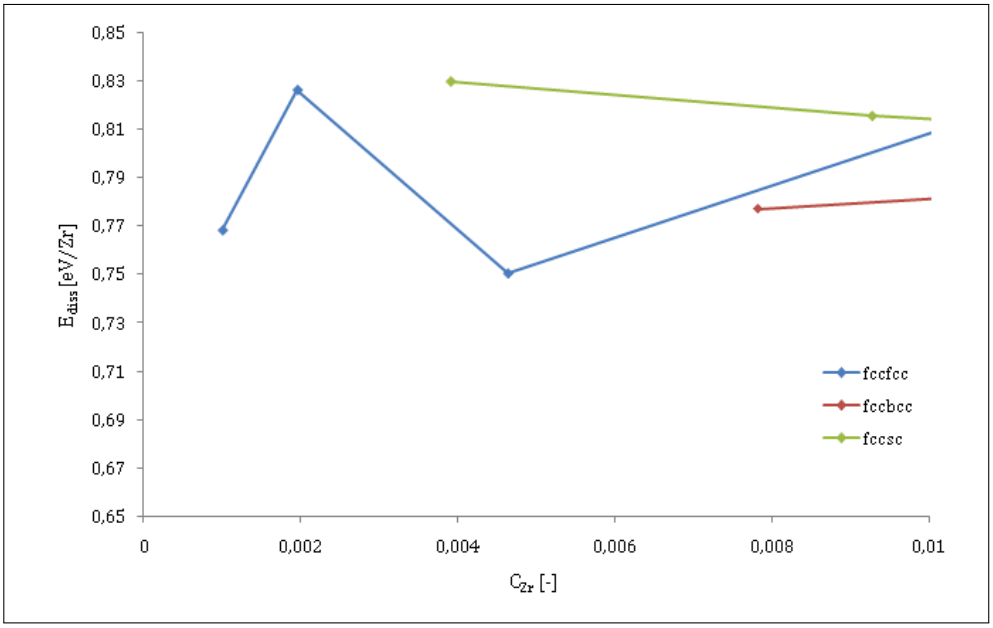

(b)

Figure 4.13: (a) Supercell finite-size convergence of the Zr dissolution energy as a function of Zr-concentration (b) Detailed picture of the finite-size convergence towards the dilute limit.

Caestecker already found that the *relaxed* Zr dissolution energy converges the most difficult for supercells with a fcc Zr sublattice. Results from his supercell finite-size convergence tests in Fig. 3.1 indicate energy differences in the order of 0.1 eV for fccfcc supercells up to 125 atoms, while energies of supercells with other sublattice symmetry vary in the order of 0.01 eV. The relative positions and convergence rates of the different trends in our supercell finite-size convergence investigation of the *unrelaxed* Zr dissolution energy are in good agreement with Caestecker's results. The fccfcc cells show a similar convergence rate at equal Zr-concentration, but differences decrease towards 0.04 eV at the lowest concentrations. Finite-size effects for the cells with fcc sublattice symmetry are hence somewhat reduced when larger supercells are included in the data set. The supercells of the other sublattice symmetries appear to converge faster towards the dilute limit of the dissolution energy, since at similar Zr-concentrations, energies obtained with bcc and sc sublattice supercells are closer to the dilute limit value than fccfcc supercells. Differences between energies of subsequent fccsc cells are in the order of 0.01 eV and thus appear to have the highest rate of convergence towards the isolated Zr dissolution energy. However, it also appears from Fig. 4.13b that all sublattice symmetries converge towards different dilute limit dissolution energies.

If only geometrical effects from the Zr sublattice and number of nearest-neighbor Zr-atoms are taken into account, the defect formation energy should converge fastest towards the dilute limit value in the case of sc sublattice symmetry since it minimizes defect interactions at a certain defect-defect separation. Probert and Payne also suggested that the directionality of the defect-defect interactions influences the energy convergence rate. According to these authors, the convergence proceeds faster if the spurious electronic charge redistribution is commensurate with the underlying charge distribution of the host lattice [13]. Since we consider a fcc Cu host lattice, the fcc symmetry should yield the highest convergence rate. This contradicts our observation that dissolution energies of fccfcc supercells convergence slowest of all towards the dilute limit value. Hence, it seems that in the case of the Cu-Zr system, the electronic charge redistribution that is commensurate with the underlying fcc lattice affects the ground-state energy of the supercell - and hence the dissolution energy - more significantly than the presence of interstitial charge at places of lower electron density, which is the case for the sc and bcc sublattice symmetries.

Supercell finite-size convergence with a constant relative accuracy

The Cu-Zr mixing enthalpy, which is the property of interest in Caestecker's work, was experimentally found to be in the order of 10 kJ/mol (depending of the Zr-concentration in the alloy) [53]. To reduce the error below 1 kJ/mol in ab initio calculations of the mixing enthalpy, Cu and Zr dissolution energies need to be known up to an accuracy of 0.01 eV/(impurity atom), since the mixing enthalpy is determined by means of these quantities. It is hence desirable to reduce the uncertainty on the Zr dissolution energy below 0.01 eV/Zr. All trends in our investigation are at first glance observed to satisfyingly converge towards a similar Zr dissolution energy of roughly 0.8 eV. However, when looking in more detail at the lowest Zr-concentrations (Fig. 4.13b), the dissolution energy can still not be considered to be accurate up to 0.01 eV.

Especially the energy difference of 0.05 eV between the 512- and 1000-atom fccfcc supercells is very significant: while the largest supercells were expected to further reduce the finite-size error, it remains in the same order as for the smaller supercells.

To get an indication of how the energy differences evolve for even lower Zr-concentrations, an additional calculation for the 1728-atom fccfcc12 cell was conducted, with only one k-point. This resulted in a Zr dissolution energy of 0.37 eV, which differs approximately 0.4 eV from the fccfcc10 energy. Such large errors cannot be attributed to finite-size errors alone anymore. First of all, the energy difference between the 1000- and 1728-atom cells is almost 10 times as large as the difference between the 512- and 1000-atom cells. This contradicts the expectation that lowering the Zr-concentration should yield a dissolution energy that is more converged with supercell size. Second, the unrelaxed energy of 0.37 eV is roughly equal to the relaxed energies found by Caestecker for the smallest Zr-concentrations considered (Fig. 3.1). Atomic relaxations will however reduce the dissolution energy since they make the Zr-dissolved supercell energetically more favorable. The relaxed energy for the 1728-cell would hence yield a far too low dissolution energy. Obviously, something else is going on.

When we return to eq. (4.1), which was used for all our Zr dissolution energy calculations, $E(Zr)$ remains constant (because the dissolution energy is calculated for the addition of one Zr-atom), while both $E(\mathrm{Cu}_{N-1}\mathrm{Zr})$ and $E(\mathrm{Cu}_N)$ express energies of the entire supercell and will hence vary with supercell size. Convergence tests for the total ground-state energy of Cu-Zr cells in chapter 3 were however conducted to achieve a certain accuracy of the energy *per atom*. In this case, values for E_{cut}, k-mesh and EDIFF were determined in order to reduce the error on the ground-state energy below 0.001 eV/atom. The optimized values for these parameters were then also found to be valid for pure Cu. Such convergence tests are the usual way of attaining a certain accuracy per atom before calculations with larger cells are performed. $E(\mathrm{Cu}_{N-1}\mathrm{Zr})$ and $E(\mathrm{Cu}_N)$ however correspond to energies of the *entire* supercell. This implies that with an accuracy of 0.001 eV/atom from convergence tests, the error is expected to be in the order of 0.1 eV for a cell of approximately 108 atoms. The same holds of course for the equally large pure Cu cell. Hence, in the worst case, the error on the dissolution energy can amount to roughly 0.2 eV. Using the same reasoning, the accuracy of the energy for supercells containing thousands of atoms, such as fccfcc10 and fccfcc12, will be even lower, in the order of 1 eV!

Because convergence tests were conducted to achieve a constant *relative* accuracy (i.e. error on the total ground-state energy per atom) in all supercells, as is usually done, the *absolute* error will differ for each supercell size that is considered. The convergence trends that are visualized in Fig. 4.13 can hence not be interpreted correctly concerning finite-size convergence since absolute errors with respect to E_{cut}, number of k-points and EDIFF differ for various supercells. This problem becomes especially important for the largest supercells, since errors for these cells become so large that any comparison with energies from smaller cells become irrelevant. This error was so far not recognized in the literature because generally only supercells containing roughly 100 atoms are considered: absolute errors in these studies will be maximally around 0.1 eV and are hence not large enough to be distinguished from finite-size errors. While large supercells were here included to further reduce finite-size errors in the Zr dissolution energy,

the absolute error on the same energy with respect to. the earlier mentioned parameter settings increases and becomes the dominant error term for the largest supercells considered. Hence, to attain a similar absolute error in all supercells that is also low enough to generate an accurate value for the Zr dissolution energy, the relative accuracy will need to increase as a function of supercell size. An optimization of the parameter settings, such as E_{cut} and the k-points, will hence be critical for the largest supercells in order to obtain sufficiently accurate values for E_{diss}^{Zr} [16].

Supercell finite-size convergence with a constant absolute error

The effect of a constant absolute error, instead of relative accuracy, on the supercell finite-size convergence behavior for the lowest Zr-concentrations, was investigated with respect to the k-point sampling density in particular. By means of a k-point convergence study as a function of supercell size, the upper limit k-meshes were determined for a constant absolute error of 0.01 eV on the Zr dissolution energy. The methodology behind this investigation and the obtained results will be discussed in more detail in the next section. The k-meshes for a constant absolute error (k-mesh$_{abs.\ error}$) of 0.01 eV are listed in the first column of Table 4.1. Each k-mesh is accompanied by its calculated Zr dissolution energy (the k-mesh was used for both the Cu-Zr- and corresponding pure Cu-calculation). The k-meshes that were used for a constant relative accuracy of 0.001 eV/atom (k-mesh$_{rel.\ accuracy}$) and their Zr dissolution energies are also summed up in this table, in order to compare the results from both sets of calculations. It also needs to be emphasized that the 'constant absolute error' k-meshes for the fccfcc8 and fccfcc10 supercells are lower limits for an absolute error of 0.01 eV, i.e. the observed absolute error with respect to k-points was still observed to be less than 0.01 eV, but computational limitations did not allow to increase the k-mesh size any further.

The results in Table 4.1 indicate that the differences between energies calculated with a different number of a k-points become larger as the supercell size grows: the largest cells (fccfcc8 and fccfcc10) already show differences in the order of 0.1 eV/Zr. This of course a consequence of the growing absolute error with increasing supercell size for 'constant relative accuracy' calculations. This can be made more clearly with, for example, the total ground-state energy calculations for the fccfcc10 Cu-Zr supercell. With the 'constant relative accuracy' k-mesh, an energy of -3729.640 eV is obtained. The absolute error on the total ground-state energy for this cell will be at most 1 eV (for a relative accuracy of 0.001 eV/atom). The same calculation, but now with the lower limit k-mesh for a constant absolute error of 0.01 eV, results in -3733.023 eV. These results are also listed in the next section in Table 4.2. The large difference between both energies is a result of the different absolute errors for the different k-meshes. The difference for the Zr dissolution energy is much smaller - approximately 0.07 eV/Zr - because the difference in the total ground-state energy for the fccfcc10 supercell is partially compensated by the total ground-state energy difference for the pure Cu cell, which will be of the same order since the same k-meshes

[16]The parameter EDIFF is not considered to be critical since the total ground-state energy per atom of the fccsc1 supercell was already found to be converged up to approximately 10^{-6} eV/atom. The absolute error with respect to EDIFF will hence still be smaller than the desired accuracy for the Zr dissolution energy.

	$\mathbf{k\text{-}mesh_{abs.error}}$ [$\mathbf{k} \times \mathbf{k} \times \mathbf{k}$]	$\mathbf{E^{Zr}_{diss,abs.error}}$ [eV/Zr]	$\mathbf{k\text{-}mesh_{rel.accuracy}}$ [$\mathbf{k} \times \mathbf{k} \times \mathbf{k}$]	$\mathbf{E^{Zr}_{diss,rel.accuracy}}$ [eV/Zr]
fccsc1	25×25×25	1.9727	21×21×21	1.9700
fccfcc2	16×16×16	1.6647	11×11×11	1.6721
fccbcc2	16×16×16	0.8691	11×11×11	0.8847
fccsc2	16×16×16	0.7456	11×11×11	0.7754
fccfcc3	12×12×12	0.9396	7×7×7	0.9501
fccsc3	12×12×12	0.7586	7×7×7	0.8153
fccfcc4	10×10×10	0.8749	6×6×6	0.8691
fccbcc4	10×10×10	0.7421	6×6×6	0.7771
fccsc4	10×10×10	0.7458	6×6×6	0.8294
fccfcc6	11×11×11	0.7679	7×7×7	0.7503
fccfcc8	7×7×7	0.7263	3×3×3	0.8261
fccfcc10	5×5×5	0.6971	3×3×3	0.7681

Table 4.1: Zr dissolution energies as calculated with the k-meshes satisfying a constant absolute error of 0.01 eV and the k-meshes satisfying a constant relative accuracy of 0.001 eV/atom, respectively. In the case of fccfcc8 and fccfcc10, the 'constant absolute error' k-meshes are lower limits for the k-point sampling density that is required for an absolute error of 0.01 eV, due to computational limitations.

were used. This clearly illustrates the need for a constant, low absolute error for Zr dissolution energy calculations in the case of supercells containing 100s or 1000s of atoms. Still, care must be taken with the values obtained for the 'constant absolute error' k-meshes in the case of the fccfcc8 and fccfcc10 supercells, since their energies were still not completely converged up to an absolute error of 0.01 eV with respect to k-points. In the case of the fccsc2 (32-atom) supercell, the difference in total ground-state energy for the two k-meshes is much smaller: for the 'constant relative accuracy' k-mesh, an energy of -123.149 eV is found, whereas the 'constant absolute error' k-mesh gives -123.147 eV. As shown in Table 4.1, this results in much smaller differences in the Zr dissolution energy compared to the largest supercells. In conclusion, 'constant relative accuracy'-calculations for the Zr dissolution energy can be considered to be accurate enough for the smaller supercells (10s of atoms), since the absolute error is still of approximately the same order as the relative accuracy, while calculations with supercells containing 100s or 1000s of atoms cannot be performed with the same relative accuracy, because the absolute error can increase up to 0.1/1 eV.

In Fig. 4.14 it can be observed how these differences in Zr dissolution energy affect the supercell finite-size convergence behavior: the energy oscillations in the fccfcc-trend from Fig. 4.13b, as a consequence of the large absolute error for the 512-atom and 1000-atom cells, have disappeared. The energies calculated for both cells can be expected to be more accurate, but are still unreliable since their accuracy can only be ensured to be up to 0.1 eV/Zr. If these data points are not considered, the trends for different sublattice symmetries seem to converge more towards the

same dilute limit value: the spread in Zr dissolution energy between the largest fccsc and fccbcc supercell has decreased from about 0.08 eV to 0.04 eV. The dilute limit value of E_{diss}^{Zr} has changed as well and appears to be around 0.72 eV/Zr instead of 0.8 eV/Zr. Performing calculations with 'constant absolute error' k-meshes instead of 'constant relative accuracy' k-meshes hence clearly improves the supercell finite-size convergence behavior of the Zr dissolution energy significantly. Remark also that in the case of fccfcc supercells a Zr-concentration of $\frac{1}{64}$ is still not small enough to approximate the dilute limit of E_{diss}^{Zr}: errors remain in the order of 0.1 eV. Most supercell calculations of defect energies are however performed with defect concentrations in this order. This agrees with our observation from the charge distribution analysis that the magnitude of spurious defect interactions is system-dependent. Hence, Cu-Zr again proves to be a system for which finite-size effects are very difficult to eliminate.

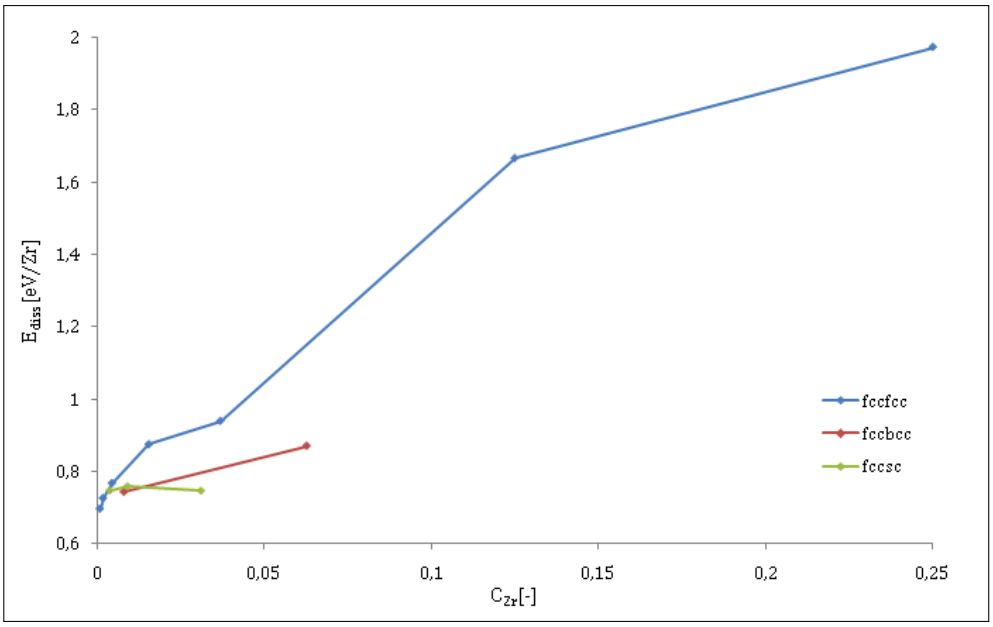

(a)

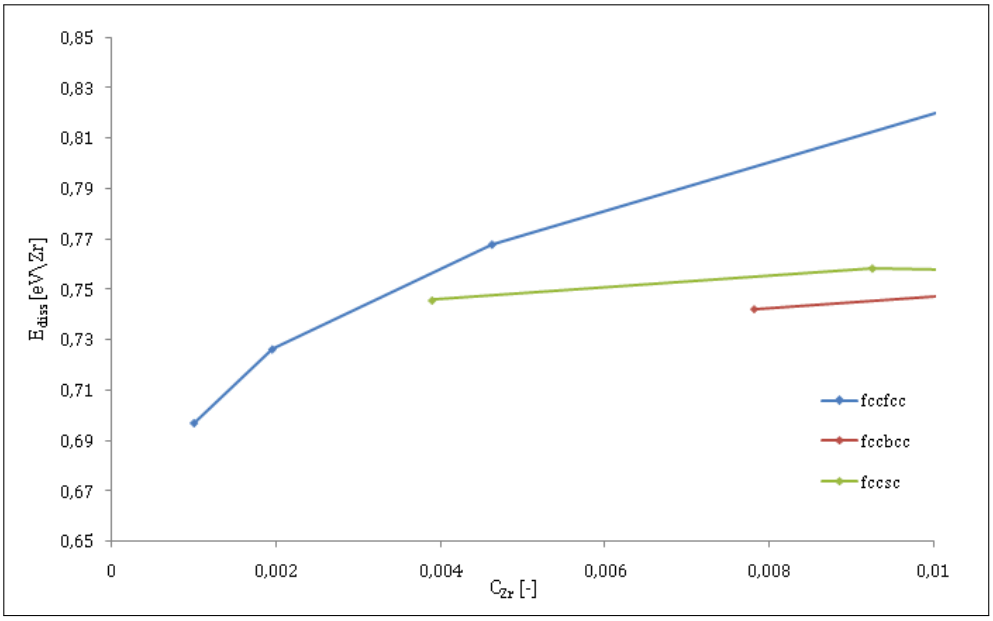

(b)

Figure 4.14: Supercell finite-size convergence of the Zr dissolution energy as a function of Zr-concentration, using 'constant absolute error' k-meshes.

4.1.4 Force

In unrelaxed supercell calculations, the positions of the nuclei are kept fixed. In this way, any relaxation of these nuclei toward a lower-energy state is prevented when a defect such as substitutional Zr is introduced. Hence, Cu host lattice atoms in the vicinity of a Zr-defect will experience a net force that drives them toward equilibrium. These forces can be calculated with ab initio codes such as VASP by using the Hellmann-Feynman theorem, as explained in subsection 3.4.2. However, when spurious interactions between Zr-atoms are present, the net force

on such a nucleus will not represent the force it would feel from an isolated defect. As a consequence, relaxation procedures are not guaranteed to produce the correct equilibrium structure anymore. In order to be able to calculate accurate forces and equilibrium structures, the force convergence was investigated with respect to Zr-concentration for particular Cu-atoms in the Cu-Zr system. As in the case of the LDOS, forces were investigated on Cu-nuclei in the vicinity of Zr and on the most bulk-like Cu-nucleus.

Force on a bulk-like nucleus

In the ideal situation of isolated Zr-defects, the Cu-atoms at a maximum distance from all nearest Zr-atoms behave as in a pure Cu-lattice and hence would feel a zero net force on their nuclei: they are neither influenced by the Zr-atom nor by the spurious interactions between Zr and its images. Investigating the force on the most bulk-like Cu-nucleus would therefore give a good indication of the accuracy of the calculated forces for the lowest Zr-concentrations considered. As explained in the previous section however, the most bulk-like Cu-atom generally resides at the middle of the primitive cell and hence will be influenced by the sublattice symmetry. The net force on this nucleus will be zero even in the presence of defect interactions. The force was therefore determined at the nearest neighbor nucleus of the middle of the primitive cell. Supercells with Zr-concentrations above $\frac{1}{64}$ were not considered because the nearest neighbor nucleus is either non-existent or a first, second or third nearest neighbor to Zr. All calculations were performed with the 'constant relative accuracy' k-meshes from Table 4.1.

Fig. 4.15a shows that the bulk-force can be quite accurately determined for smaller supercells, since fluctuations in the force are in the order of 0.01 eV/Å. It is also clear from Fig. 4.15b that these oscillations can be reduced even more if different sublattice symmetries are considered individually. As in the case of the Zr dissolution energy, different convergence trends appear for different sublattice symmetries. Hence, as long as Zr interacts with its images, the net force on a Cu-nucleus is not guaranteed to vary monotonically with decreasing Zr-concentration if the sublattice symmetry changes as well. The forces calculated in supercells with simple cubic sublattice symmetry converge faster towards zero, the true dilute limit net force on a bulk Cu-atom. For similar Zr-concentrations, fccfcc cells appear to contain a smaller error on the bulk-force than fccbcc cells, which is opposite to the convergence trends of the Zr dissolution. Attention must be paid, however, since only one data point is available for the fccbcc cells. The same figure shows that the different convergence trends are related to the distance of the Cu-nuclei with respect to Zr, as suggested by Probert and Payne . For similar Zr-concentrations, the distance of the most bulk-like Cu-nucleus to Zr is smallest for supercells with an fcc sublattice symmetry while the sc sublattice supercells maximize the Cu-Zr distance. Hence, for similar Zr-concentrations, the net force on the most bulk-like Cu-nucleus in a sc sublattice symmetry supercell will be lower than for supercells with any other sublattice symmetry. Overall, errors remain in the order of 0.001 eV/Åfor the larger supercells with respect to the dilute limit. A zero net force can not yet be obtained for the bulk-force with these Zr-concentrations, but an accuracy of 0.001 eV/Åcan be considered to be sufficiently high for most applications, such as atomic relaxation procedures.

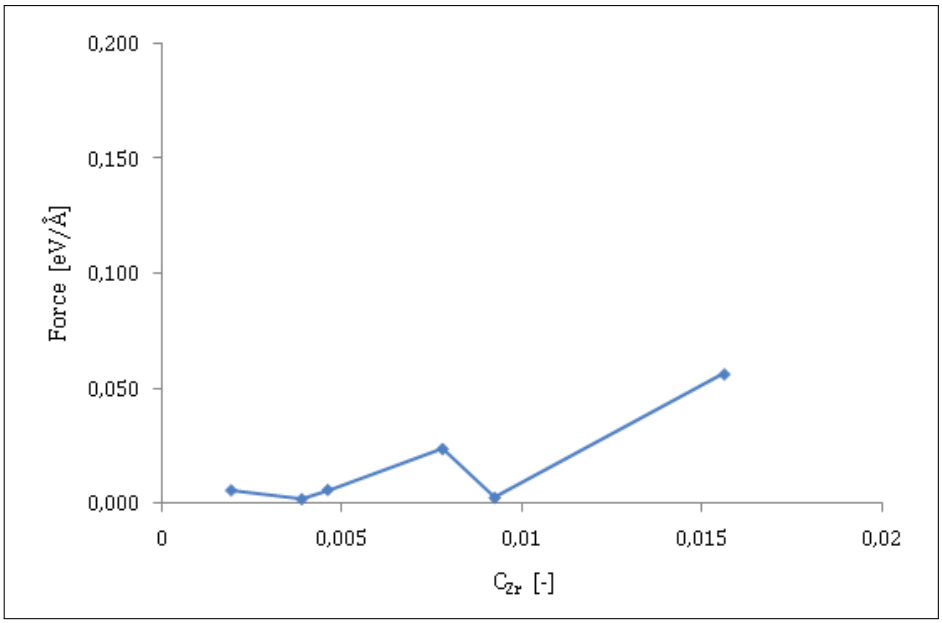

(a)

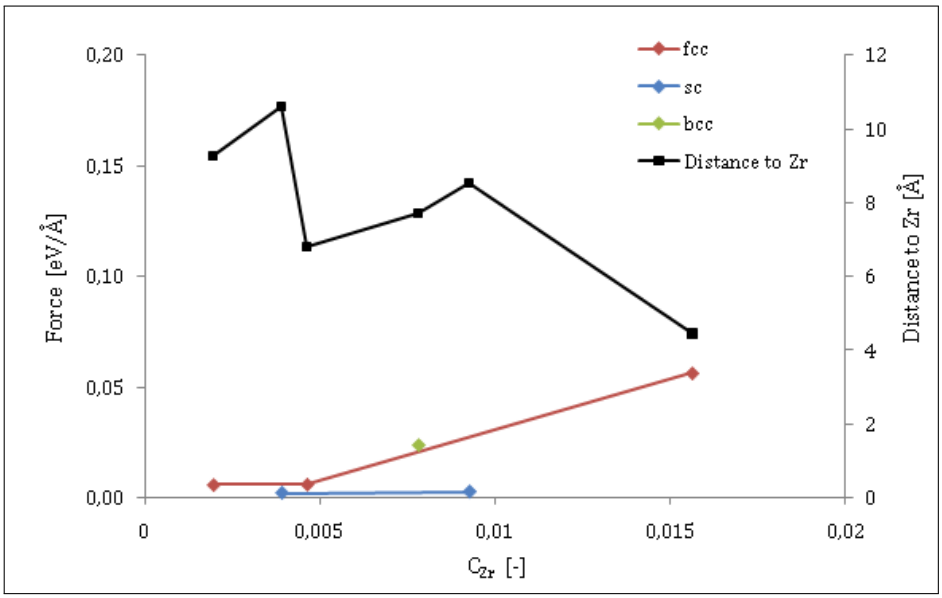

(b)

Figure 4.15: (a) Forces on the most bulk-like Cu-atom that is not influenced by Zr sublattice symmetry for Cu-Zr supercells with a maximum Zr-concentration of $\frac{1}{64}$ (b) The same forces, but with separate trends for different sublattice symmetries. The distance of the Cu-nuclei with respect to Zr are also shown.

Force on nearest neighbors

Since Cu-nuclei closer to Zr will experience a larger net force, the relaxed (equilibrium) structure and hence the total ground-state energy of this relaxed cell will predominantly depend on the accuracy of these forces. In order to investigate the convergence of the force on Cu-nuclei close to Zr, forces were determined on the first (NN1), second (NN2) and third (NN3) nearest neighbors to Zr for supercells with a Zr-concentration equal to and below $\frac{1}{27}$. Higher concentrations were

not considered since at least one of these forces then adds up to zero due to the same symmetry effect as described in the section about the LDOS, and is therefore irrelevant. The nearest-neighbor-nuclei of Zr can of course be expected to experience the largest forces. The results from these calculations in Fig. 4.16a indicate a well converging trend of the forces on NN2 and NN3 Cu-atoms, with oscillations of at most 0.01 eV/Å. Larger oscillations, in the order of 0.1 eV/Å, however remain for the net force on NN1, especially for the lowest Zr-concentrations of $\frac{1}{256}$ and $\frac{1}{512}$.

As in the case of the bulk force in the previous subsection, oscillations turn out to be related to some extent to the sublattice symmetry. This is shown for the fcc sublattice symmetry in particular in Fig. 4.16b. The oscillations for the force on NN2 and NN3 are clearly reduced if only the fcc symmetry is considered. With differences in the order of 0.005 eV/Å between the two lowest concentrations, these forces show a very pleasing convergence trend with increasing supercell size. However, even lower Zr-concentration supercells need to be considered in order to determine the accuracy of the NN1 forces in our supercells. The force on the first nearest neighbor still cannot be considered to be converged with supercell size up to the highest considered Zr-concentration of $\frac{1}{512}$. The large difference in NN1-force between the $\frac{1}{216}$ and $\frac{1}{512}$ Zr-concentration, which correspond to supercells with a different sublattice symmetry, also indicate that Zr still interacts with its periodic images. Even larger supercells are required in order to converge the NN1-force. Hence, finite-size effects seem to appear in the atomic force on a Zr-neighbor as well, despite the fact that it is a local property. On the other hand, the Hellmann-Feynman theorem guarantees that the force on a particular nucleus is proportional to the derivative of the total ground-state energy with respect to the position of the nucleus. The differences between Zr dissolution energies (and hence also supercell total ground-state energies), calculated with a 'constant relative accuracy' and a 'constant absolute error' k-mesh, were already found to grow with increasing supercell size, up to approximately 0.1 eV/Zr for the 1000-atom supercell. This was found to be a consequence of the increasing absolute error on the total ground-state energy of the supercell with respect to parameter settings, as supercells become larger. This becomes especially important for cells containing 100s to 1000s atoms. Forces can hence be expected to suffer from the same problem as the total ground-state energy itself, i.e. large errors for cells containing 100s or 1000s of atoms. The large oscillations of the NN1-force that appear for the largest supercells (lowest Zr-concentration) could then maybe explained by the large absolute error on the total ground-state energy of these cells as well. In order to find the true source of these large oscillations, forces could be calculated for each supercell with the 'constant absolute error' k-meshes, as done for the Zr dissolution energy. To obtain these forces, the self-consistent procedure for each supercell calculation needs to be completely executed. Calculations for the 216-atom and 512-atom supercells crashed, however, before the procedure had finished completely. Whereas total ground-state energies could still be recovered, forces could not be obtained. In order to obtain forces for the largest supercells, the amount of computational resources thus needs to be large enough.

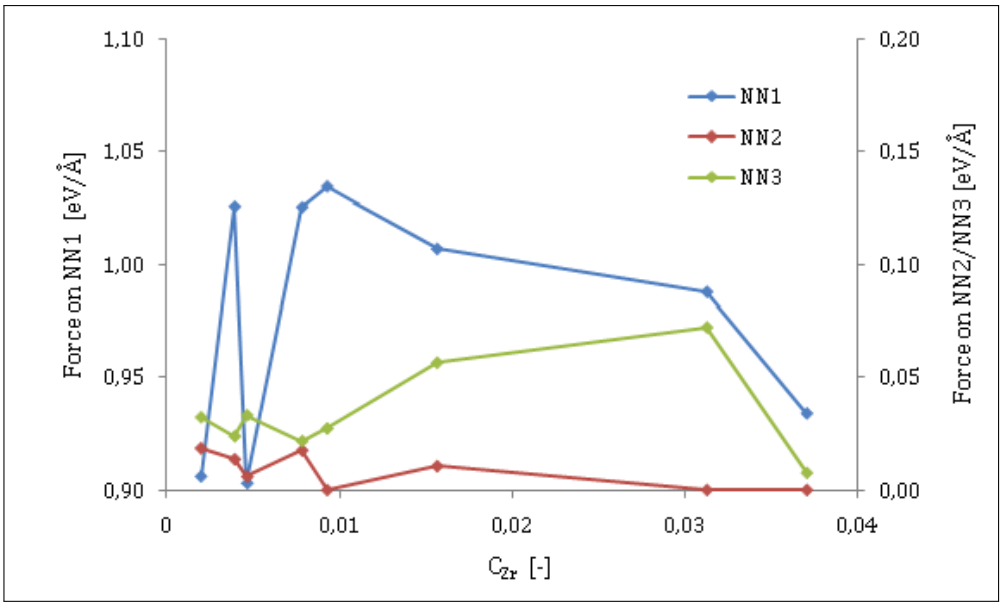

(a)

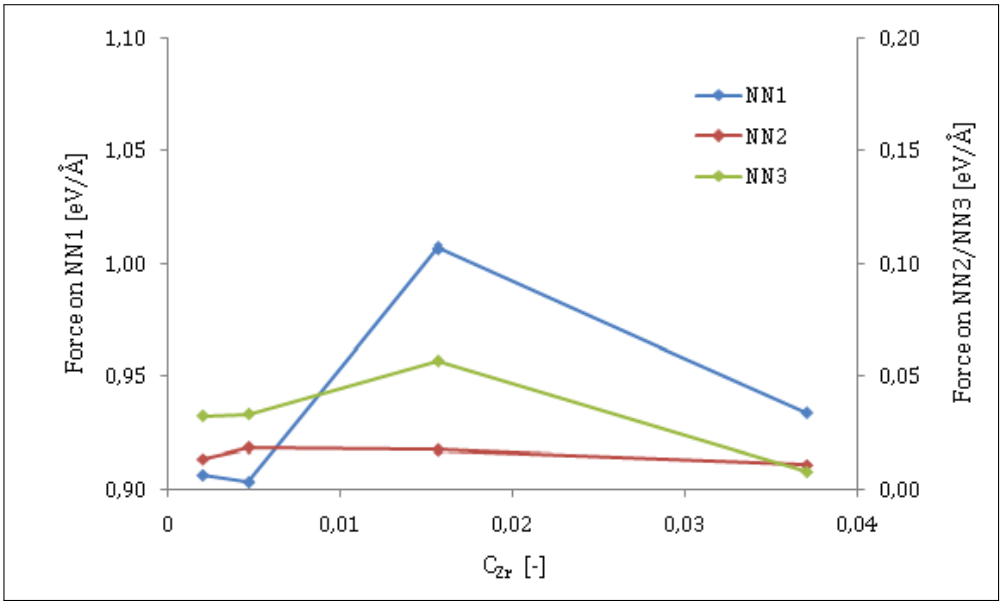

(b)

Figure 4.16: Forces on the first- (NN1), second- (NN2) and third- (NN3) nearest-neighbor Cu-atoms to Zr (a) for all Zr sublattice symmetries and (b) for the fcc sublattice symmetry exclusively.

4.2 K-point requirements for 'constant absolute error' calculations

4.2.1 System-size-dependent k-point requirements

The supercell finite-size convergence behavior of the Zr dissolution energy could not be interpreted correctly so far for the lowest Zr-concentration since the absolute error on the ground-state

energy of a supercell with respect to the parameter settings was found to be dependent on the size of the system, i.e. how many atoms the supercell contains. As a consequence, the relative accuracy needs to increase as supercells become larger, in order to produce a constant absolute error for each supercell. The relative accuracy is determined via parameter settings such as E_{cut} and the number of k-points. An optimization of these parameters is therefore indispensable for each individual supercell. This is especially the case for supercells containing 100s or 1000s of atoms, since for the fccfcc8 and fccfcc10 supercells, 'constant relative accuracy' calculations (0.001 eV/atom) for the Zr dissolution energy were found to differ quite significantly from those obtained with the lower limit k-meshes for a constant absolute error of 0.01 eV. In order to find the required values for E_{cut} and the k-point sampling density for each supercell to attain a constant, low absolute error, E_{cut} and k-point convergence tests on each individual supercell would be necessary.

Ironically however, performing VASP calculations for various cut-off energies and k-meshes becomes computationally unfeasible for the largest and at the same time most critical supercells due to high calculation times. For the most accurate calculations in Table 4.1 for example, the VASP calculation for the 4-atom supercell requires only 25 seconds on 1 node of 8 CPU's, while for the 256-atom cell a calculation time of approximately 688 hours would be necessary on the same node. Parallellisation of the calculation over different nodes can ideally reduce the calculation time in a proportional way (i.e. performing the calculation over 8 nodes requires roughly 1/8 of the calculation time on 1 node), but since the calculation time scales with the third power of the system size, convergence tests on 512-atom cells and larger are clearly unfeasible. If the evolution of the required parameter settings could however be predicted adequately for each supercell, convergence tests would not be necessary anymore. Such a procedure is much more time-efficient, but requires that a mathematical description exists for the behavior of the parameter requirements as a function of system size that is consistent with calculated data. Therefore, as a start, the k-point requirements were analyzed for several supercells in the Cu-Zr system.

The accuracy of the Zr dissolution energy with respect to supercell size was already mentioned to be preferably in the order of 0.01 eV. To ensure such a high accuracy, the errors introduced due to k-point effects must be at most in the same order. Therefore, both a 0.1 eV and 0.01 eV accuracy of the Zr dissolution energy were chosen as reference values for the k-point convergence tests, i.e. the number of k-points required to achieve these accuracies were investigated. An accuracy of 0.1 eV for the Zr dissolution energy means that its value may deviate $\pm$ 0.05 eV from the dissolution energy at infinite accuracy, i.e. for a hypothetical calculation with an infinite number of k-points. The maximum error $|\Delta E^{\mathrm{Zr}}_{diss}(N,k)|$ is hence equal to half the desired accuracy. In Appendix C it is shown that the error on the total ground-state energy of the supercell $|\Delta E(\mathrm{Cu}_{N-1}\mathrm{Zr})(k)|$ should be approximately equal to half the maximum dissolution energy error. Hence, the supercell error is related to the desired accuracy as:

$$|\Delta E(\mathrm{Cu}_{N-1}\mathrm{Zr})(k_{crit})| \cong \frac{A}{4} \tag{4.2}$$

with A the accuracy of E_{diss}^{Zr} and k_{crit} the number of k-points necessary to reach an accuracy A for a Cu-Zr supercell containing N atoms. This means that errors on the total ground-state energy of Cu-Zr cells need to be reduced below 0.025 eV and 0.0025 eV to achieve a 0.1 eV and 0.01 eV accuracy of the Zr dissolution energy, respectively.

K-point convergence tests were performed on 5 Cu-Zr supercells with different numbers of atoms N:

- fccsc1 ($N = 4$)
- fccsc2 ($N = 32$)
- fccfcc4 ($N = 64$)
- fccsc3 ($N = 108$)
- fccfcc6 ($N = 216$)

As already mentioned for fccsc1 in the previous section, the error on the total ground-state energy of the Cu-Zr supercell was determined by taking the energy of the most accurate calculation (i.e. the calculation with the highest number of k-points) as a reference. The most accurate k-mesh was selected in such a way that the smallest error $|\Delta E(\mathrm{Cu}_{N-1}\mathrm{Zr})(k)|$ was reduced below 0.0025 eV, which corresponds to $A = 0.01$ eV, the smallest Zr dissolution energy accuracy considered. This however implies that the density of the reference k-mesh will vary for the different cells: the accuracy of the calculated errors will nevertheless be similar and at most of the same order as the lowest error $|\Delta E(\mathrm{Cu}_{N-1}\mathrm{Zr})(k)|$ for each N. K-point convergence tests for the different supercells can therefore without any problem be compared with each other.

The evolution of the absolute error on $E(\mathrm{Cu}_{N-1}\mathrm{Zr})$ with the number of k-points is shown for all 5 supercells in Fig. 4.17. Green and red lines indicate in each figure the upper limit for an accuracy of 0.1 eV and 0.01 eV for the Zr dissolution energy, respectively. All graphs are on a logarithmic scale in order to investigate the lowest errors in more detail. The absolute error decreases in an oscillatory fashion with increasing number of k-points for all supercells, except in the case of $\mathrm{Cu}_{215}\mathrm{Zr}$. This is however a consequence of the limited number of data points available for this supercell: performing a k-point convergence test on a 216-atom supercell already requires a significant amount of calculation time. The error for the 9×9×9 k-mesh (last data point in Fig. 4.17e) is already below the upper limit for an accuracy of 0.01 eV. This does not ensure that such a k-mesh is already large enough to achieve an accuracy of 0.01 eV. No denser k-point sampling grids were considered anymore, however, because calculations for these grids became computationally unfeasible. Therefore, the 9×9×9 k-mesh is hence considered as a lower limit for a 0.01 eV accuracy in the case of $\mathrm{Cu}_{215}\mathrm{Zr}$.

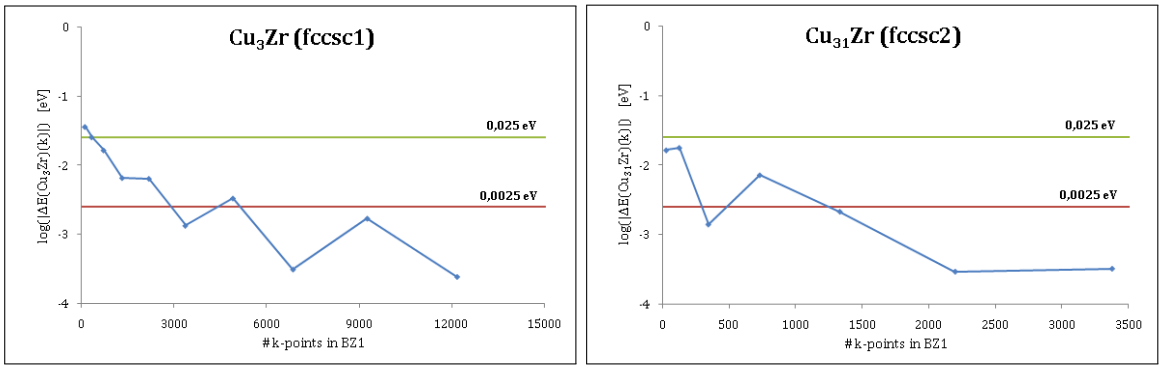

(a)

(b)

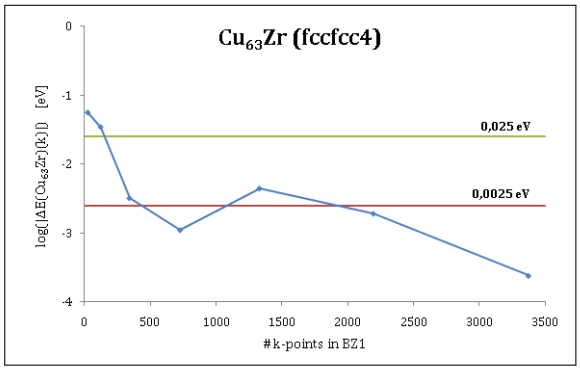

(c)

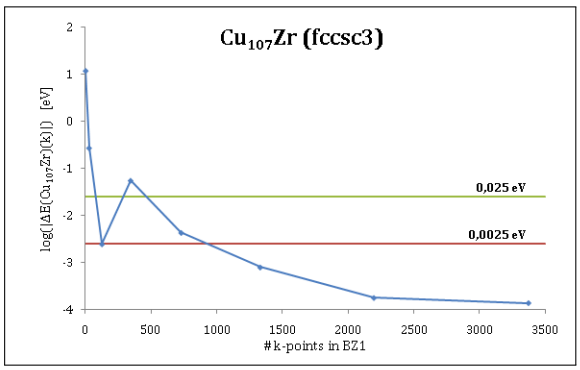

(d)

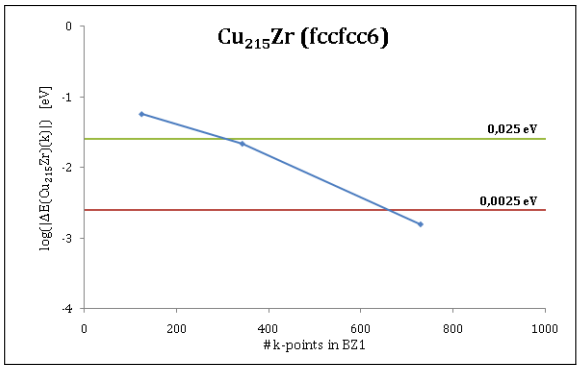

(e)

Figure 4.17: Evolution of $|\Delta E(\mathrm{Cu}_{N-1}\mathrm{Zr})(k)|$ with the number of k-points for (a) fccsc1 (Cu_3Zr), (b) fccsc2 ($Cu_{31}Zr$), (c) fccfcc4 ($Cu_{63}Zr$), (d) fccsc3 ($Cu_{107}Zr$) and (e) fccfcc6 ($Cu_{215}Zr$)

The k-mesh was also varied to some extent for the 1000-atom supercell (fccfcc10). Results from these calculations are summarized in Table 4.2. The difference in total ground-state energy between the largest k-meshes in this table, was already discussed in subsection 4.1.3. Since all total ground-state energy differences are in the order of 1 eV, a Zr dissolution energy calculation with a relative accuracy of 0.001 eV/atom (which is roughly achieved with the 3×3×3 k-mesh) will not suffice for an absolute error below 0.01 eV/Zr (or even 0.1 eV, as shown in Table 4.1). The 5×5×5 k-mesh can be considered as the expected k-point requirement for an accuracy of 0.1 eV/Zr. To reach an even higher accuracy, a calculation with a 7×7×7 k-mesh on 105 16-core (!) nodes was performed as well. This calculation crashed, however, due to virtual memory

# k-points in BZ1	E($Cu_{999}Zr$) [eV]
1	-3714.617
27	-3729.640
125	-3733.023

Table 4.2: Total ground-state energy of the fccfcc10 supercell for various numbers k-points.

limitations, indicating that even moderately accurate calculations are becoming computationally unfeasible for such large cells. The 5×5×5 k-mesh can hence be considered as a lower limit for the k-point requirements for $A = 0.01$ eV/Zr.

Based on all these k-point convergence tests, the number of k-points required to achieve an accuracy of 0.1 eV and 0.01 eV is plotted as a function of system size (Fig. 4.18). The data points for the 1000-atom supercell are the same in both figures: for $A = 0.1$ eV/Zr, it is the expected k-point requirement, while for $A = 0.01$ eV/Zr it is the lower limit k-point requirement. It is observed that a higher desired accuracy for the Zr dissolution energy requires an increase of the k-point sampling density over the whole system-size range. This could be expected, since a higher accuracy implies a reduced absolute error $|\Delta E(\mathrm{Cu}_{N-1}\mathrm{Zr})|$: k-point convergence tests in Fig. 4.17 have already shown that a denser k-point sampling of the first Brillouin zone, despite some oscillations, systematically reduces the absolute error.

The data obtained from the k-point convergence tests indicate that for each individual accuracy A, the required number of k-points rapidly decreases as the supercell size is increased in the small supercell-size range (10s of atoms), while this decrease is slowed down significantly in the 100-1000 atom region. This behavior can be understood from two competing effects. On the one hand, an increase of the supercell size implies that the volume of the first Brillouin zone (V_{BZ1}) decreases proportionally. This means that if the first Brillouin zone of a one-atom supercell has a volume $V_{BZ1,1}$, the BZ1-volume of an N-atom cell will be $\frac{V_{BZ1,1}}{N}$. In order to keep the relative accuracy constant, the k-point sampling density of the Brillouin zone needs to be similar. A larger supercell hence requires less k-points to sample its first Brillouin zone to attain the same relative accuracy. If k_1 k-points are required to sample the first Brillouin zone of the one-atom cell, the N-atom supercell needs to be sampled with a number of k-points equal to:

$$k_N = \frac{k_1}{N} \tag{4.3}$$

On the other hand, to attain a constant absolute error, the relative accuracy cannot remain constant but needs to be enhanced if the supercell size increases. This effect hence calls for an increase of the number of k-points. According to Fig. 4.18, the first effect clearly dominates for small supercells: for small values of N, k_N decreases rapidly, corresponding to eq. (4.3), while the relative accuracy does not need to be increased very much for the same absolute error[17]. As supercells become larger, containing 100s of atoms or more, the absolute error rapidly increases for a constant relative accuracy. For such supercells, the relative accuracy needs to be enhanced

[17]Recall that the absolute error is roughly equal to N times the relative accuracy.

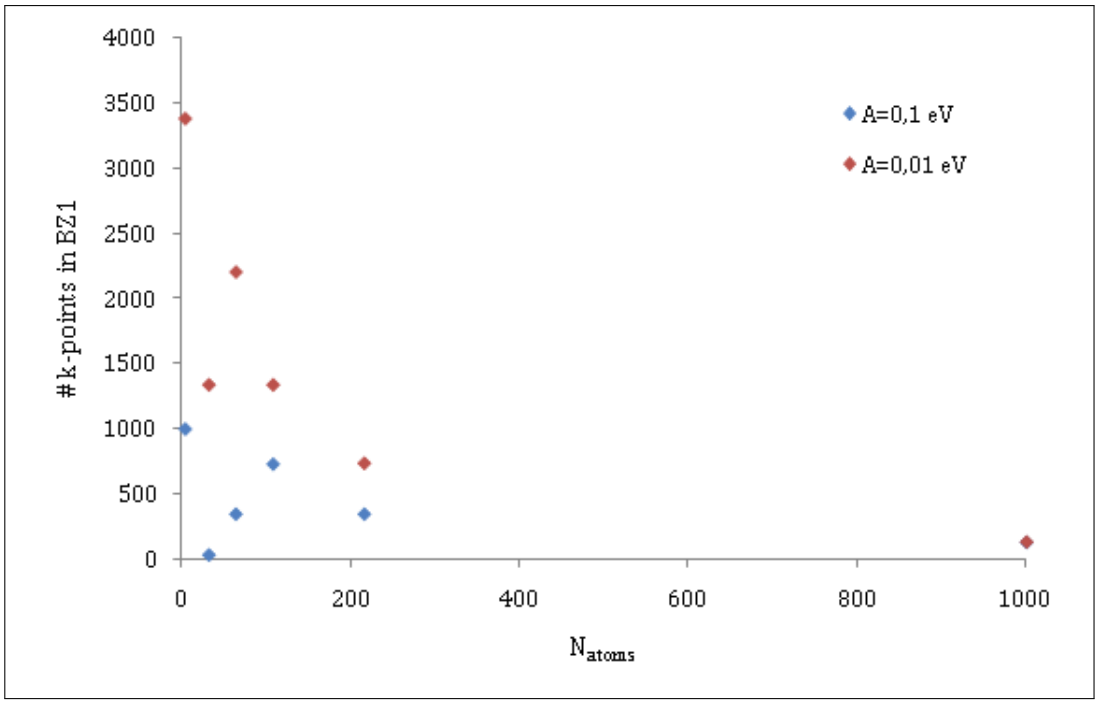

Figure 4.18: Number of k-points required to attain an accuracy of 0.1 eV and 0.01 eV as a function of system size.

by a factor of 100 or 1000, depending on the supercell size: this required increase of k-points will largely compensate the k-point reduction allowed by the smaller Brillouin zone volume. This explains why the k-point requirements decrease more slowly in the large-supercell limit.

4.2.2 Prediction of the k-point requirements

The data points in Fig. 4.18 only give an indication of the way the k-point requirements appear to evolve with supercell size. In addition, data points are not available for cells in the large-supercell limit due to the large computational cost for k-point convergence tests on such cells. Hence, k-point requirements cannot be exactly deduced on sight, especially not for large supercells since the true behavior of the requirements in this limit is uncertain. One possibility to obtain more accurate predictions of the number of k-points in the large-supercell limit, is to fit the (k, N)-data from Fig. 4.18 directly to various possible fitting functions. However, note that the evolution of k-point requirements as a function of system size for a particular accuracy can also be derived from the k-point convergence of the relative accuracy. Consider a fitting function $f(a, b, k_1)$, with a and b fitting parameters, that describes the absolute value of the relative accuracy $|\Delta E_{atom}|$ as a function of the number of k-points in a one-atom supercell:

$$|\Delta E_{atom}| = f(a, b, k_1) \tag{4.4}$$

The effect of the decreasing first Brillouin zone volume with supercell size N can be taken into account with eq. (4.3). The required increase in relative accuracy with N can be included as

well: a cell containing N atoms will have an absolute error on its ground-state energy that is N times as large as the relative accuracy:

$$|\Delta E(\mathrm{Cu}_{N-1}\mathrm{Zr})| = N|\Delta E_{atom}| \tag{4.5}$$

For an accuracy A of the Zr dissolution energy, the absolute error on the supercell can be at most $\frac{A}{4}$. Hence, eq. (4.4) can be rewritten as:

$$\frac{A}{4} = Nf(a, b, Nk_N) \tag{4.6}$$

If a and b are known from the fitting procedure, this equation allows to determine the behavior of the required number of k-points k_N as a function of system size N. Data from our k-point convergence tests on the Cu-Zr supercells were therefore used to analyze the convergence behavior of the relative accuracy as a function of the one-atom number of k-points. Only data from the 4-atom, 32-atom and 64-atom supercells were used since too few data points are available from the 108-atom and 216-atom cells. Both errors and k-points were rescaled for each data set to properties for one atom, using eqs. (4.4) and (4.5). These data points are plotted in Fig. 4.19, showing that the relative accuracy rapidly increases with a denser k-point sampling. An appropriate fitting function $f(a, b, k_1)$ that shows such a large curvature is an exponential function of the form $a\exp(-bk_1)$, where $a > 0$ and $b > 0$. By means of eq. (4.6), the expression for the required number of k-points as a function of system size N for this particular fitting function becomes:

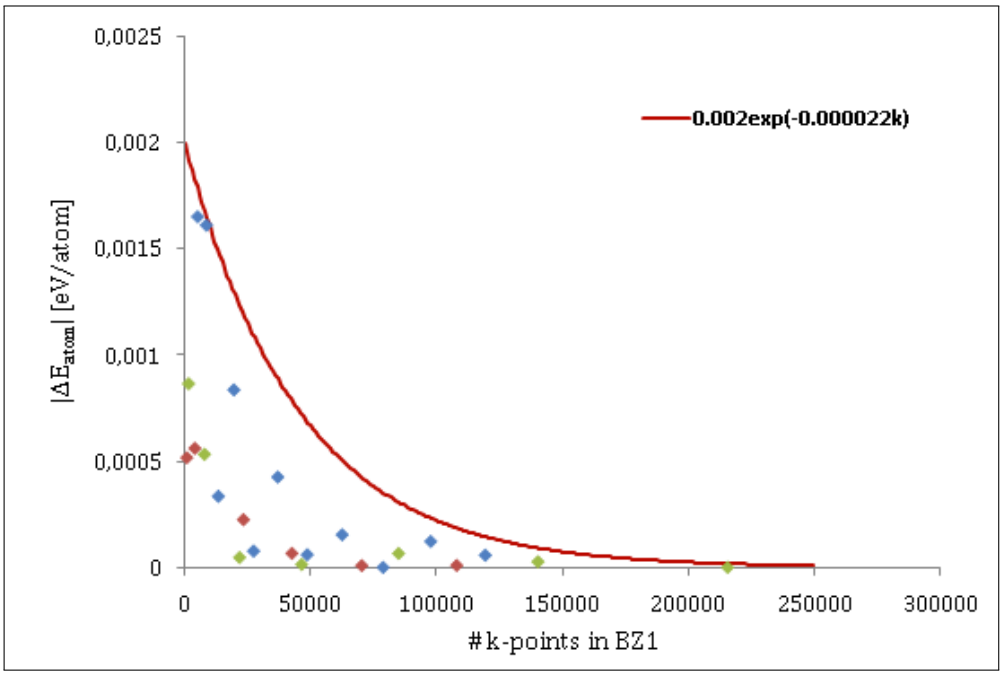

Figure 4.19: Evolution of the relative accuracy with the number of k-points in a one-atom supercell. The enveloping exponential function,'fitted' to the highest positioned data points, is also shown.

$$k_N = \frac{1}{bN} \ln(\frac{4aN}{A}) \tag{4.7}$$

Such an expression is certainly useful for the prediction of the required number of k-points for the large supercells: it predicts that no k-points are required for an 'infinitely' large supercell (i.e. $\lim_{N\to\infty} \frac{1}{bN} \ln(\frac{4aN}{A}) = 0$ for $a > 0$ and $b > 0$), which is in good agreement with the expectation that a single k-point calculation will suffice for such an infinite supercell, since the volume of its first Brillouin zone is zero.

In order to determine appropriate values for the fitting parameters a and b, the data points in Fig. 4.19 need to be fitted with the proposed exponential function. A large scatter can be observed in these data points, however. It would therefore be safer to determine the fitting parameters in such a way that the exponential function envelops the data points in the upper limit, i.e. the fitting function lies as close as possible to the data points, but still above them. In this way, the error on the total ground-state energy per atom is (slightly) overestimated for each k-point sampling density, which means that the required number of k-points will be overestimated for each supercell size. The predicted k-point requirements will hence be an upper limit for a certain accuracy of the Zr dissolution energy, implying that with these amounts of k-points, supercell finite-size convergence tests can be safely performed for every supercell size. Remark that the exponential function is no longer fit to the data points. Values for the parameters a and b are determined in such a way that the exponential function envelops the data points in Fig. 4.19 as good as possible. The result of this procedure is also shown in Fig. 4.19. The curvature is not optimal for the smaller amounts of k-points, but, most importantly, the enveloping function lies above all data points. The obtained parameters of the enveloping function are $a = 0.002$ eV and $b = 0.000022$. An optimal correspondence between the enveloping function and the data points for the highest relative accuracies is not the most important issue. Such relative accuracies are required for the smaller supercells to attain a particular accuracy A on the Zr dissolution energy. This implies that the lower k-point range of the enveloping function will result in the upper-limit k-point requirements of the smallest supercells (10s of atoms). An accurate prediction of the k-point requirements is not so important for such supercells, because k-point convergence tests can be relatively easy performed for them.

Now the values for the parameters of the enveloping function a and b are determined, the upper-limit k-point requirements for any accuracy A can be predicted for each supercell size N by means of eq. (4.7). The functions are visualized in Fig. 4.20 for $A = 0.1$ eV/Zr and $A = 0.01$ eV/Zr in particular, together with the data points (N, k_N) from Fig. 4.18. For $A = 0.1$ eV/Zr, the expected trend for the k-point requirements with supercell size, as visualized in Fig. 4.18, is not very well reproduced for very small supercells: when decreasing the supercell size, the function reaches a maximum, subsequently decreases very fast and even becomes negative for the smallest supercells (12 atoms and less). This is the result of the parameter a (0.002 eV) being much smaller than the accuracy A (0.1 eV/Zr): for small N, the fraction in the ln-factor of eq. (4.7) then becomes < 1 and the whole term on the right-hand side of this equation becomes negative. This indicates that an exponential function is not a physically correct description of the decreasing relative accuracy with increasing k-point sampling density, as visualized in Fig.

4.19. There is of course no reason to believe why an exponential function should be the most appropriate enveloping function. Most importantly, however, the predicted k-point requirements in Figs. 4.20a and 4.20b are closer to and still above the data points in the large-supercell limit, which is the supercell range of interest. The enveloping function predicts an upper limit requirement of 200 k-points for the 1000-atom supercell, which is approximately equivalent with a 6×6×6 k-mesh. This is slightly larger than the 5×5×5 k-mesh that was found to suffice from our calculations, but is still within reasonable agreement. The best results are clearly obtained for $A = 0.01$ eV/Zr, except for the large overestimation of the k-point requirements for the smaller supercells. This is however a consequence of the too small curvature of the exponential function in Fig. **??**. For the 1000-atom supercell, the envelopng function predicts a 7×7×7 k-mesh to be sufficient. This is the smallest possible k-mesh that is still larger than the 6×6×6 k-mesh, which was found as an upper limit for the same cell for $A = 0.1$ eV/Zr. The absolute error on the 1000-atom supercell is hence predicted to decrease fast with increasing k-point sampling density.

With appropriate parameters a and b, the enveloping exponential function appears to produce reliable upper-limit k-point requirements for the larger supercells (100s of atoms). Care must be taken with too low accuracies ($A \geq 0.1$ eV/Zr), however, since the (k_N, N)-trend as observed from the data points in Fig. 4.18 is then not correctly reproduced for the smaller supercells.

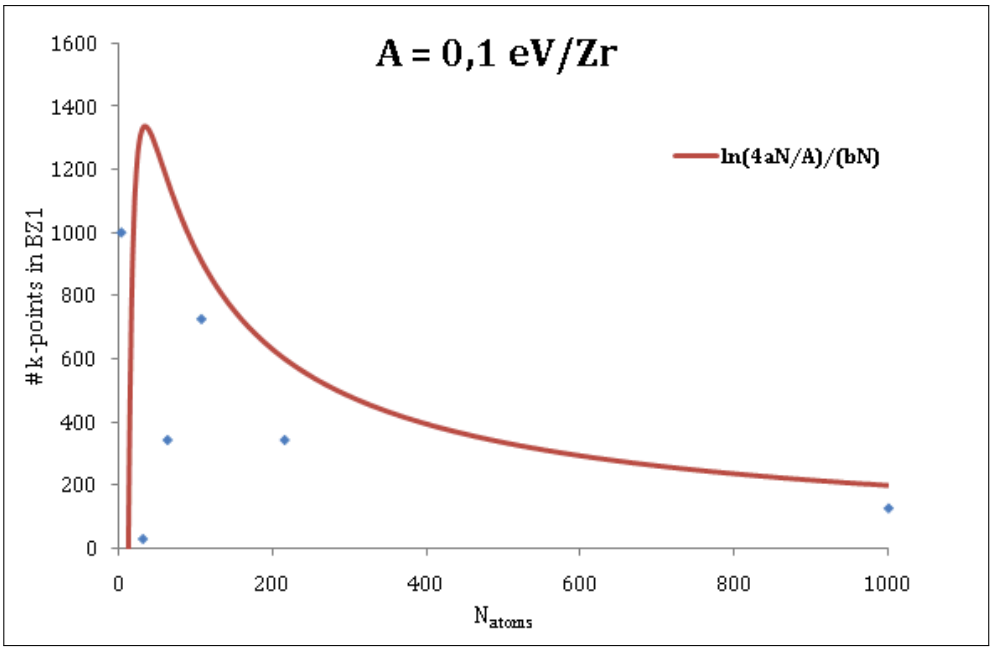

(a)

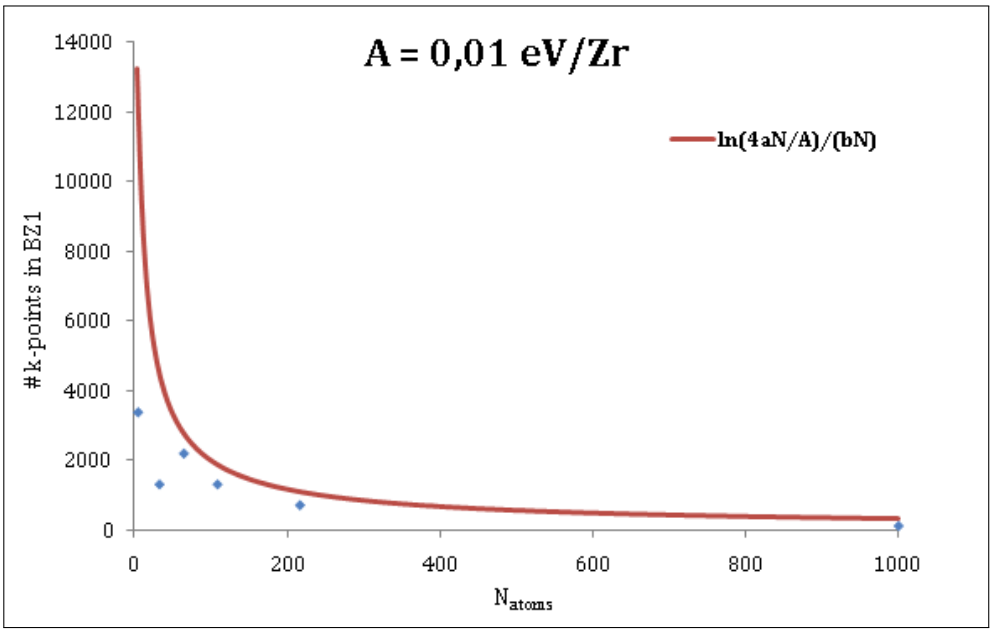

(b)

Figure 4.20: The predicted upper-limit k-point requirements as a function of supercell size for (a) $A = 0.1$ eV/Zr and (b) $A = 0.01$ eV/Zr.

The k-meshes that were used for the 'constant absolute error' calculations in subsection 4.1.3 are based on the prediction of the k-point requirements for $A = 0.01$ eV/Zr in Fig. 4.20b, except for the fccfcc8 (512-atom) and fccfcc10 (1000-atom) supercells, for which lower limit k-mesh sizes were used (due to the lack of calculation time and amount of computational resources for the predicted, larger k-meshes). If both supercells were not included in the data set, the supercell finite-size convergence was observed to be significantly improved with respect to the 'constant relative accuracy' calculations. This procedure of performing 'constant absolute error' calcula-

tions, by means of upper-limit k-point requirements as predicted by an enveloping exponential function, hence proves to be a useful way of removing large absolute errors from ground-state energy calculations of large supercells. However, despite the fact that the predicted upper-limit k-point requirements for supercells such as fccfcc8 (512 atoms) and fccfcc10 (1000 atoms) would produce Zr dissolution energies which can be safely included in the supercell finite-size convergence investigation, VASP calculations with such k-meshes (8×8×8 for fccfcc8 and 7×7×7 for fccfcc10 for $A = 0.01$ eV/Zr) become unfeasible due to computational resource and calculation time limitations: recall that the calculation for the fccfcc10 supercell with the 7×7×7 k-mesh had even crashed on 105 16-core nodes. While such supercells could be very interesting for the supercell finite-size investigation of the Zr dissolution, because spurious Zr interactions and hence finite-size errors become small(er), they probably cannot be considered since a too high k-point sampling density is required to attain a low absolute error (0.01 eV/Zr). Hence, when performing a supercell finite-size convergence investigation of the defect formation energy, the size of the largest supercell that can be used will depend on the desired accuracy of the defect formation energy.

Absolute errors with respect to other parameters that induce significant absolute errors with increasing supercell size, need to be removed in a similar way in order to further enhance the supercell finite-size convergence behavior of the Zr dissolution energy, or any defect formation energy in general. The relative accuracy then needs to be visualized as a function of this parameter for a hypothetical one-atom supercell. Remark however that it is not guaranteed that an exponential function will be equally suitable as for the case of the k-point requirements.

4.3 Fe-H: Supercell finite-size convergence of the H dissolution energy

The H dissolution energy can be calculated by means of eq. (3.4). In the particular case of the Fe-H system, this equation can be rewritten as:

$$E_{diss}^{\mathrm{H}} = E(\mathrm{Fe}_N\mathrm{H}) - E(\mathrm{Fe}_N) - \frac{1}{2}E(\mathrm{H}_2) \tag{4.8}$$

Computational details about ground-state energy calculations of Fe-H and pure bcc Fe supercells were already mentioned in Chapter 3. However, in order to calculate the H dissolution energy, the total ground-state energy of H in its pure equilibrium state needs to be known as well. Before discussing results from the supercell finite-size investigation, details about the calculation of $E(\mathrm{H}_2)$ are briefly described.

4.3.1 Total ground-state energy of H_2

Our reference state for hydrogen at 0 K is H_2, i.e. molecular hydrogen. Its ground-state energy can be determined with VASP by conducting a gamma point calculation[18] of a H_2-molecule in a 10×10×10 $\AA^3$ cell. In this way, interactions with unphysical images are minimized. The position of one of the H-atoms is relaxed in order to find the equilibrium bond length of the molecule and its corresponding ground-state energy. The bond length was found to be 0.749 Å which is in excellent agreement with results from Jiang and Carter [33]. A ground-state energy of -6.788 eV was calculated for the relaxed H_2-molecule and was applied for all H dissolution energy calculations.

DFT calculations are known to yield inaccurate energies for molecular hydrogen [61]. This will however not affect the supercell finite-size convergence behavior since the same H_2-related error is introduced in every dissolution energy.

4.3.2 Supercell finite-size convergence of the H dissolution energy

The Zr dissolution energy in the Cu-Zr system has proved to be a property that is difficult to converge with supercell size due to the combined effect of strong, persistent interactions between Zr and its periodic images up to the largest supercells and the large absolute errors on the total ground-state energy at the traditional 'constant relative accuracy' settings. In the case of the Fe-H system, finite-size effects will undoubtedly appear in supercell calculations of the H dissolution energy as well. The magnitude of spurious defect interactions was already found in subsection 4.1.1 to be heavily dependent on the type of defect system, but it was concluded at the same time that an accurate prediction of the degree of interaction is so far impossible. In the literature review in chapter 2, about the computational study of point defects in iron, both relaxed an unrelaxed H dissolution energy were found to converge very fast with supercell size (Table 2.1): $Fe_{128}H$ supercells already reduced the error on this energy to approximately 0.01 eV/H, which is accurate enough for most H-defect binding energy calculations. These finite-size convergence tests were however performed with a constant relative accuracy. As we have shown earlier in this chapter, this procedure is potentially unsafe. The apparent supercell finite-size convergence behavior could hence be a coincidental one, since absolute errors could become already quite large for the $Fe_{128}H$ supercell (in the order of 0.1 eV). The supercell size convergence study of the unrelaxed H dissolution energy was performed by Jiang and Carter with a relative accuracy for the ground-state energy of a supercell that lower than 0.001 eV/atom (i.e. the error is higher than 0.001 eV/atom). They used a 12×12×12 k-mesh and a 350 eV cut-off energy for the Fe_2H calculation with VASP, while we found for the same cell that a 19×19×19 k-mesh and a E_{cut} = 400 eV reduce the error below 0.001 eV/atom. The unrelaxed H dissolution energy calculations were therefore first repeated with the higher parameter settings from our convergence tests. The relative accuracy was held constant for all supercell calculations. The $Fe_{250}H$ supercell was also concluded. Since absolute errors can be up to approximately 0.2 eV for this supercell, the difference between the H dissolution energy of the $Fe_{128}H$ and $Fe_{250}H$ supercells could become

[18] A calculation with only one k-point, at the origin of the reciprocal space.

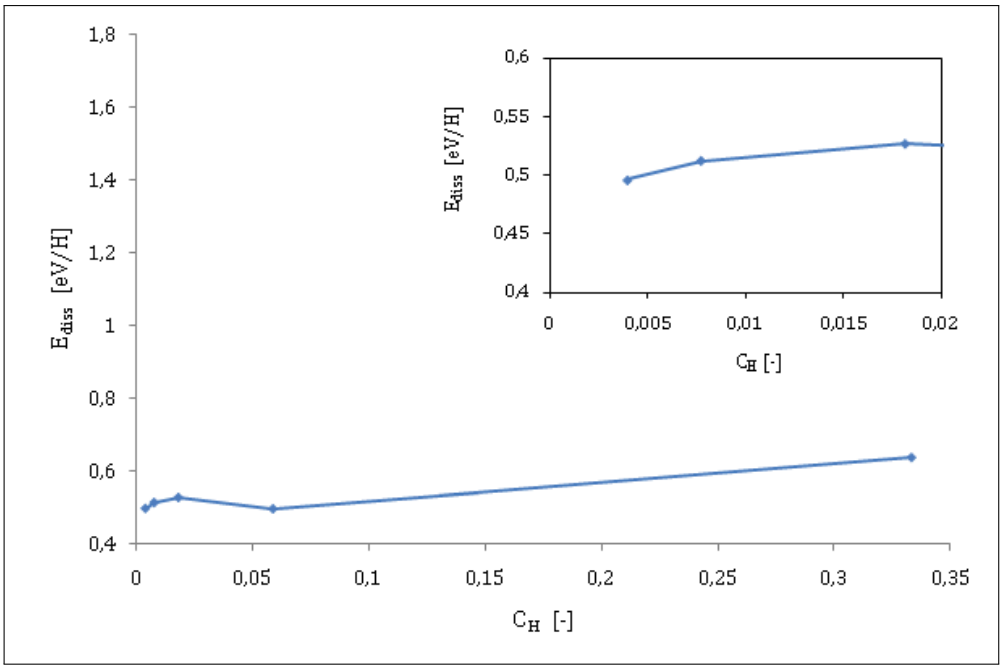

Figure 4.21: Supercell finite-size convergence of the H dissolution energy as a function of H-concentration. Inset: The H dissolution energy convergence in more detail for the smallest H-concentrations.

larger than expected in the literature, since growing absolute errors with respect to parameter settings for increasing supercell sizes were not taken into account.

The calculated H dissolution energies are plotted in Fig. 4.21 as a function of the H-concentration. The H dissolution energy as calculated with the Fe_2H supercell differs significantly from the other values, in the order of 0.15 eV. This indicates that this supercell can rather be considered as a Fe-hydride rather than a H-atom dissolved in a Fe bulk lattice. The spread in the H dissolution energy as obtained from the other supercells, appears to be very small, especially compared to the supercell finite-size convergence behavior of the Zr dissolution energy in Cu (Fig. 4.21). When looking in more detail in the dilute limit (inset of Fig. 4.21), energy oscillations are at most 0.02 eV/H, the $Fe_{250}H$ supercell calculation included, and this for a constant relative accuracy of 0.001 eV/atom in each supercell. This convergence trend is in good agreement with the supercell finite-size convergence behavior of the unrelaxed H dissolution energy as obtained Jiang and Carter, despite their lower relative accuracy. In the case of the Cu-Zr system, on the other hand, differences in the order of 0.1 eV/Zr are observed between Zr dissolution energies obtained from subsequent Cu-Zr supercells (if all sublattice symmetries are considered together). Even if every sublattice symmetry is considered individually, energy differences are larger compared to the H dissolution energy, especially in the case of the fcc sublattice symmetry. Hence, finite-size errors in the Fe-H system appear to diminish much faster with decreasing defect concentration than in the Cu-Zr system.

All these calculations were performed with a constant relative accuracy of 0.001 eV/atom on the total ground-state energy. This is the usual procedure for defect calculations by means of the supercell method, if different supercell sizes are considered. Despite the fact that finite-size

errors even appear to be already negligible for the $Fe_{54}H$ supercell, the apparent convergence behavior could still be completely coincidental because the absolute error with respect to parameter settings could become quite large for the largest considered supercells, in the order of 0.1 eV/H. It would therefore be safer, as in the case of the Zr dissolution energy in Cu, to perform all calculations for supercell finite-size convergence investigation of the H dissolution energy with a constant absolute error (that is equal to or lower than the desired maximum error on the H dissolution energy). As discussed in the previous sections, this would require k-point and E_{cut} convergence tests for each considered supercell. Such a procedure becomes very time-inefficient for supercells containing several 100s of atoms. Instead, upper limits for the k-mesh and E_{cut} could be determined for these cells by means of the procedure that was discussed in the previous section for the k-points in particular. In conlusion, to investigate the supercell finite-size convergence of the unrelaxed H dissolution energy, without the risk of obtaining misleading H dissolution energies for the largest supercells due to possibly large absolute errors, can be conducted by means of the following methodology:

- Define the desired relative accuracy of the H dissolution energy (e.g. 0.01 eV/atom) with respect to parameter settings;
- Determine how large the absolute error on the total ground-state energy of the Fe_NH and corresponding Fe_N supercells may be for this desired accuracy: check if the convergence behavior of the ground-state energy with respect to E_{cut} and k-points is similar for Fe_NH and Fe_N by means of convergence tests on the smallest supercell. If so, then the absolute error on the ground-state energy of the supercell can be at most $\frac{A}{4}$ (with a definition of the accuracy A as in section 4.2) and only convergence tests are necessary for the Fe-H supercells;
- Perform a k-point convergence test of the total ground-state energy for the smallest Fe_NH supercell. Determine for each calculation with a different k-mesh the absolute value of the error on the ground-state energy with respect to the most accurate calculation (i.e. the calculation with the highest amount of k-points). Reduce these errors to relative accuracies using eq. (4.5). Determine for each k-mesh, with k_N k-points in the first Brillouin zone, the equivalent number of k-points in the first Brillouin zone of a hypothetical one-atom supercell k_1 via eq. (4.3). Plot the relative accuracies as a function of k_1;
- Do the same for one or two other, small Fe_NH supercells. Plot all data points in the same figure;
- Determine the parameters of the enveloping function a and b for which (preferably) the function $|\Delta E_{atom}| = a\exp(-bk_1)$ lies as close as possible to the data points, but high enough for the data points to be still below this function. In this way, an upper limit for the k-point requirements can be obtained for each supercell size;
- Plot the upper limit for the required amount of k-points for the desired accuracy A as a function of supercell size N, using the parameters a and b, by means of eq. (4.7);
- Do the same for requirements as a function of supercell size of other parameters that induce significant absolute errors with increasing supercell size, by means of the previous

4 steps, with an appropriate enveloping function;

- Calculate the H dissolution energy for each Fe_NH with these parameter requirements;
- Determine the dilute limit value of E^H_{diss} by plotting the H dissolution energy as a function of H-concentration.

Finally, remark that the obtained unrelaxed H dissolution energies differ significantly from the calculated values of Jiang and Carter (Table 2.1): while their energies are approximately 0.28 eV/H, our calculations resulted in energies for the largest supercells of roughly 0.50 eV/H. A different choice of exchange-correlation functional (Jiang and Carter: PBE $\leftrightarrow$ here: GGA-PW91) and parameter settings (Jiang and Carter: E_{cut} = 350 eV and 12×12×12 k-mesh for the Fe_2H supercell $\leftrightarrow$ here: E_{cut} = 400 eV and 19×19×19 k-mesh) evidently has an influence on these values, but was not found to be critical: in the case of the Fe_128H cell, the dissolution energy was only altered by 0.02 eV/H. However, Jiang and Carter used the experimental value of the bcc Fe lattice parameter (2.86 Å), while the calculated equilibrium lattice parameter of 2.826 Å , as determined via a Birch-Murnaghan fit, was used in our calculations. Changing the lattice parameter as well leads to a H dissolution energy of 0.33 eV/H for the same cell, which agrees better with the results from Jiang and Carter. The choice of lattice parameter hence proves to be very critical with regards to the value of the H dissolution energy: a difference in the order of 0.03 Å already induces a change of approximately 0.2 eV. Since the values of Jiang and Carter are similar to computational results from other authors and experimental results, the experimental lattice parameter appears to be a better choice for DFT calculations of defect formation energies.

Chapter 5

Conclusions and outlook

5.1 Conclusions

DFT calculations of defect properties by means of the supercell method are generally found to be accompanied by spurious interactions between the defect and its periodic images. This a consequence of the limited supercell sizes, generally a few 100s of atoms at most, that can be handled computationally. Such interactions will however affect the charge distribution in the system. Hence, calculated properties that depend on the charge distribution will contain errors due to the limited supercell size. The most important property suffering from finite-size errors is the defect formation energy. In the literature, various studies have been performed on the different types of finite-size induced errors with respect to this property and possible correction schemes, especially in the research domain of defects in semiconducting materials. Spurious defect interactions can however be expected in any system that includes some kind of lattice defect. In particular, the dissolution energies of a substitutional Zr-atom in a sc, bcc and fcc Cu host lattice have already been observed to converge difficultly with supercell size: errors in the order of 0.1 eV even remained for cells containing about 128 atoms. In the case of hydrogen-related defects in bcc Fe, the literature is quite conclusive that point defect formation energies are already well converged with supercell size for similar system sizes, without consideration of larger systems. In order to judge the accuracy of these convergence tests, the tetrahedral interstitial H atom in bcc Fe was chosen as a reference system to investigate the finite-size convergence of the H dissolution energy: in the context of possible hydrogen traps in steel, calculated H-defect binding energies can only be interpreted correctly if finite-size related errors in defect formation energies are removed up to a certain degree of accuracy. Since data from Cu-Zr convergence tests were already available, the supercell finite-size convergence behavior was considered first for this system, thereby using the correction scheme as proposed by Probert and Payne in the case of the Zr dissolution energy. The study was performed for a Cu host lattice in particular. Results were subsequently transferred to the Fe-H system.

The analysis of the charge density distribution has showed that in the case of the Cu-Zr system, spurious interactions between Zr and its periodic images are very persistent: charge density difference oscillations were even observed along the entire nearest-defect axes in fccfcc12, the

largest considered supercell with $c_{Zr} = \frac{1}{1728}$. Supercells for routine defect calculations however have defect concentrations in the order of $\frac{1}{100}$, implying that in the particular case of Cu-Zr properties, finite-size induced errors cannot be avoided. At the same time, the magnitude of the spurious defect interactions was observed to depend on the type of substitutional impurity element. In the specific cases of Ag, Cd and Mg, these interactions were found to be much smaller than for Zr. Hence, it is the specific combination of a Zr-defect in a Cu host lattice that induces such strong defect interactions.

Properties that depend on the local charge distribution, such as the local electronic density of states (LDOS) and the integrated charge around a nucleus, were found to converge very well with supercell size. Supercells containing a few 100s of atoms already produced reliable LDOS and reduced errors on the integrated charge below 0.01 electrons, which is accurate enough for most practical applications (such as X-ray diffraction). On the other hand, the Zr dissolution energy suffers to a larger extent from finite-size errors, as was also observed in a previous Cu-Zr study. Up to a Zr-concentration of $\frac{1}{256}$, the uncertainty about its dilute limit value is still in the order of 0.1 eV. Remarkably, deviations from the convergence trends increased again for larger supercells, while the finite-size errors are expected to further decrease. A thorough investigation of the defect formation energy equation revealed that these large errors, in the order of 0.1-1 eV for the largest supercells, were a consequence of keeping the relative accuracy constant in each supercell, thereby causing the absolute error on the total ground-state energy to increase with supercell size. The same problem was observed in the case of the supercell finite-size convergence of the atomic forces: while errors fluctuate around 0.02 eV/Å up to the 128-atom cells, large deviations in the order of 0.1 eV/Å or the NN1-force appear for even larger cells. This is expected to be a consequence of the force being proportional to the derivative of the total ground-state energy with respect to the nucleus position.
The dissolution energy of H in bcc Fe appears to be less critical with regard to finite-size errors, in agreement with the literature. For a constant relative accuracy of 0.001 eV/atom in each supercell, dissolution energy values oscillate in the order of 0.01 eV/H as a function of H-concentration, even up to the $Fe_{250}H$ supercell, which is generally not considered in supercell finite-size convergence investigations in the literature. Absolute errors on the total ground-state energy with respect to the parameter settings hence appear not to dominate the convergence behavior of the H dissolution energy. Nevertheless, since such errors can be in the order of 0.1 eV for the largest cells, a completely correct interpretation of the convergence trend still requires individual E_{cut} and k-point convergence tests for each considered supercell. In addition, an adequate choice of the lattice parameter was found to influence the value of the H dissolution energy significantly: differences were observed to be in the order of 0.2 eV/H for a change in the lattice parameter of 0.03 Åfor the conventional bcc Fe unit cell. Hence, calculations with a constant, low absolute error with respect to all parameter settings appear to be indispensable for properties that depend on the electronic structure of the entire supercell.

To achieve the same absolute error for each defect formation energy, the relative accuracy needs to be increased as supercells become larger. A more accurate estimate of all parameter requirements can be made by optimizing the k-mesh via convergence tests for each individual supercell. However, such tests become impossible for cells containing 100s or 1000s of atoms due to excessive

calculation times. A procedure was therefore developed to estimate the required k-point settings for these supercells. K-point convergence tests were conducted on the smallest Cu-Zr supercells. From these tests, the relative accuracy was plotted as a function of the number of k-points in the one-atom first Brillouin zone. An enveloping exponential function was determined for these data, which was subsequently translated to the upper-limit k-point requirements as a function of supercell size. The predicted upper-limit 'constant absolute error' k-point requirements (for $A = 0.01$ eV/Zr) were used to replace the 'constant relative accuracy' k-meshes in the supercell finite-size convergence investigation of the Zr dissolution energy. These k-meshes improved the supercell finite-size convergence of this property significantly up to the 256-atom supercells. This result suggests that, for properties that depend on the electronic structure of the entire supercell, 'constant absolute error' calculations are indispensable in their supercell finite-size convergence investigation in order to interpret the observed convergence trend correctly. However, due to the very high upper-limit k-point density for the larger supercells, calculations became unfeasible for these cells as a consequence of limited computational resources and calculation time. These supercells were therefore excluded from the investigation. Hence, when performing a supercell finite-size convergence investigation of a supercell-size-dependent property, the largest supercell that can be included will depend on the degree of accuracy of this property.

Our investigation suggests that the settings for supercells in recent studies of supercell-size-dependent defect properties can be expected to be insufficient. Such properties are influenced by unphysical finite-size effects if the considered supercell(s) are too small. On the other hand, when large supercells are effectively considered (in order to diminish the finite-size effects), large absolute errors can appear due to an incorrect scaling with respect to supercell size of parameter settings that induce significant absolute errors for large supercells, such as the number of k-points. Hence, to interpret the supercell finite-size convergence behavior of supercell-size-dependent properties correctly, supercell calculations should be conducted with a constant absolute error (within the necessary degree of accuracy). In order to achieve this constant degree of accuracy for each supercell, the suggested procedure could be useful to estimate the upper-limit parameter requirements.

5.2 Outlook

Due to an increasing absolute error with supercell size (as the relative accuracy is kept constant), parameter requirements can become so severe for very large supercells (several 100s or 1000s of atoms) that calculations for such supercells become unfeasible due to the limited amount of computational resources and calculation time. Despite the fact that finite-size effects will have diminished significantly in these supercells, they can (currently) not be included in a supercell finite-size convergence investigation. As a suggestion for future work, it could be useful to investigate the parameter requirements as a function of supercell size for a certain amount of calculation time. Superimposing this curve on a plot as in Fig. 4.20 would then allow to investigate the maximum supercell size that can be considered for a certain degree of accuracy of the supercell-size-dependent property, given a certain amount of calculation time.

The suggested supercell finite-size convergence procedure was applied in this thesis to the Cu-Zr system (and to some extent to the Fe-H system) in particular. Other defect-lattice combinations were also shortly discussed, in the investigation of spurious defect interactions by means of charge density difference plots. The magnitude of these defect interactions were observed to be system-dependent, which suggests that the supercell finite-size convergence of the defect formation energy will also depend on the particular choice of defect-lattice combination. To substantiate this statement, supercell finite-size convergence investigations could be performed for the defect formation energy of these systems, by means of the proposed procedure in this work.

If the magnitude of finite-size errors depends on the particular choice of defect-lattice combination, there must be an underlying reason for this phenomenon. An investigation of all possible physical and chemical properties of lattices and defects that influence the magnitude of spurious defect interactions, and to what extent they influence the interactions would therefore be very useful. In this way, the maximum supercell size that needs be considered in order to eliminate finite-size errors, could be somewhat predicted in the supercell finite-size convergence investigation for a particular defect-lattice system.

It has been showed that calculations for large supercells do not necessarily improve the supercell finite-size convergence behavior. All parameters that induce errors who scale with system size, such as the number of k-points, will cause problems for such supercells if calculations are performed with a constant relative accuracy. A procedure was however developed that enables us to estimate the necessary parameter requirements for each supercell size and, taking computational limitations into consideration, which supercell sizes can be included in the supercell finite-size convergence investigation. Hence, if all parameter requirements with respect to the defect property of interest are taken into account, reliable supercell finite-size convergence studies can be performed for any defect/lattice-system.

Appendix A

List of supercells

A.1 Cu-Zr

	$\mathbf{n_{unit}}$ [N×N×N]	$\mathbf{n_{atoms}}$	Zr sublattice symmetry	$\mathbf{c_{Zr}[n_{atoms}^{-1}]}$
fccsc1	1×1×1	4	sc	$\frac{1}{4}$
fccfcc2	2×2×2	32	fcc	$\frac{1}{8}$
fccbcc2	2×2×2	32	bcc	$\frac{1}{16}$
fccsc2	2×2×2	32	sc	$\frac{1}{32}$
fccfcc3	3×3×3	108	fcc	$\frac{1}{27}$
fccsc3	3×3×3	108	sc	$\frac{1}{108}$
fccfcc4	4×4×4	256	fcc	$\frac{1}{64}$
fccbcc4	4×4×4	256	bcc	$\frac{1}{128}$
fccsc4	4×4×4	256	sc	$\frac{1}{256}$
fccfcc6*	6×6×6	216	fcc	$\frac{1}{216}$
fccfcc8*	8×8×8	512	fcc	$\frac{1}{512}$
fccfcc10*	10×10×10	1000	fcc	$\frac{1}{1000}$
fccfcc12*	12×12×12	1728	fcc	$\frac{1}{1728}$

Table A.1: Overview of all Cu-Zr supercells for which the investigation of the supercell finite-size convergence was conducted. The number of unit cells in each dimension, the number of atoms per supercell, the Zr sublattice symmetry and the Zr-concentration are given for each supercell. The cells denoted with * are primitive cells.

A.2 Fe-H

	$\mathbf{n_{unit}}$ [N×N×N]	$\mathbf{n_{Fe}}$	$\mathbf{c_H}$ [$\mathbf{n_{atoms}^{-1}}$]
Fe_2H	1×1×1	1	$\frac{1}{3}$
$Fe_{16}H$	2×2×2	16	$\frac{1}{17}$
$Fe_{54}H$	3×3×3	54	$\frac{1}{55}$
$Fe_{128}H$	4×4×4	128	$\frac{1}{129}$
$Fe_{250}H$	5×5×5	250	$\frac{1}{251}$

Table A.2: Overview of all Fe-H supercells for which the H dissolution energy was calculated, for the investigation of the supercell finite-size convergence. The number of unit cells in each dimension, the number of atoms per supercell and the H concentration are given for each supercell.

Appendix B

Computational parameter settings

B.1 Cu-Zr

	$\mathbf{n_{unit}}$ [N×N×N]	$\mathbf{E_{cut}}$ [eV]	EDIFF [eV]	k-mesh [k×k×k]
fccsc1	1×1×1	400	1E-7	21×21×21
fccfcc2	2×2×2	400	1E-7	11×11×11
fccbcc2	2×2×2	400	1E-7	11×11×11
fccsc2	2×2×2	400	1E-7	11×11×11
fccfcc3	3×3×3	400	1E-7	7×7×7
fccsc3	3×3×3	400	1E-7	7×7×7
fccfcc4	3×3×3	400	1E-7	6×6×6
fccbcc4	4×4×4	400	1E-7	6×6×6
fccsc4	4×4×4	400	1E-7	6×6×6
fccfcc6	6×6×6	400	1E-7	7×7×7
fccfcc8*	8×8×8	400	1E-7	3×3×3
fccfcc10*	10×10×10	400	1E-7	3×3×3
fccfcc12*	12×12×12	400	1E-7	1×1×1

Table B.1: Overview of the parameter settings that were used for all property calculations of each Cu-Zr supercell, as determined by convergence tests on the fccsc1 cell. The cells denoted with * are primitive cells.

B.2 Fe-H

	$\mathbf{n_{unit}}$ [N×N×N]	$\mathbf{E_{cut}}$ [eV]	EDIFF [eV]	k-mesh [k×k×k]
$\mathbf{Fe_2H}$	1×1×1	400	1E-6	21×21×21
$\mathbf{Fe_{16}H}$	2×2×2	400	1E-6	11×11×11
$\mathbf{Fe_{54}H}$	3×3×3	400	1E-6	7×7×7
$\mathbf{Fe_{128}H}$	4×4×4	400	1E-6	5×5×5
$\mathbf{Fe_{250}H}$	5×5×5	400	1E-6	4×4×4

Table B.2: Overview of the parameter settings that were used for the dissolution energy calculation of each Fe-H supercell, as determined by convergence tests on the Fe_2H cell.

Appendix C

Absolute error on the Zr dissolution energy

Before any k-point convergence tests can be performed, a criterion needs to be established that relates the maximum allowed error on the Zr dissolution energy with respect to the number of k-points to the absolute error on the Cu-Zr and corresponding pure Cu cell for which this maximum error is attained. Therefore, consider eq. (4.1), by which all Zr dissolution energies are calculated. It is slightly rewritten, by mentioning the dependence on the number of k-points explicitly:

$$E_{diss}^{\mathrm{Zr}}(N,k) = E(\mathrm{Cu}_{N-1}\mathrm{Zr})(k) - \frac{N-1}{N}E(\mathrm{Cu}_N)(k) - E(\mathrm{Zr})(k) \tag{C.1}$$

$E(\mathrm{Zr})(k)$ is the total ground-state energy of only one Zr-atom in its pure equilibrium state. The error on this energy with respect to the parameter settings was already found to be in the order of 10^{-4} eV and can hence be considered to be accurate enough for all dissolution energy calculations. The other energies on the right-hand side of the equation are the ones that scale with supercell size and hence the absolute error on their values do as well. In order to determine how $E_{diss}^{\mathrm{Zr}}(N,k)$ varies with a change in the total ground-state energy of the Cu-Zr and its corresponding pure Cu cell, the total differential of the Zr dissolution energy with respect to these variables can be taken:

$$\Delta E_{diss}^{\mathrm{Zr}}(N,k) = \Delta E(\mathrm{Cu}_{N-1}\mathrm{Zr})(k) - \frac{N-1}{N}\Delta E(\mathrm{Cu}_N)(k) \tag{C.2}$$

As expected, the error on the Zr dissolution energy is directly proportional to the error on the supercell energies. $\Delta E_{diss}^{\mathrm{Zr}}(k)$ will be maximal when the error terms on the right-hand side of eq. (C.2) have opposite signs. The maximum error on the Zr dissolution energy can hence be determined by adding up absolute values of the absolute error terms:

$$|\Delta E_{diss}^{\mathrm{Zr}}(N,k)| = |\Delta E(\mathrm{Cu}_{N-1}\mathrm{Zr})(k)| + \frac{N-1}{N}|\Delta E(\mathrm{Cu}_N)(k)| \tag{C.3}$$

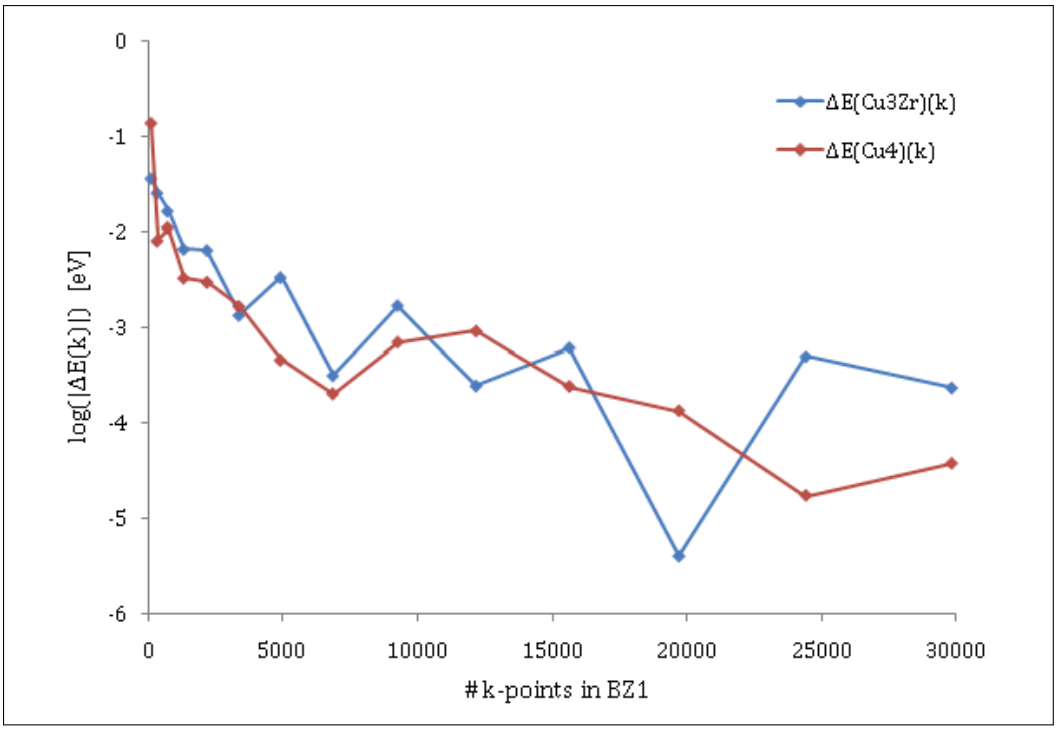

Figure C.1: Convergence of the absolute error on the total ground-state energy of Cu_3Zr and its corresponding pure Cu cell with the number of k-points in BZ1.

By means of the above equation, the maximum tolerance on the total ground-state energy of the Cu-Zr and Cu supercell can be determined for a degree of accuracy of the Zr dissolution energy. In this way, however, k-point convergence tests for both the Cu-Zr and its corresponding pure Cu cell would be required for each system size. To further reduce the calculation time, notice that the values of both terms to the right-hand side of eq. (C.3) can be expected be approximately the same and this for two reasons. First of all, both terms correspond to systems that are nearly equal in size, with the pure Cu-term accounting for a system that contains one atom less than the Cu-Zr term. Second, the difference between both systems is the substitution of a single Cu-atom by Zr, which is like Cu a transition metal. The k-point convergence behavior of the total ground-state energy for both systems is therefore expected to be quite similar.

Both hypotheses are tested by comparing the k-point convergence behavior of the error on the total ground-state energy of the smallest supercell in Table A.1 (chemical composition Cu_3Zr) with an equally large pure Cu cell. As in subsection 4.2.1, the energy error for a certain number of k-points was determined by taking the total ground-state energy of the most accurate calculation (a 33×33×33 k-mesh for both systems) as a reference. Results from these calculations are shown in Fig. C.1, with errors plotted on a logarithmic scale. The absolute errors for both systems are indeed observed to be of the same order for nearly all calculations, with only a deviation of one order as from the calculations with a 27×27×27 k-mesh (roughly 20000 k-points). Because the factor $\frac{N-1}{N}$ in the pure-Cu-term in eq. (C.3) converges to 1 for large N, it seems to be appropriate to approximate the maximum error on the Zr dissolution energy by twice the absolute error on the total ground-state energy of the Cu-Zr cell:

$$|\Delta E^{\mathrm{Zr}}_{diss}(N,k)| \cong 2|\Delta E(\mathrm{Cu}_{N-1}\mathrm{Zr})(k)| \tag{C.4}$$

In this way, the calculation time for k-point convergence tests for a specific supercell size could be approximately halved since only the Cu-Zr cells need to be investigated. In Fig. C.2 the maximum error on the Zr dissolution energy, calculated by adding up $\Delta E(\mathrm{Cu_3Zr})(k)$ and $\Delta E(\mathrm{Cu_4})(k)$ according to eq. (C.3), is compared with the twice the absolute error on the $E(\mathrm{Cu_3Zr})$, as a function of k-points. Both errors are in good agreement with each other, with only a deviation of one order for the 27×27×27 k-mesh, as expected. The error for this amount of k-points is already very small, in the order of 10^{-4} eV and hence does not require special attention: the general convergence trends of both systems are still very similar over the complete k-point range. $|\Delta E^{Zr}_{diss}(N,k)|$ can therefore safely be approximated by twice the absolute error on the total ground-state energy of the Cu-Zr cell.

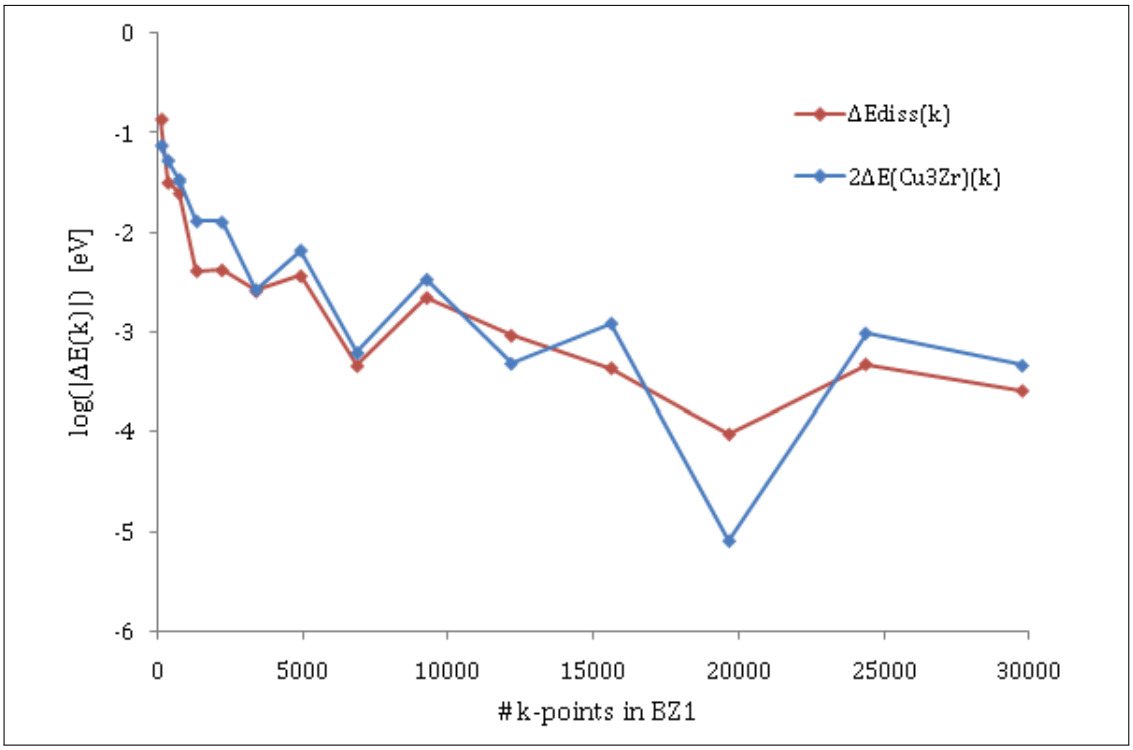

Figure C.2: Comparison between the convergence behavior of the absolute error on E^{Zr}_{diss} and twice the absolute error on the total ground-state energy of $\mathrm{Cu_3Zr}$.

Bibliography

[1] S. Cottenier, *Density Functional Theory and the family of (L)APW-methods: a step-by-step introduction.* Instituut voor Kern- en Stralingsfysica, K.U. Leuven, Belgium, 2002.

[2] D. S. Scholl and J. A. Steckel, *Density Functional Theory: A practical introduction.* John Wiley & Sons, Inc., 2009.

[3] S. Cottenier, "Slides from the *Computational Materials Physics* course." pdf, 2012.

[4] P. Hohenberg and W. Kohn, "Inhomogeneous Electron Gas," *Physical Review*, vol. 136, pp. B864 – B871, Nov 1964.

[5] J. P. Perdew, J. A. Chevary, S. H. Vosko, K. A. Jackson, M. R. Pederson, D. J. Singh, and C. Fiolhais, "Atoms, molecules, solids, and surfaces - Applications of the Generalized Gradient Approximation for exchange and correlation," *Physical Review B*, vol. 46, no. 11, pp. 6671–6687, 1992.

[6] J. P. Perdew, K. Burke, and M. Ernzerhof, "Generalized gradient approximation made simple," *Physical Review*, vol. 77, pp. 3865–3868, 1996.

[7] Wikipedia, "Brillouin Zone — Wikipedia, The Free Encyclopedia." `http://en.wikipedia.org/w/index.php?title=Brillouin_Zone&oldid=174793526`, 2007.

[8] H. Monkhorst and J. D. Pack, "Special points for Brillouin-Zone integrations," *Physical Review B*, vol. 13, p. 5188, 1976.

[9] P. E. Blochl, "Projector augmented-wave methods," *Physical Review B*, vol. 50, p. 17953, 1994.

[10] G. Kresse and D. Joubert, "From ultrasoft pseudopotentials to the projector augmented-wave method," *Physical Review B*, vol. 59, p. 1758, 1999.

[11] C. Rostgaard, "The Projector Augmented-wave Method," 2009.

[12] C. W. M. Castleton and S. Mirbt, "Finite-size scaling as a cure for supercell approximation errors in calculations of neutral native defects in InP," *Physical Review B*, vol. 70, p. 195202, Nov 2004.

[13] M. I. J. Probert and M. C. Payne, "Improving the convergence of defect calculations in supercells: An ab initio study of the neutral silicon vacancy," *Physical Review B*, vol. 67, no. 7, 2003.

[14] F. Corsetti and A. A. Mostofi, "System-size convergence of point defect properties: The case of the silicon vacancy," *Physical Review B*, vol. 84, p. 035209, Jul 2011.

[15] C. W. M. Castleton, A. Höglund, and S. Mirbt, "Density functional theory calculations of defect energies using supercells," *Modelling and Simulation in Materials Science and Engineering*, vol. 17, no. 8, p. 084003, 2009.

[16] C. W. M. Castleton, A. Höglund, and S. Mirbt, "Managing the supercell approximation for charged defects in semiconductors: Finite-size scaling, charge correction factors, the band-gap problem, and the *ab initio* dielectric constant," *Physical Review B*, vol. 73, p. 035215, 2006.

[17] A. Höglund, C. W. M. Castleton, and S. Mirbt, "Relative concentration and structure of native defects in GaP," *Physical Review B*, vol. 72, p. 195213, Nov 2005.

[18] R. Nazarov, T. Hickel, and J. Neugebauer, "Vacancy formation energies in fcc metals: Influence of exchange-correlation functionals and correction schemes," *Physical Review B*, vol. 85, p. 144118, Apr 2012.

[19] P. Blaha, K. Schwarz, G. K. H. Madsen, D. Kvasnicka, and J. Luitz, *WIEN2k, An Augmented Plane Wave + Local Orbitals Program for Calculating Crystal Properties*. Karlheinz Schwarz, Techn. Universität Wien, Austria.

[20] M. J. Puska, S. Poykko, M. Pesola, and R. M. Nieminen, "Convergence of supercell calculations for point defects in semiconductors: Vacancy in silicon," *Physical Review B*, vol. 58, no. 3, pp. 1318–1325, 1998.

[21] N. Chetty, M. Weinert, T. S. Rahman, and J. W. Davenport, "Vacancies and impurities in Aluminum and Magnesium," *Physical Review B*, vol. 52, no. 9, pp. 6313–6326, 1995.

[22] J. Moreno and J. M. Soler, "Optimal meshes for integrals in real-space and reciprocal-space unit cells," *Physical Review B*, vol. 45, no. 24, pp. 13891–13898, 1992.

[23] G. Makov and M. C. Payne, "Periodic boundary-conditions in ab-initio calculations," *Physical Review B*, vol. 51, no. 7, pp. 4014–4022, 1995.

[24] F. El-Mellouhi, N. Mousseau, and P. Ordejón, "Sampling the diffusion paths of a neutral vacancy in silicon with quantum mechanical calculations," *Physical Review B*, vol. 70, p. 205202, Nov 2004.

[25] M. Wierzbowska and A. Fleszar, "Density functional theory calculations for a single Re impurity in silicon," *Physical Review B*, vol. 83, p. 184418, May 2011.

[26] C. Castleton and S. Mirbt, "Ab initio study of neutral vacancies in InP using supercells and finite size scaling," *Physica B: Condensed Matter*, vol. 340-342, pp. 407 – 411, 2003.

[27] D. J. Wilson, A. A. Sokol, S. A. French, and C. R. A. Catlow, "Defect structures in the silver halides," *Physical Review B*, vol. 77, p. 064115, Feb 2008.

[28] K. Levasseur-Smith and N. Mousseau, "Ab initio study of the diffusion mechanisms of gallium in a silicon matrix," *European Physical Journal B*, vol. 64, no. 2, pp. 165–172, 2008.

[29] B. Puchala and D. Morgan, "Atomistic modeling of As diffusion in ZnO," *Physical Review B*, vol. 85, p. 064106, Feb 2012.

[30] N. D. M. Hine, K. Frensch, W. M. C. Foulkes, and M. W. Finnis, "Supercell size scaling of density functional theory formation energies of charged defects," *Physical Review B*, vol. 79, p. 024112, Jan 2009.

[31] D. R. Saravia, A. Juan, G. Brizuela, and S. Simonetti, "Comparative study of H-atom location, electronic and chemical bonding in ideal and vacancy containing-FCC iron," *International Journal of Hydrogen Energy*, vol. 34, no. 19, pp. 8302 – 8307, 2009.

[32] D. P. Escobar, *Evaluation of Hydrogen Trapping in Iron-Based Alloys by Thermal Desorption Spectroscopy*. PhD thesis, University of Ghent, 2012.

[33] D. E. Jiang and E. A. Carter, "Diffusion of interstitial hydrogen into and through bcc fe from first principles," *Physical Review B*, vol. 70, p. 064102, Aug 2004.

[34] R. Nazarov, T. Hickel, and J. Neugebauer, "First-principles study of the thermodynamics of hydrogen-vacancy interaction in fcc iron," *Physical Review B*, vol. 82, p. 224104, Dec 2010.

[35] J. Au and H. Birnbaum, "Magnetic relaxation studies of the motion of hydrogen and deuterium in iron," *Acta Metallurgica*, vol. 26, no. 7, pp. 1105 – 1116, 1978.

[36] J. L. Gu, K. D. Chang, H. S. Fang, and B. Z. Bai, "Delayed Fracture Properties of 1500 MPa Bainite/Martensite Dual-phase High Strength Steel and Its Hydrogen Traps," *ISIJ International*, vol. 42, pp. 1560–1564, 2002.

[37] G. M. Pressouyre and I. M. Bernstein, "A Quantitative Analysis of Hydrogen Trapping," *Metallurgical Transactions A - Physical Metallurgy and Materials Science*, vol. 9, no. 11, pp. 1571–1580, 1978.

[38] F. Besenbacher, S. M. Myers, P. Nordlander, and J. K. Nørskov, "Multiple hydrogen occupancy of vacancies in Fe," *Journal of Applied Physics*, vol. 61, no. 5, pp. 1788–1794, 1987.

[39] W. Y. Choo and J. Y., "Thermal-analysis of trapped hydrogen in pure iron," *Metallurgical Transactions A - Physical Metallurgy and Materials Science*, vol. 13, no. 1, pp. 135–140, 1982.

[40] H. Dogan, D. Li, and J. R. Scully, "Controlling Hydrogen Embrittlement in Precharged Ultrahigh-Strength Steels," *Corrosion*, vol. 63, no. 7, pp. 689–703, 2007.

[41] S. M. Myers, S. T. Picraux, and R. E. Stoltz, "Defect trapping of ion-implanted deuterium in Fe," *Journal of Applied Physics*, vol. 50, no. 9, p. 5710, 1979.

[42] L. S. R. Thomas, D. Li, R. P. Gangloff., and J. R. Scully, "Trap-governed hydrogen diffusivity and uptake capacity in ultrahigh-strength AERMET 100 steel," *Metallurgical and Materials Transactions A*, vol. 33, pp. 1991–2004, 2002.

[43] R. Gibala, "Internal friction in hydrogen-charged iron," *Transactions of the Metallurgical Society of AIME*, vol. 239, no. 10, p. 1574, 1967.

[44] W. Counts, C. Wolverton, and R. Gibala, "First-principles energetics of hydrogen traps in α-Fe: Point defects," *Acta Materialia*, vol. 58, no. 14, pp. 4730 – 4741, 2010.

[45] B.-J. Lee and J.-W. Jang, "A modified embedded-atom method interatomic potential for the Fe-H system," *Acta Materialia*, vol. 55, no. 20, pp. 6779 – 6788, 2007.

[46] A. T. Paxton and C. Elsässer, "Electronic structure and total energy of interstitial hydrogen in iron: Tight-binding models," *Physical Review B*, vol. 82, p. 235125, Dec 2010.

[47] A. Ramasubramaniam, M. Itakura, and E. A. Carter, "Interatomic potentials for hydrogen in α-iron based on density functional theory," *Physical Review B*, vol. 79, p. 174101, May 2009.

[48] Y. Tateyama and T. Ohno, "Stability and clusterization of hydrogen-vacancy complexes in alpha-Fe: An ab initio study," *Physical Review B*, vol. 67, no. 17, p. 174105, 2003.

[49] D. Psiachos, T. Hammerschmidt, and R. Drautz, "Ab initio study of the modification of elastic properties of α-iron by hydrostatic strain and by hydrogen interstitials," *Acta Materialia*, vol. 59, no. 11, pp. 4255 – 4263, 2011.

[50] J. Sanchez, J. Fullea, C. Andrade, and P. L. de Andres, "Hydrogen in α-iron: stress and diffusion," 2011.

[51] L. Ismer, T. Hickel, and J. Neugebauer, "*Ab initio* study of the solubility and kinetics of hydrogen in austenitic high Mn steels," *Physical Review B*, vol. 81, p. 094111, Mar 2010.

[52] Y. A. Du, L. Ismer, J. Rogal, T. Hickel, J. Neugebauer, and R. Drautz, "First-principles study on the interaction of H interstitials with grain boundaries in alpha- and gamma-Fe," *Physical Review B*, vol. 84, no. 14, 2011.

[53] F. Caestecker, "Nauwkeurigheidsstudie voor het ab-initio berekenen van de mengingsenthalpie bij bulk metallic glasses," Master's thesis, Universiteit Gent, 2012.

[54] G. Kresse and J. Furthmüller, "Efficiency of ab-initio total energy calculations for metals and semiconductors using a plane-wave basis set," *Computational Materials Science*, vol. 6, p. 15, 1996.

[55] G. Kresse and J. Furthmüller, "Efficient iterative schemes for ab initio total-energy calculations using a plane-wave basis set," *Physical Review B*, vol. 54, p. 11169, 1996.

[56] G. Kresse, M. Marsman, and J. Furthmüller, *VASP the GUIDE*. Universität Wien, 2009.

[57] S. R. Bahn and K. W. Jacobsen, "An object-oriented scripting interface to a legacy electronic structure code," *Computing in Science Engineering*, vol. 4, no. 3, pp. 56 – 66, 2002.

[58] K. Lejaeghere, V. Van Speybroeck, G. Van Oost, and S. Cottenier, "Supplementary material at arxiv:1204.2733 [cond-mat.mtrl-sci] to 'Error estimates for solid-state density-functional theory predictions: an overview by means of the ground-state elemental crystals'."

[59] K. Momma and F. Izumi, "VESTA 3 for three-dimensional visualization of crystal, volumetric and morphology data," *Journal of Applied Crystallography*, vol. 44, no. 6, pp. 1272–1276, 2011.

[60] "Zirconium Facts: Chemical and Physical properties." `http://en.wikipedia.org/w/index.php?title=Brillouin_Zone&oldid=174793526`.

[61] L. A. Curtiss, K. Raghavachari, P. Redfern, and J. Pople, "Assessment of Gaussian-2 and density functional theories for the computation of enthalpies of formation," *Journal of Chemical Physics*, vol. 106, no. 3, p. 1063, 1997.

List of Figures

List of Tables